universität wien

MASTERARBEIT | MASTER'S THESIS

Titel | Title

Sustainable biotechnological conversion and storage of carbon dioxide with methanogenic archaea

verfasst von | submitted by

Nicolás Antonio Salas Wallach

angestrebter akademischer Grad | in partial fulfilment of the requirements for the degree of

Master of Science (MSc)

Wien | Vienna, 2025

Studienkennzahl lt. Studienblatt | Degree programme code as it appears on the student record sheet:	UA 066 830
Studienrichtung lt. Studienblatt | Degree programme as it appears on the student record sheet:	Masterstudium Molecular Microbiology, Microbial Ecology and Immunobiology
Betreut von | Supervisor:	Mag. Mag. Dr.techn. Simon Karl-Maria Rasso Rittmann Privatdoz. Bakk.

Acknowledgements

"Caminante, no hay camino, se hace camino al andar" — Antonio Machado. With this phrase, I want to thank life for the people I've met and the choices I've made during my studies in Vienna.

First, I would like to thank my parents, my brother, and my grandmother for their unconditional support—for listening to me, making me smile on my darkest days, and sharing the joy of the brightest ones. Although more than 12,000 km separate us, we've always been connected.

Secondly, to my first friends in Vienna who welcomed me so warmly—María, Alejandro, Fernanda, and Paolo—you will always hold a special place in my heart.

Next, to the amazing people I met along the way: Martino, Maddi, Ale, Ina, Alonso, Yassin, Fran, Alma, Hanin, Michael, Nadinne, Cesc, Arnau, Selina, Drew, and Adri, just to name a few. Sharing my time with you made my stay feel like being part of a family—people I could trust and count on.

To my Chilean diaspora friends—Seba, Felipe, Enzo, and Benja—thank you. It was always a pleasure to meet and talk with you. Moving to Austria wouldn't have been the same without your company.

Finally, I would like to acknowledge Dr. Simon Rittmann and his team for trusting me to work and share this experience with them. Special thanks to Walter for being a close supervisor, colleague, and friend. We went through adversity together and still managed to survive.

Abstract

Archaeal biotechnology remains an understudied field in science with significant potential for the development of novel technologies. The unique metabolism and adaptations of Archaea position them as promising candidates for several applications including biomining, enzyme bioprospecting, amino acid synthesis, bioplastic production and methane generation. In the first chapter of this work, it was explored for the first time the polyhydroxyalkanoate (PHA) biosynthesis pathway in the ammonia-oxidizing archaeon (AOA) *Nitrososphaera viennensis*. The PHA pathway enzymes (PhaAa, PhaAb, PhaB, PhaC, and PhaE) were cloned and expressed in *Escherichia coli* and subsequently purified. Kinetic parameters were determined for PhaB with a k_{cat} of 40.92 ± 1.62 s^{-1} and a K_m of 2.81 · 10^{-2} ± 3.29 · 10^{-3} mmol L^{-1}. Detected values are consistent with other already characterized ortholog proteins from related organisms. Additionally, the quaternary structure of the PHA synthase (PhaCE) was found to be putatively tetrameric. These findings might enable the application of novel archaeal enzymes for PHA synthesis and potentially new PHA polymers.

In the second chapter, the operation of a novel device was presented, the Gas and Pressure Controller (GPC), designed to identify physiological and biotechnological characteristics of gas fermentation microbial cell factories. The GPC allows for automated control of the headspace gas pressure in closed batch cultivation systems, enabling gassing, sparging, monitoring in real time. As proof of concept, four autotrophic, hydrogenotrophic, methanogenic archaea were cultured, achieving unprecedented maximum specific methane production rates (qCH_4): *Methanothermobacter marburgensis* (169.59 ± 12.52 mmol g^{-1} h^{-1}), *Methanotorris igneus* (420.21 ± 89.46 mmol g^{-1} h^{-1}*), Methanocaldococcus jannaschii* (364.52 ± 25.50 mmol g^{-1} h^{-1}), and *Methanocaldococcus villosus* (356.38 ± 20.79 mmol g^{-1} h^{-1}). The GPC also operated reliably and autonomously during long-term cultivation of *Methanococcus maripaludis*. This device enables precise pressure regulation and holds great promise for optimizing a wide range of gas-fermenting bioprocesses.

Zusammenfassung

Die Archaeen-Biotechnologie ein bis jetzt noch wenig erforschtes Gebiet in der Wissenschaft, welche jedoch ein erhebliches Potenzial für die Entwicklung neuer Technologien besitzt. Die einzigartigen Stoffwechselwege der Archaea kennzeichnen sie als vielversprechenden Kandidaten für eine Vielzahl von verschiedenen Anwendungen z.B. für das „Biomining“, die Enzymbioprospektion, Aminosäuresynthese- und produktion, die Biokunststoffproduktion und die Methanerzeugung. Im ersten Kapitel dieser Arbeit wird erstmalig der natürliche Polyhydroxyalkanoat (PHA)-Biosyntheseweg des ammoniakoxidierenden Archaeon (AOA) *Nitrososphaera viennensis* untersucht. Die für die Produktion des Bioplatiks verantwortlichen Gene (PhaAa, PhaAb, PhaB, PhaC und PhaE) wurden in *Escherichia coli* kloniert und die Enzyme anschließend exprimiert und aufgereinigt. Die kinetischen Parameter wurden mit einem k_{cat} von 40,92 ± 1,62 s^{-1} und einem K_m von 2,81 · 10^{-2} ± 3,29 · 10^{-3} mmol L^{-1} für PhaB bestimmt. Die ermittelten Werte stimmen in ihrer Größe mit orthologen Proteine überein. Des Weiteren wurde eine neuartige quaternäre Struktur der PHA-Synthase (PhaCE) (Tetramer) ermittelt. Diese Ergebnisse ermöglichen die Anwendung neuartiger archaeischer Enzyme für die PHA-Synthese in Kombination mit neuartigen PHA-Polymeren.

Im zweiten Kapitel wird die Funktionsweise eines neu entwickelten Prototypen unter dem Namen des „Gas and Pressure Controller“ (GPC) vorgestellt. Diese Maschine kann zur Ermittlung von physiologischer und biotechnologischer Merkmale von mikrobiellen Zellfabriken verwendet werden, die in Gasfermentierungsprozessen angewandt werden können. Die GPC ermöglicht die Überwachung und Regelung des Gasdrucks im Kopfraum von geschlossenem satzverfahrenbasierten Kultivierungssystemen durch automatisches Begasen und Spülen von Kultivierungsflaschen in Echtzeit. Zum Nachweis der Funktionalität des Systems wurden vier autotrophe und hydrogenotrophe methanogene Archaeen mit der GPC kultiviert. Es konnten dadurch bisher unerreichte maximale spezifische Methanproduktionsraten (qCH_4) der untersuchten Organsimen erfasst werden: *Methanothermobacter marburgensis* (169,59 ± 12,52 mmol g^{-1} h^{-1}), *Methanotorris igneus* (420,21 ± 89,46 mmol g^{-1} h^{-1}), *Methanocaldococcus jannaschii* (364,52 ± 25,50 mmol g^{-1} h^{-1}), und *Methanocaldococcus villosus* (356,38 ± 20,79 mmol g^{-1} h^{-1}). Außerdem konnte die Zuverlässigkeit und autonome Anwendung der GPC während einer Langzeitkultivierung von *Methanococcus maripaludis* erfolgreich bestätigt werden. Die neu entwickelte Maschine ermöglicht eine präzise Druckregulierung und ist ein vielversprechendes Werkzeug für die Optimierung eines breiten Spektrums von gasfermentierender Bioprozesse.

Content

General introduction

Biotechnology

Throughout human civilization, microorganisms have played a fundamental role in various processes, ranging from food production to the generation of raw materials and energy [1]. The earliest records of biotechnological applications date back to approximately 6,000 BC, involving anaerobic fermentation such as the production of beer and wine, the preservation of food through pickling in acetic acid and the use of enzymes in cheese production [1,2]. However, it was not until the 1860s that Louis Pasteur demonstrated that yeasts and certain bacteria are responsible for these processes, forever revolutionizing our understanding of microorganisms and their roles in biological processes [3]. In this context, industrial biotechnology emerges as a sustainable and promising alternative.

The United Nations Convention on Biological Diversity defines biotechnology as „*any technological application that uses biological systems, living organisms, or derivatives thereof, to make or modify products or processes for specific use.*" Therefore, the different applications can be classified in the following categories such as [1,4]:

- White biotechnology (industrial biotechnology): Research and development on the biocatalysis in industrial processes, production of biodegradable polymer, renewable fuel and industrially relevant enzymes or microorganisms.
- Blue biotechnology: Explores the ocean and sea resources to create products and applications of industrial interest, focusing in new materials (hydrocolloids and gelling agents), production of next generation biofuels with microalgae and enzymatically active molecules useful for medicine, diagnostics and processes.
- Green biotechnology: Related to the improvement of agriculture with molecular engineering for selection of plants with desired properties, as well as tissue and plant cells propagation, among other techniques.
- Red biotechnology: Involves health and pharmaceutical applications. It considers the production of vaccines and antibiotics, discovery of new drugs, construction of artificial organs and new diagnostic techniques.
- Yellow biotechnology: Related to food production and quality. It aims to improve food to obtain a more nourishing and fortified version of it.
- Brown biotechnology: Considers the management and possible applications of arid lands and deserts. It additionally focusses in drought-resistant crops and saline agriculture.
- Violet biotechnology: Associated with developing proper regulations and a platform for discussion for biotechnology applications.

To date, biotechnology has primarily focused on fungal systems, bacterial systems, or enriched microbial consortia. Among the most commonly used organisms are the bacteria *Escherichia coli* and *Bacillus subtilis*, as well as the yeasts *Saccharomyces cerevisiae* and *Pichia pastoris*. These organisms are notable for their rapid growth, well-characterized genomes, and ease of genetic manipulation [5,6]. Other approach is utilizing microbial consortia, which have proven to be effective in processes such as bioremediation, wastewater treatment, and biomining, leveraging the synergistic interactions between different species [7]. Despite significant advancements and a wide range of established cell factories, archaeal systems remain underrepresented [1]. However, archaea represent an intriguing frontier in biotechnological research due to their unique metabolic pathways. As members of the third domain of life, archaea inhabit almost every terrestrial habitat, including those with extreme conditions (extreme temperature, high salinity, extreme pHs, among others) [8]. Their resilience and their metabolic versality make them crucial players in the global carbon and nitrogen cycles [9].

Applications of archaea in environmental biotechnology

The extreme adaptations and metabolic capabilities of the archaea hold an immense potential for novel biotechnological applications. For instance, hyperthermophilic archaea, with cultivation temperatures of 80 °C and higher, are excellent sources of thermostable enzymes used in biofuel production, molecular biology (e.g., polymerase chain reaction - PCR) and in the food industry [1,8,10]. Ammonia oxidizing archaea (AOA) found in almost all environments are key players in the nitrogen cycle through their ability to perform ammonium oxidation and maintain the nitrogen balance in wastewater treatment [11] and in soil health [12]. Haloarchaea, are remarkable microorganisms capable of growing in high salinity environments, making them suitable for bioremediation of saline wastewater [1,8]. Furthermore, methanogenic archaea are a group of organisms that produce methane (CH_4) from various organic substrates and play a crucial role in anaerobic digestion processes for the production of biogas [1,8]. Finally, *Sulfolobales* thrive in thermophilic and acidic conditions. Their metabolism often involves interactions with heavy metals, being particularly useful in bioleaching and in bioremediation of acidic and metal-contaminated environments [8].

Amino acids

Recent studies have found that certain autotrophic, hydrogenotrophic methanogenic archaea, such as *Methanothermococcus marburgensis*, *Methanococcus villosus*, and *Methanocaldococcus okinawensis*, are capable of excreting proteinogenic amino acids. Each microorganism exhibits a distinct amino acid excretion profile, which can be influenced by environmental conditions. Although the excretion rates of these wild-type methanogenic archaea are lower than those observed in genetically engineered bacteria, their hydrogenotrophic metabolism combined with advances in synthetic biology offer a promising biotechnological application [13,14].

Enzymes

Extremophilic archaea have developed enzymes with unique structure-function properties, also known as extremozymes. They show increased stability at high temperatures, extreme pH and in the presence of organic solvents or heavy metals, in addition to being more resilient against proteolytic attacks [8]. Mainly proteolytic, lipases, DNA processing and glycosyl esterases enzymes are studied, particularly the most successful use for archaeal enzymes is the DNA polymerase originally isolated from archaea from the genera *Thermococcus* and *Pyrococcus* utilized in PCR reactions. Most of the studies for enzyme applications are in hyperthermophilic and halophilic archaea [1,8].

Biomining

The extraction of metals from minerals is usually performed by different chemical processes, pyrometallurgy and hydrometallurgy, that use high temperatures and are energy intensive demanding [1]. However, microorganisms can offer an alternative process through increasing the solubility of certain insoluble minerals by biological acidification, oxidation or complexation [15]. This technology has been established for recovering copper, gold, uranium, cadmium, nickel, zinc among other metals [1]. Notable approximately 20% of the copper mined today is extracted through biomining with a consortia of archaea and bacteria[16]. Some archaea utilized in biomining and isolated from mines belong to the genera *Acidianus*, *Ferroplasma*, *Sulfolobus*, and *Metallosphaera* [8].

Molecular hydrogen production

Nowadays more than 75% of the global molecular hydrogen (H_2) production origins from fossil fuel, while only a small fraction is produced from renewable resources [17]. However, H_2 can be additionally produced biologically by microorganisms in 4 distinct metabolic pathways: bio-photolysis, which uses light energy to power the lysis of water (direct photolysis) or to degrade

carbohydrates with photosynthetic origin (indirect); photo-fermentation, where organic compounds are degraded in a light-driven process; dark fermentation, which breaks down organic compounds via acetate mediated pathway; and CO-gas fermentation, in which carbon monoxide (CO) is oxidized and water is reduced [18]. Additionally, the hydrogen-producing microorganisms are classified into three main groups: oxygenic phototrophs, anoxygenic phototrophs and facultative or strict anaerobes, which includes all known archaeal H_2 producing strains [1]. Due to a higher catalytic activity at high temperatures, the most studied and promising archaea for H_2 production are hyperthermophilic as *Desulfurococcus amylolyticus*, *Pyrococcus furiosus*, *Thermococcus barophilus*, *Thermococcus kodakarensis*, *Thermococcus litoralis, Thermococcus onnurineus* and *Thermococcus paralvinellae*, via dark fermentation or CO gas fermentation [1].

Methane production

The only microorganisms capable of producing methane (CH_4) as part of their central metabolism are methanogenic archaea or methanogens [10]. Methanogens grow strictly anaerobic and their energy metabolism is mostly facilitated autotrophic, although for certain methanogens the degradation of organic as energy source was reported [1,10]. They can be classified into 3 groups based on their substrate usage: hydrogenotrophic (oxidize H_2, formate or simple alcohols and reduce CO_2), aceticlastic (consume acetate) and methylotrophic methanogens (use methylated compounds) for CH_4 generation. This unique metabolic capability has driven efforts to develop new waste treatment technologies for biogas production mainly with aceticlastic methanogens [19]. Additionally, when a voltage or molecular hydrogen (H_2) is applied, as an electron donor, to the hydrogenotrophic methanogen culture, these organisms can (bioelectrochemically) convert CO_2 into CH_4, offering a potential solution for demand-oriented and power storage of excess electrical energy [1,10]. Some of the main organisms studied are *Methanothermobacter marburgensis*, *Methanothermobacter thermoautotrophicus*, *Methanocaldococcus jannaschii* and *Methanococcus maripaludis* [1].

Polyhydroxyalkanoates (PHAs)

PHAs are natural biopolyesters composed of (R)-hydroxy fatty acid monomers (hydroxyalkanoates, HAs), which are linked by ester bonds [20,21]. They are produced by certain microorganisms functions as an energy and redox storage mechanism, typically occurring under nutrient-limited conditions in the presence of excess carbon [20], while also serving as a mechanism to cope with various stress conditions[22]. Their wide range of physical and chemical properties—including hydrophobicity, biodegradability, crystallinity, elasticity, and biocompatibility—make PHAs a promising substitute for conventional fossil-based plastics [20,23]. One of their most distinctive properties is its biodegradability, as PHAs can degrade into water and CO_2 after approximately seven months when buried in soil [23]. Studies suggested that they can be utilized in medicine for making artificial blood vessels or wound dressings. Additionally, they can be used in packaging, pharmacy, agriculture and food industry. Most of the archaeal studies are focused on haloarchaea. However, the cost of substrates remains a major challenge, as many microbial production systems rely on expensive carbon sources [1,10].

Chapter 1

Purification and characterization of the enzymes responsible for the PHA biosynthesis pathway of *Nitrososphaera viennensis*.

Contribution

My contribution to this chapter includes cloning, expression and purification of the responsible enzymes for PHA biosynthesis, the evaluation of quaternary structure for the PHA synthase, as well as the performance and analysis of the enzyme kinetics of one of the enzymes (PhaB).

Introduction

Nitrososphaera viennensis

Ammonia-oxidizing archaea (AOA) exhibit highly conserved evolutionary adaptations for energy and carbon metabolism. Their energy metabolism primarily relies on ammonia oxidation, catalyzed by an ammonia monooxygenase (AMO), while their carbon metabolism depends on an extremely efficient version of the 3-hydroxypropionate/4-hydroxybutyrate pathway (HP/HB) for CO_2 fixation [1]. One notable AOA species is *N. viennensis*, which belongs to the class *Nitrososphaeria* within the *Nitrososphaerota* phylum. *N. viennensis* has been extensively studied, and its proteome and metabolism have been thoroughly investigated, revealing its ability to synthetize the biopolymers polyhydroxyalkanoates (PHAs).

Polyhydroxyalkanoates (PHAs)

These polymers are composed of (R)-hydroxy fatty acid monomers – hydroxyalkanoates (HAs), to date, more than 150 different HAs have been reported as monomers for PHAs, influencing the physicochemical properties of the resulting polymer [2]. Based on the number of carbon atoms in their monomer units, PHAs are categorized into three distinct classes: short-chain-length PHAs (SCL-PHAs) consisting of 3 to 5 carbon atoms, medium-chain-length PHAs (MCL-PHAs) with 6 to 14 carbon atoms, and long-chain-length PHAs (LCL-PHAs) containing more than 14 carbon atoms. The former are characterized by their rigidity and hardness, similar to conventional plastics, with prominent examples including poly(3-hydroxybutyrate) (PHB) and poly(3-hydroxyvalerate) (PHV) [2–4]. Meanwhile, MCL-PHAs exhibit elastomeric and adhesive properties, such as poly(3-hydroxyoctanoate) (PHO) [2–4].

PHA biosynthesis

Although many microorganisms are able to synthesize PHAs, *Cupriavidus necator* (formerly known as *Ralstonia eutropha*), *Bacillus* sp., *Haloferax mediterranei, and Pseudomonas sp.* are among the most well-studied [2,5]. They have been identified of being capable of synthesizing a wide range of different PHAs from compounds related to several central metabolic pathways, including fatty acid and amino acid metabolism, the Krebs cycle, and the pentose phosphate pathway. Among these pathways, acetyl-CoA serves as a key precursor for the synthesis of SCL- and MCL-PHAs across the 14 identified biosynthetic pathways [4]. The three most common biosynthetic pathways for PHA synthesis are shown in Figure 1 and are briefly introduced here.

Pathway 1: This is the best representative pathway for PHA synthesis and allows for the sole synthesis of SCL-PHAs. The pathway begins with the condensation of two molecules of acetyl-CoA into acetoacetyl-CoA by the enzyme β-ketothiolase [2,4]. The product is then reduced to 3-hydroxybutyryl-CoA by the acetoacetyl-CoA reductase and subsequently polymerized by the PHA synthase via ester bond formation to produce poly(3HB) [2,4].

Pathway 2: Fatty acids from the β-oxidation pathway are converted into hydroxyalkanoate monomers by (R)-enoyl-CoA hydratase, acyl-CoA oxidase, and 3-ketoacyl-CoA reductase. These monomers, which can be MCL or LCL, are then polymerized by the PHA synthase [4].

Pathway 3: (R)-hydroxy acyl intermediates in the acyl-carrier protein (ACP) are converted into hydroxyalkanoate (CoA form) using simple carbon sources like glucose, sucrose, and lactose by the enzyme acyl-ACP-CoA transacetylase, before being condensed by the PHA synthase [4].

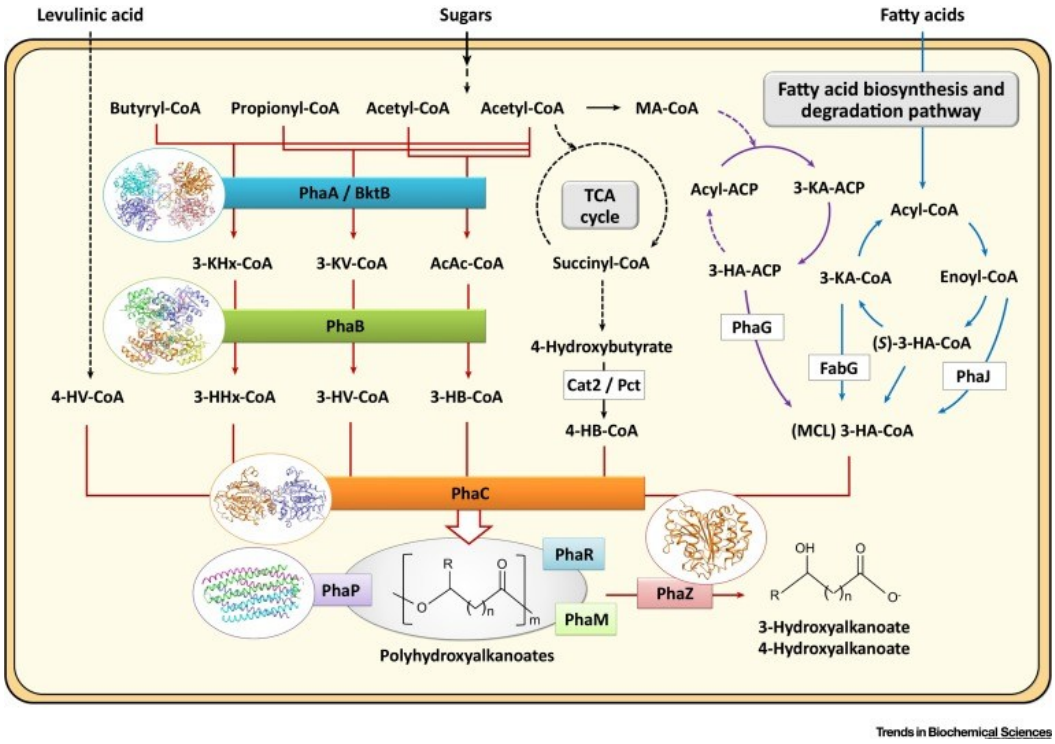

Figure 1: Overview of the most common pathways for polyhydroxyalkanoate (PHA) synthesis. "Key enzymes are shown in boxes, while metabolic pathways are indicated by arrows; dashed arrows represent sequences involving more than two enzymatic conversions. AcAc-CoA, acetoacetyl-CoA; 3-HA-ACP, 3-hydroxyacyl-ACP; 3-HA-CoA, 3-hydroxyacyl-CoA; 3-HB-CoA, 3-hydroxybutyryl-CoA; 4-HB-CoA, 4-hydroxybutyryl-CoA; 3-HHx-CoA, 3-hydroxyhexanoyl-CoA; 3-HV-CoA, 3-hydroxyvaleryl-CoA; 4-HV-CoA, 4-hydroxyvaleryl-CoA; 3-KA-ACP, 3-ketoacyl-ACP; 3-KA-CoA, 3-ketoacyl-CoA; 3-KHx-CoA, 3-ketohexanoyl-CoA; 3-KV-CoA, 3-ketovaleryl-CoA; MA-CoA, malonyl-CoA; TCA, tricarboxylic acid." [2]

Genes related to PHA synthesis in pathway 1

a. β-ketothiolase: PhaA

The protein PhaA, encoded by the *phaA* gene, is a β-ketothiolase responsible for the condensation of two acetyl-CoA molecules into acetoacetyl-CoA in a two-step catalytic process, a covalent catalysis step and condensation step. In the former, one molecule of acetyl-CoA enters the catalytic center of the enzyme and forms an acetyl-S-enzyme intermediate; in the subsequent condensation step, the second acetyl-CoA molecule is deprotonated and attacks the intermediate forming acetoacetyl-CoA [2].

Previous studies have identified different traits depending of the enzymes bacterial or archaeal origin. For the most studied bacteria for PHA production, *C. necator*, PhaA (CnPhaA) has determined a homotetrameric structure and a similar fold to other thiolases, recognizing three catalytic residues that function as covalent catalyst, second nucleophile and a general base respectively [2,5]. Additionally, another β-ketothiolase has been identified in *C. necator* (CnBktB) which can perform the same function (ketothiolase) for bigger substrates, resulting in different monomers [2]. On the other hand, in the haloarchaea *Haloferax mediterranei* two β-ketothiolases were identified, each one composed of two subunits, PhaAα and PhaAβ, involved in acetoacetyl-CoA generation and BktBα and BktBβ which are involved in acetoacetyl-CoA and 3-ketovaleryl-CoA generation [5].

b. Acetoacetyl-CoA reductase: PhaB

The second step in the synthesis is catalyzed by a reversible acetoacetyl-CoA reductase, known as PhaB and encoded by the *phaB* gene. This enzyme from the superfamily of short-chain dehydrogenase/reductase (SDR) reduces, stereospecificly acetoacetyl-CoA to (*R*)-3-hydroxybutyryl-CoA utilizing as coenzyme one molecule of NADH or NADPH, depending on the enzyme variant [5–7]. The crystal structure of the *C. necator* PhaB (*Cn*PhaB) reveals a homotetramer configuration with specificity to NADPH, alternatively PhaB from *Bacillus* sp. SG-1 can utilize NADH as reducing power [2,8]. On the other hand, two types of PhaB have been identified in archaea, a monomer present in *N. maritimus* [7] and a heterodimer (PhaB1/PhaB2) in *Haloferax mediterranei* [5].

c. PHA synthase: PhaC

The PHA synthase (PhaC) is the key enzyme responsible for the polymerization of the hydroxyalkanoate (HA) monomers. Its ability to incorporate SCL, MCL and/or LCL monomers into the polymer has garnered significant interest in industry-related research [9,10]. The PHA synthases are composed of different subunits, allowing them to catalyze different substrates polymerizations and are classified into different classes [9,10] (Table 1). In order to obtain a product similar to conventional plastics, an enzyme capable of producing a copolymer composed of both SCL- and MCL-monomers is required [10].

Table 1: Classes of PHA synthases (PhaC) and their properties

Class	Length of substrate [Carbon atoms]	Subunits	Predominant reported quaternary structure
Class I	3 - 5	PhaC	Dimer
Class II	6 - 14	PhaC	Dimer
Class III	3 - 5	PhaC / PhaE	Dimer
Class IV	3 - 5	PhaC / PhaR	Dimer

d. Other related genes

Additionally, other enzymes regulate PHA granule formation. For example, PHA granule-associated protein (PhaM) interacts with and activates PhaC in *C. necator*, while phasins (PhaP) determine the number, size, and distribution of granules in the cell. PHA depolymerase (PhaZ) and its regulatory enzyme (PhaR) are additionally critical for this process [2].

The PHA synthesized by *N. viennensis* follows putative this pathway depending in acetyl-CoA, catalyzed by the genes *phaAa1* and *phaAb1* encoding for the β-ketothiolase, *phaB* for acetoacetyl-CoA reductase and *phaC* and *phaE* for a PHA synthase class III [11].

Hypothesis and objectives

Hypothesis

The enzymes PhaAa1, PhaAb1, PhaB, PhaC and PhaE are responsible for the biosynthesis of polyhydroxyalkanoates (PHA) in *N. viennensis*, can be recombinantly expressed and purified in active form in *Escherichia coli*.

Objectives

- Recombinant expression of PhaAa1, PhaAb1, PhaB, PhaC and PhaE in *Escherichia coli* and subsequent purification in soluble form
- Characterization of the quaternary structure of the enzymes.
- Determination of kinetic parameters from the enzymatic activity including V_{max}, k_{cat} and K_m, and comparison of reported values from ortholog enzymes.

Materials and Methods

Media, strains and cultivation

The bacterial strain *Escherichia coli* DH5α was used for plasmid propagation and the strain *Escherichia coli* BL21(DE3) for protein expression. Strains were cultured in Luria Broth (LB) media with kanamycin (50 mg L^{-1}), according to the antibiotic resistant in transformed plasmid, in Erlenmeyer flasks at 37 °C and 120 rpm in an incubator (Labwit ZWYR-2102C, Lab Xperts Laboratory Solutions Austria, Klosterneuburg, Austria).

Cultures for protein expression were cultivated with the DASGIP® Bioblock (76DGTBLOCK) system with 2.2 L (working volume of 1.5 L) Bioblock stirrer reactors (Eppendorf AG, Hamburg, Germany). The temperature was set to 37 °C with a steady airflow of 0.06 vvm (gas flow per unit culture volume per min). Stirring was increasing by 100 rpm each h, starting at 300 rpm until 700 rpm is reached. The OD_{600} was measured every h. After 3 h, protein expression was inducted by adding IPTG with a final concentration 1 mmol L^{-1} and cultured for additional 4 h. The culture was then harvested at 5,000 g for 30 min (Sorvall LYNX 4,000 Superspeed Centrifuge, Thermo Fisher Scientific, Austria), subsequent weighted and flash frozen with liquid nitrogen before storage at -70 °C.

Plasmids construction and transformation

The 5 genes coding for the proteins responsible for the PHA biosynthesis pathway in *N. viennensis* (*phaAa1*, *phaAb1*, *phaB*, *phaC*, *phaE*) were previously isolated from the genome in a pET-15b plasmid backbone and cloned individually, with the exception of *phaAa1* and *phaAb1* which was cloned in a singular expression cassette. The genes were amplified from the genome and from the previous isolated vectors utilizing the primers from Table 2 and inserted into a pET-15b plasmid backbone containing a His-Tag and a SUMO (Small Ubiquitin-like Modifier) cleavage site, positioned upstream (N-terminal) of the desired gene, to improve solubility [12] and facilitate removal of the purification tag, along with a kanamycin resistance gene, and was assembled via Gibson Assembly (E5510S, Gibson Assembly® Cloning Kit, New England Biolabs). Primers were designed using SnapGene software (GSL Biotech, Chicago, IL, USA) and can be found in Table 2. The BL21(DE3) cells were transformed with the plasmids following the 5-min transformation protocol from New England Biolabs. The recombinant strains were screened via colony PCR amplifying the inserts between the T7 promoter and T7 terminator and sequencing of the construct (Table 2). The PCR products were visualized in a 1% Agarose TAE gel with SYBR™ Safe DNA Gel Stain.

Table 2: Primers used for constructing the plasmid with Gibson Assembly and for PCR amplification.

phaAa1 + *phaAb1*	FW	5'- CGAACAGATTGGTGGCATGACCAACAAGGTTTG -3'
	RV	5'- GTTAGCAGCCGGATCTTTACGCCTTCTCAAG -3'
phaB	FW	5'- CGAACAGATTGGTGGCATGTCCGTCTCAATAAAC -3'
	RV	5'- TTAGCAGCCGGATCTCTAGGCCCGATAGCT -3'
phaC	FW	5'- CGAACAGATTGGTGGCATGACACAGCAAGAAAC -3'
	RV	5'- GTTAGCAGCCGGATCTCTATTGGGACCTTGC -3'
phaE	FW	5'- GAACAGATTGGTGGCATGACGACTGATGAC -3'
	RV	5'- CTTTGTTAGCAGCCGGATCTTCATTGTTTTTCTAGG -3'
T7	FW	5'- TAATACGACTCACTATAGG -3'
	RV	5'- CTAGCATAACCCCTTGGGGCCTCTAAACGGGTCTTGAGGGGTTTTTTG -3'

Expression assay

To evaluate the synthesis of PhaAa1 and PhaAb1, an expression assay was conducted under various conditions. The strain was cultivated in LB medium at 120 rpm, followed by induction with 1 mmol L^{-1} IPTG after 3 h of growth, and compared to cultivation in 2-YT autoinduction medium. Additionally, the impacts of culturing at room temperature (22 °C) versus 37 °C were assessed. The OD was measured and an aliquot of 1 mL was collected and centrifuged at 16,000 g for 5 min (Eppendorf 5415R Refrigerated Centrifuge, Eppendorf AG, Hamburg, Germany). The supernatant was discarded and the pellet is resuspended in loading dye (LD) with 100 µL of LD per an OD_{600} of one. The samples were cooked for 5 min at 96 °C with 1,050 rpm in a Thermomixer comfortable (Eppendorf AG, Hamburg, Germany), transferred to ice for 5 min and finally centrifuged at 4 °C at 16,000 g for 30 min. The supernatant was then collected and loaded in a 10% SDS-PAGE gel and stained with InstantBlue® Coomasie Protein Stain for visualizing the protein bands.

Protein purification

The molecular weights and pI's of the proteins were calculated using ProtParam from Expasy bioinformatics resource portal (Swiss Institute of Bioinformatics, Lausanne, Switzerland). The proteins PhaB and PhaC were purified from their corresponding pellet with the following protocol. The pellet was resuspended in 15 mL of Lysis Buffer containing 50 mmol L^{-1} Tris/HCl, 500 mmol L^{-1} NaCl, 20 mmol L^{-1} imidazole and 10% glycerol with an adjusted pH of 7.5 at 4 °C. Additionally, 50 µL of protease inhibitor per gram of cell pellet, 2 µL of benzonase per mL of buffer and 0.3 mg of lysozyme per mL of buffer was additionally added and subsequent incubated for 15 min on ice. As, PhaC contains cysteine and is therefore prone to form disulfide bonds, DTT was added to a final concentration of 1 mmol L^{-1} to all buffers just before use. Afterwards the resuspended cell suspension was sonicated with a sonic dismembrator (Fisherbrand™ Model 705, Waltham, Massachusetts, USA) for 10 cycles of 10 s with 50% Amplitude and 1 min cooling in between each sonication cycle. The lysate was centrifuged at 45,000 g for 30 min at 4 °C (Sorvall LYNX 4,000, Lab Xperts Laboratory Solutions Austria, Klosterneuburg, Austria). The supernatant was subsequent loaded on a His Trap FF 5 mL column with an ÄKTA Pure™ (Cytiva, Marlborough, Massachusetts, USA) chromatography system purifying the proteins through immobilized metal affinity chromatography (IMAC). 20 column volumes (CV) of IMAC-A buffer (20 mmol L^{-1} Tris/HCl, 500 mmol L^{-1} NaCl, 20 mmol L^{-1} imidazole and 10% glycerol with a pH 7.5 at 4 °C, all buffers were filtered and degassed) were used for washing and 10 CV of

IMAC-B buffer (identical recipe as IMAC-A with elevated imidazole concentration of 500 mmol L^{-1}) for elution. The eluted fractions and the lysate were screened in a 10% SDS-PAGE gel stained with InstantBlue®. Fractions containing the corresponding protein were retrieved. The pooled fractions were incubated overnight at 4 °C in a SnakeSkin™ dialysis membrane (Thermo Scientific™, Waltham, MA, USA) with 17.5 mg of ULP1 protease per mL of solution in order to remove the His-Tag and the SUMO cleavage site, and additionally dialysis with a 1:100 ratio in SEC (size exclusion chromatography) buffer (similar to IMAC-A, but with 20 mmol L^{-1} Tris/HCl and without imidazole). The dialyzed solution was collected and screened in a 10% SDS-PAGE gel stained with InstantBlue®, if the protein was not cleaved in the overnight incubation, another overnight incubation with ULP1 was done at room temperature (22 °C). The cleaved protein was then purified by a reverse immobilized metal affinity chromatography (R-IMAC) from the dialyzed solution employing the same IMAC protocol. As in the previous steps, the flowthrough fractions were screened in a 10% SDS-PAGE gel stained with InstantBlue® and the protein solution was concentrated in a 10 kDa centrifugal concentrator Vivaspin® 20 (VS2002 Sartorius Stedlm Lam Ltd, Göttingen, Germany) to approximately 5 mL. Finally, the concentrated protein was loaded in the ÄKTA for a SEC with a Cytiva HiLoad™ 16/600 Superdex™ 200 pg column (Cytiva, Marlborough, Massachusetts, USA) using SEC buffer. The fractions were pooled according to purity and the protein concentration measured with Qubit 2.0 Fluorometer (Thermo Fisher Scientific, Waltham, MA, USA). The protein solution was aliquoted and flash frozen with liquid nitrogen for their storage at -70 °C.

Similarly to the purification of the other proteins, PhaE was purified in a bench top batch chromatography utilizing the same IMAC-A, IMAC-B, SEC buffers and a 5 mL HisPur™ Ni-NTA Resin (ThermoScientific™, Waltham, MA, USA) packed column at 4 °C. It was subsequently purified via SEC, following the same procedure as the other proteins. In parallel a mix of PhaC and PhaE was prepared to investigate the stability and co-purification of the possible protein complex following the same protocol as for PhaE.

Mass Photometry

To determine the complex formation of the PHA synthase (PhaC and PhaE) a mass photometry assay was performed following the protocol described by Wu and Piszczek 2021 [13] using the Two^{MP} mass photometer (Refeyn Ltd., Oxford, UK). The individual purified proteins and the buffers (50 and 200 mmol L^{-1} NaCl, 100 mmol L^{-1} Tris/HCl, pH 7.5 at room temperature) were filtered with a 0.22 µm VWR® syringe filter (VWR International Ltd., Poole, UK.). The mass photometry was performed for each protein individually, diluted with buffer containing 200 mmol L^{-1} NaCl and 100 mmol L^{-1} Tris/HCl buffer. The two proteins were mixed and diluted with 50 mmol L^{-1} NaCl and 100 mmol L^{-1} Tris/HCl, incubated for 5 min at room temperature and subsequently measured at different concentrations: 10 nmol L^{-1} for the single proteins, and 10, 20 and 100 nmol L^{-1} for the PhaC and PhaE mix.

Michaelis-Menten kinetic model

The kinetic parameters were determined following the Michaelis-Menten model. This model suggests, at steady state, the rate of an enzymatic reaction is a function of the substrate concentration. It assumes that the substrate concentration is higher than the enzyme concentration, and that the enzyme interacts with only one substrate [14]. Mechanistically, it involves the formation of an enzyme-substrate complex, its conversion to product, and the subsequent release as represented by the following equation:

$$v = \frac{V_{max} \cdot [S]}{K_m + [S]}$$

Here, v represents the enzyme reaction rate, $[S]$ the substrate concentration, V_{max} the maximum catalytic capacity for a given amount of enzyme and K_m the dissociation constant of the enzyme-substrate complex, which corresponds to the substrate concentration at which the reaction rate reaches half of V_{max}.

Enzymatic activity and kinetic assay

An aliquot of PhaB was thawed on ice, diluted 1:16 in a buffer containing 100 mmol L^{-1} Tris/HCl 50 mmol L^{-1} NaCl pH 7.5 and centrifuged for 15 min at 4 °C at 16,000 g (Eppendorf 5415R Refrigerated Centrifuge, AG, Hamburg, Germany). The protein concentration was determined with Bradford reagent [15] utilizing bovine serum albumin (BSA) as a protein standard. The enzymatic activity was monitored by measuring oxidation of NADH to NAD at 340 nm absorbance using the Spark® Multimode Microplate Reader (Tecan Group Ltd, Männedorf, Switzerland), according to following reaction:

$$NADH + Acetoacetyl - CoA \leftrightarrow NAD^{++(R)-Hydroxybutyryl-CoA}$$

The experiment was conducted in a Greiner Bio-One UV-STAR® 96-well microplate utilizing the same buffer as described above and a total volume of 150 µL per well. The concentrations of the enzyme and NADH were kept constant at 25 nmol L^{-1} and 0.5 mmol L^{-1}, respectively, while the concentration of acetoacetyl-CoA (AcAc-CoA) varied between 0 and 0.2 mmol L^{-1}. The Michaelis-Menten kinetic parameters were determined with Microsoft Excel (Microsoft, Redmond, WA, USA) and with GraphPad Prism 10 (GraphPad Software, San Diego, CA, USA).

Results

Gene cloning

The *N. viennensis* genes (*phaAa1+phaAb1*, *phaB*, *phaC* and *phaE*) were only successfully amplified from the plasmid pET-15b already containing the respective genes. Amplification was not successful when initial PCR was performed with the genome as template. Genes were subsequently cloned into the new pET vectors using Gibson Assembly, as shown in Figure 3. The estimated molecular weights and isoelectric points (pI) reveal that the His-Tag and the SUMO cleavage site adds 12 kDa to the protein's molecular weight (Table 3). The transformation of DH5α cells resulted in different numbers of transformant colonies (two containing PhaAa1-PhaAb1, four for PhaB, four for PhaC and one for PhaE). A colony PCR confirmed the plasmid in all colonies, except for PhaC-C1 as can be seen Figure 4. The vectors amplified in DH5α were subsequent used to successfully transform BL21(DE3) cells (Figure 5).

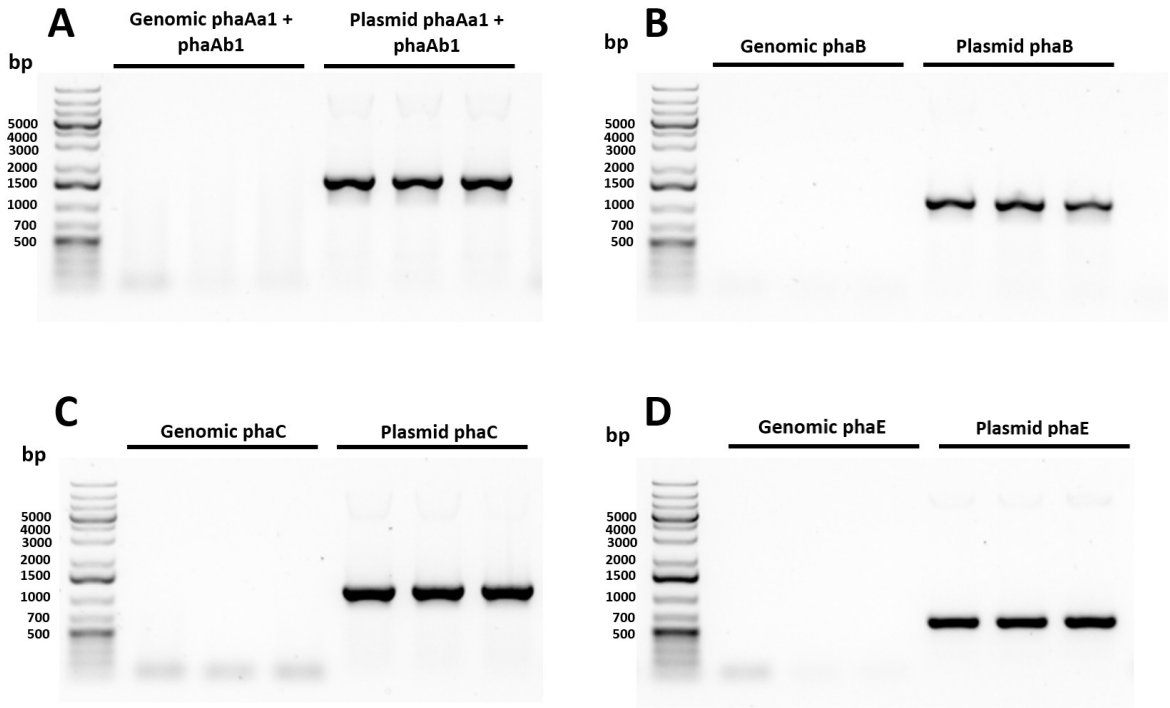

Figure 2: 1% Agarose TAE gel electrophoresis for the PCR amplification from genomic and plasmid DNA (triplicates). A: *phaAa1* and *phaAb1* genes, B: *phaB*, C: *phaC* gene and D: *phaE* gene. The PCR only amplified the genes contained in the plasmids.

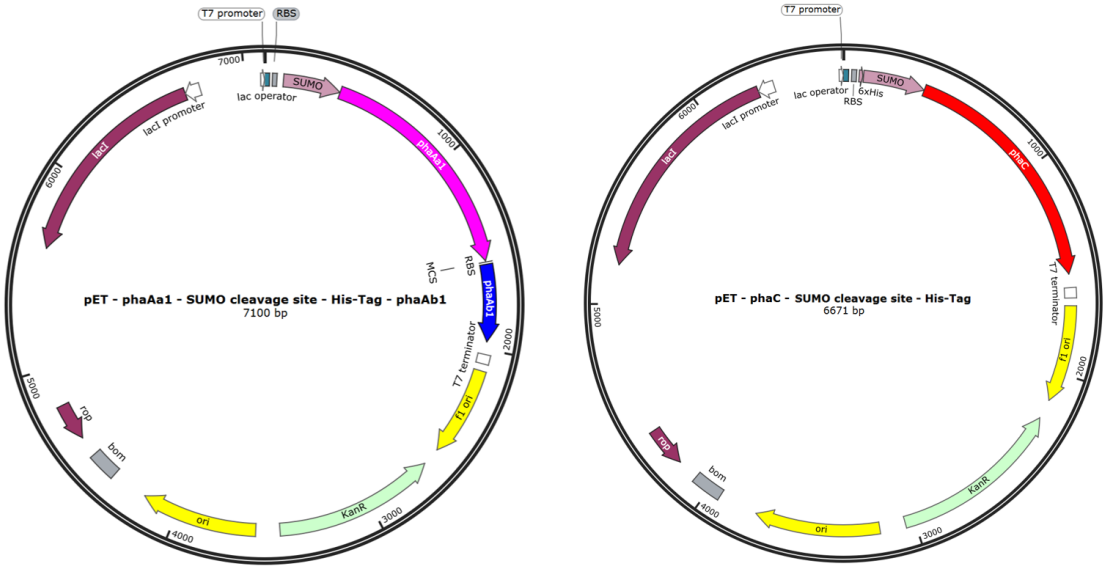

Figure 3: Examples of the plasmid construction containing the desired protein, SUMO cleavage sites and His-Tag. The images correspond to the vectors coding for PhaAa1 + PhaAb1 and PhaC visualized in SnapGene, respectively.

Table 3: Predicted molecular weights and pI's for the cloned enzymes using ProtParam.

	Protein		Protein with His-Tag and SUMO cleavage site	
	MW [kDa]	pI	MW [kDa]	pI
phaAa1	40.7	6.46	52.7	6.14
phaAb1	14	7.71		
phaAa1 + phaAb1	54.76	6.79	55.58	6.95
phaB	42.7	8.13	54.7	6.44
phaC	43.1	6.02	55.1	5.89
phaE	21.3	6.17	33.2	5.85

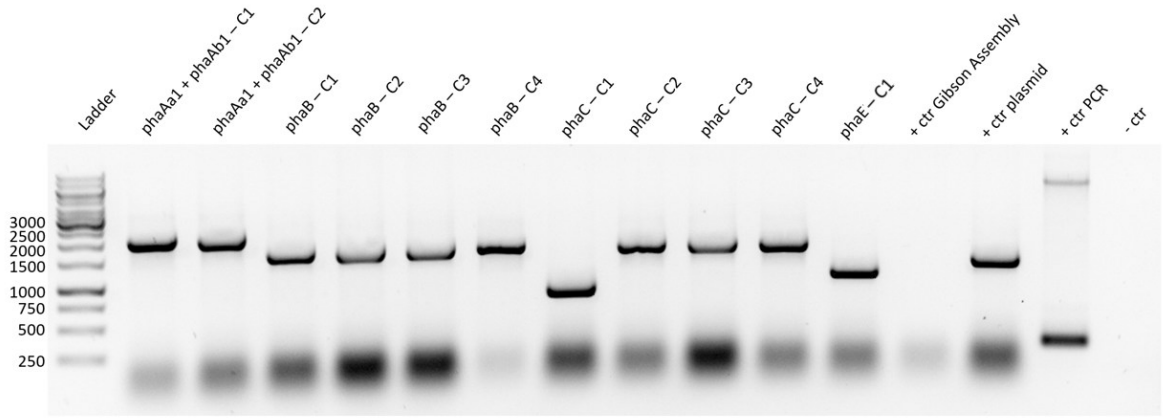

Figure 4: 1% Agarose TAE gel electrophoresis of colony PCR products using T7 primers from DH5α transformant cells obtained through Gibson Assembly. All the colonies seem to have the correct insertion, except *phaC*-C1 that differs from the expected value.

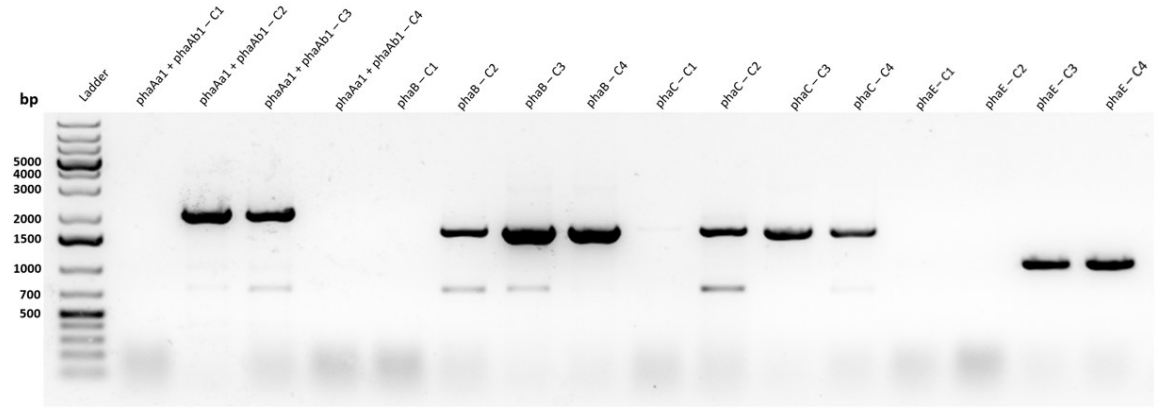

Figure 5: 1% Agarose TAE gel electrophoresis of colony PCR products from BL21(DE3) transformant cells. Four colonies per desired transformation were screened with the T7 primer pair. And the inserts could be found in 2 *phaAa1* + *phaAb1*, 3 in *phaB*, 3 in *phaC*, and 2 in *phaE* colonies.

Protein expression and expression assay

The transformed *E. coli* BL21(DE3) with plasmids containing the genes *phaB*, *phaC* and *phaE* were cultivated in 1.5 L bioreactors for protein expression. The growth curves (Figure 6) depicts an exponential growth regardless of the IPTG induction and protein expression, indicating no apparent toxic effects from the overexpression of the protein of interest (POI).

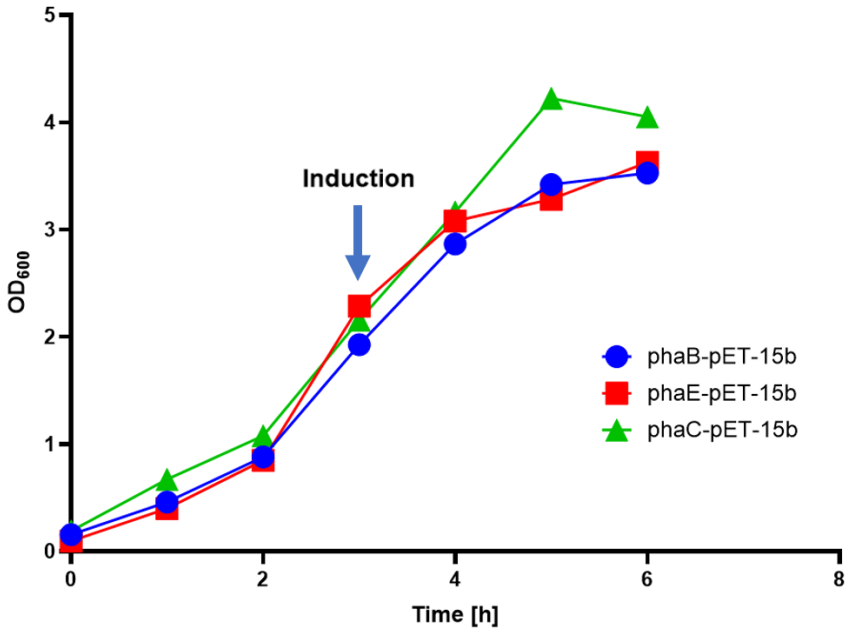

Figure 6: Growth curve of *E. coli* Bl-21(DE3) strains expressing PhaB-SUMO-His, PhaC-SUMO-His, and PhaE-SUMO-His in bioreactors with IPTG induction after 3 h. The three strains maintained an exponential growth independently of the IPTG induction.

Expression levels of PhaAa1 and PhaAb1 were significantly lower compared to PhaB and the corresponding protein bands mostly undetectable on the SDS-Gel under all tested cultivation conditions (Figure 7). However, in the transformed *E. coil* growing with auto-inducible 2YT medium at 37 °C, the protein band indicating PhaAb1 protein was present after 6 h of induction. Likewise, a band appeared at the expected position of PhaAa1 after 3 h of IPTG induction in LB medium at 37 °C, however, both bands were not observed simultaneously.

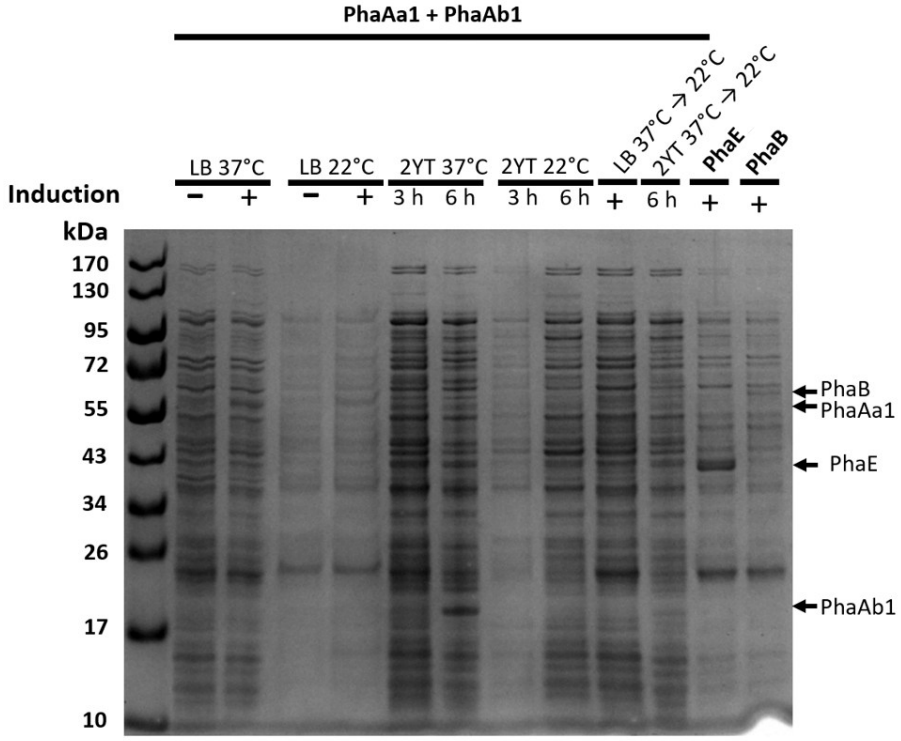

Figure 7: 10% SDS-PAGE gel with the expression assay under different conditions, media (LB and autoinducible 2YT) and temperature (22 °C and 37 °C), for proteins PhaAa1 and PhaAb1, as well as screening of PhaB and PhaE expression from bioreactors samples. Distinct bands corresponding to PhaB and PhaE were clearly visible, while only faint separate bands were observed for PhaAa1 and PhaAb1 in LB 37 °C after induction and 2YT media at 37 °C, respectively.

Purification of the enzymes

The proteins PhaB, PhaC, and PhaE were successfully purified from the bioreactor cultures using various chromatography techniques (IMAC, R-IMAC, and SEC). The obtained results are represented below.

PhaB

The overexpression of PhaB-SUMO-His Tag was clearly distinguishable in the supernatant after the lysis, showing a band near the 55 kDa ladder band (Figure 8), higher than the expected 54.7 kDa. No POI was observed in the fractions corresponding to the flowthrough and wash, with all the enzyme recovered in the elution fractions between 42 and 56 (Figure 8).

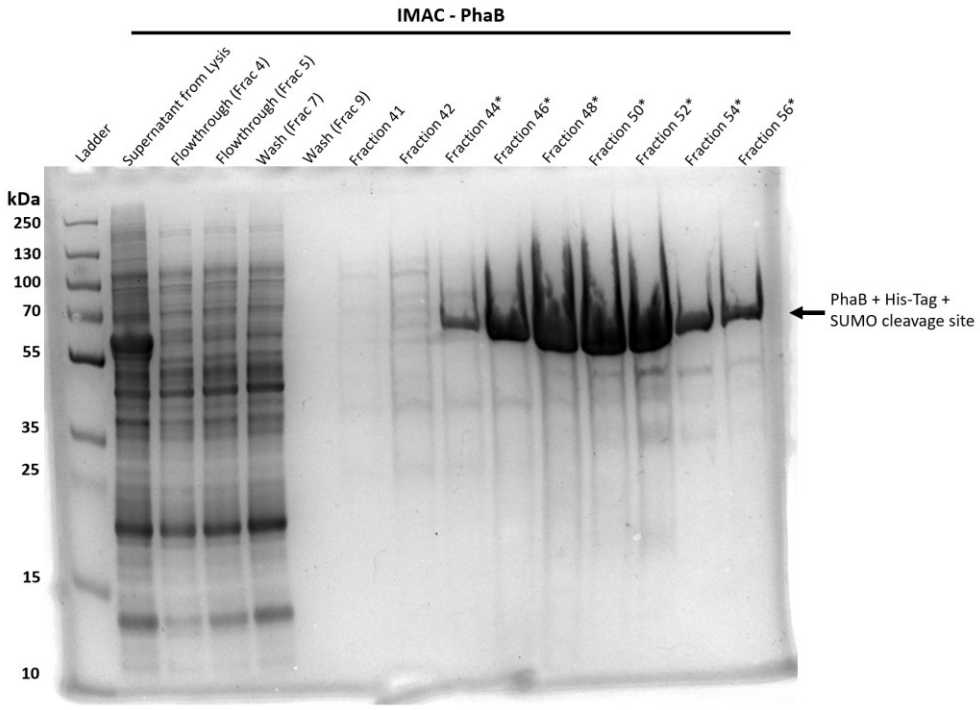

Figure 8: 10% SDS-PAGE gel of the PhaB-SUMO-His Tag purification of by IMAC, the protein could be found between the fractions 44 and 56, nevertheless only the fractions with * were pooled for further purification. The protein bands were located between 55 and 70 kDa, which is higher than expected.

Following the overnight dialysis, all protein was successfully cleaved and two distinctive protein bands appeared on the gel (Figure 9). One band represents PhaB, at approximately 42 kDa while the other band is composed of the His-Tag together with the SUMO cleavage site (~15 kDa). As the majority of the enzyme was cleaved, a clear separation during the R-IMAC purification was achieved. PhaB was found in the flowthrough, while the uncleaved protein and the His-Tag together with SUMO cleavage site was recovered in the elution fractions. The flowthrough was concentrated and subsequent loaded on SEC, archiving protein fraction with high purity. However, some smaller impurities were still present (Figure 10). Elution fractions 37 to 43 were pooled and the concentration measured with a final concentration of 1.575 mg mL^{-1}.

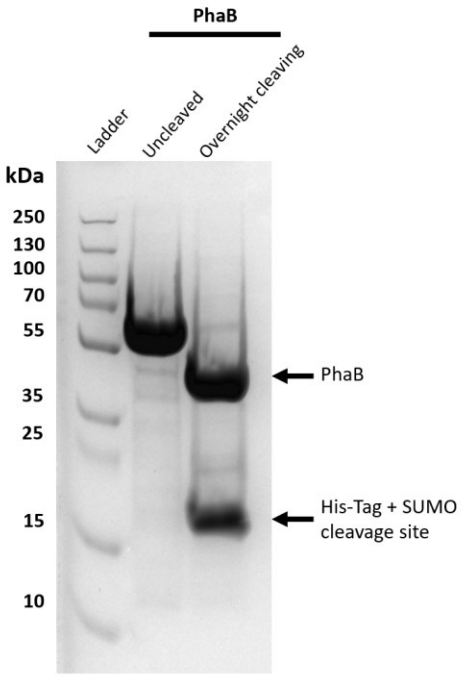

Figure 9: 10% SDS-PAGE gel of the overnight cleavage of PhaB-SUMO-His Tag by ULP1 protease. Two fractions were recognizable, cleaved PhaB (43 kDa) and His-Tag +SUMO cleavage site (15 kDa).

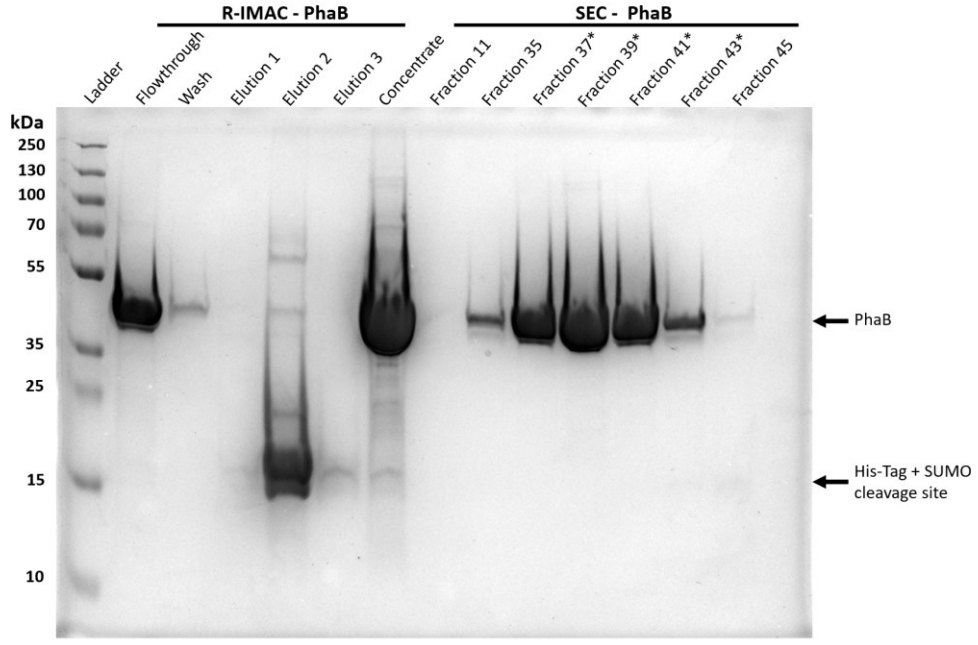

Figure 10: 10% SDS-PAGE gel of the PhaB purification by R-IMAC (first 6 samples), concentrate and subsequently SEC (last 7 samples). The protein bands were located between 35 and 55 kDa for PhaB (Flowthrough) and 15 kDa for His-Tag and SUMO cleavage site. The fractions with * correspond to the pooled fractions.

PhaC and PhaE

As depicted in the SDS-PAGE gels from the Figure 11 and Figure 12, distinguishable protein bands were observed for the pure fractions in the supernatant from the lysis, with PhaC-SUMO-His Tag located between 55 and 70 kDa (expected molecular weight 55.1 kDa) and PhaE-SUMO-His Tag between 35 and 55 kDa (expected molecular weight 33.2 kDa). Interestingly, co-purified PhaC and PhaE mixture showed with similar results when performed individually.

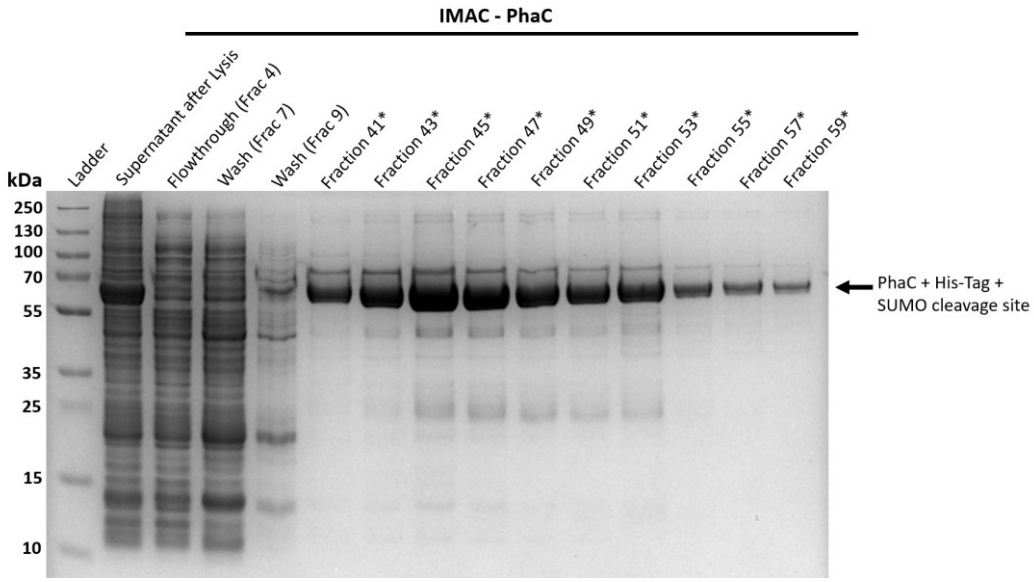

Figure 11: 10% SDS-PAGE gel of the PhaC-SUMO-His Tag purification by IMAC. The enzyme could be found from fraction 41 to 59, here the protein band was located between the bands of 55 kDa and 70 kDa. The fractions with * correspond to the pooled fractions.

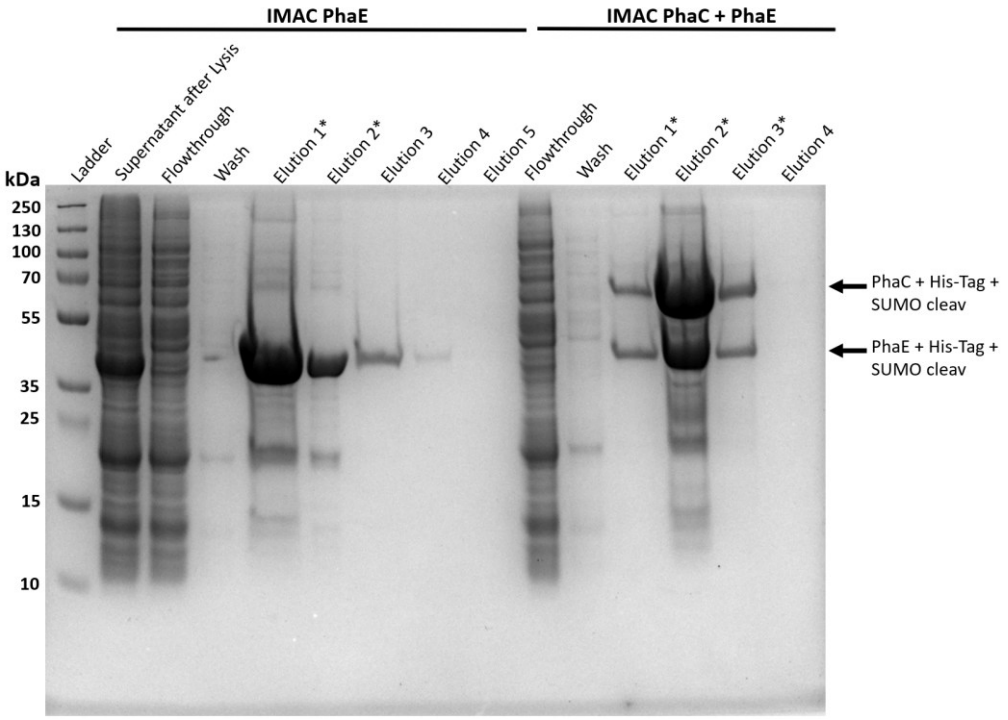

Figure 12: 10% SDS-PAGE gel of the PhaE-SUMO-His Tag and the mix of PhaC-SUMO-His Tag and PhaE-SUMO-His Tag purification by IMAC. It was possible to recognize the bands corresponding to the subunits of the PHA synthase in the elution fractions. The fractions with * correspond to the pooled fractions.

After the overnight incubation of the proteins with the protease ULP1, only PhaC-SUMO-His Tag and the mix showed a significant amount of cleaved protein (Figure 13). Therefore, PhaE-SUMO-His Tag was incubated again overnight at room temperature yielding better results as shown in the last wells of the SDS-PAGE gel from Figure 15.

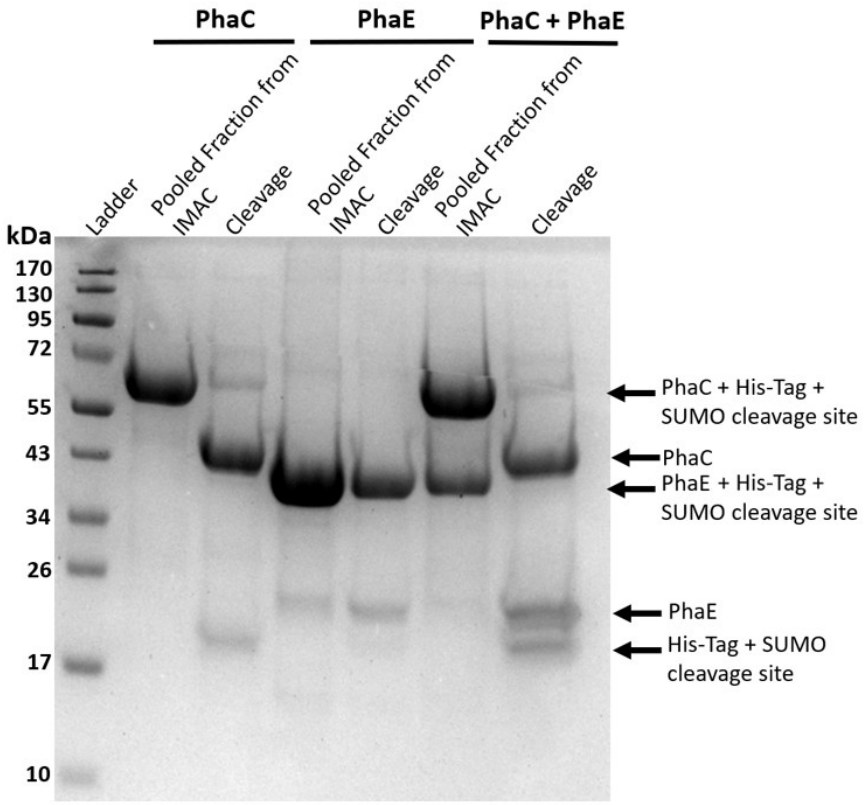

Figure 13: 10% SDS-PAGE gel of the overnight protein cleavage of PhaC-SUMO-His Tag, PhaE-SUMO-His Tag and the mix of both by ULP1 protease. In the cleaved fraction, results varied: nearly all of PhaC-SUMO-His Tag and the mix of enzymes were cleaved, while PhaE-SUMO-His Tag showed no cleavage.

The flowthrough of the R-IMAC contained PhaC and PhaE in each individual case. The protein bands in the SDS-PAGE gels from the flowthrough were located where expected according to the calculated molecular weight (Figure 14, Figure 15 and Figure 16). These fractions were then successfully purified using SEC. Notably, the fractions containing PhaE correspond to those with higher molecular weights than the fractions containing PhaC (Figure 17 and Figure 19), and in the mixture PhaC and PhaE were co-purified in the same fractions (26 - 30) suggesting a possible complex formation in both cases (Figure 18). The final concentration was 0.5 mg mL^{-1} and 0.303 mg mL^{-1} for pure PhaC and PhaE, respectively.

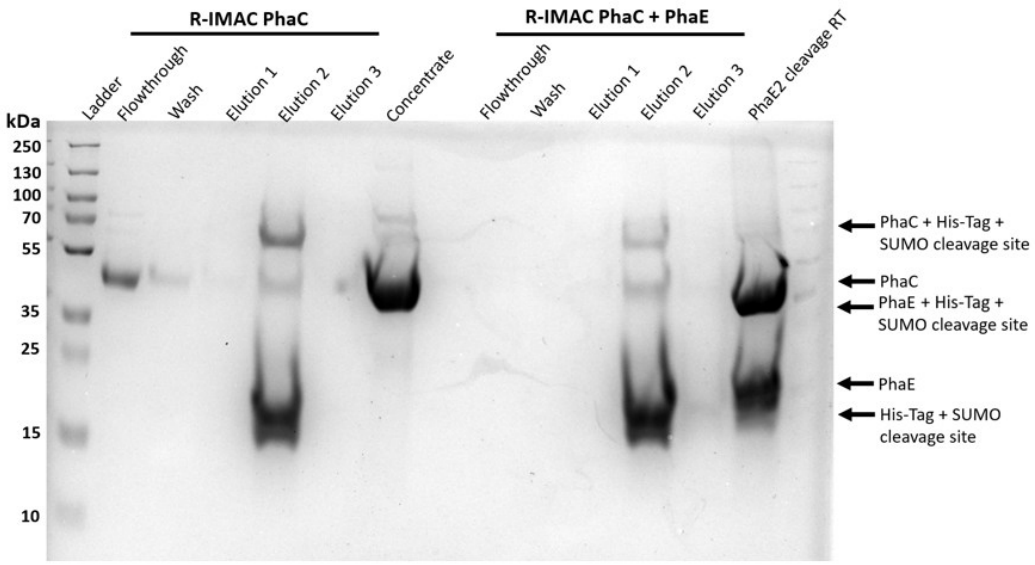

Figure 14: 10% SDS-PAGE gel of the PhaC purification by R-IMAC (first 5 samples), PhaC concentrate, fractions from the R-IMAC of PhaC and PhaE mixture and PhaE cleavage incubation (4 h) with ULP1 at room temperature (RT). The cleaved enzymes were recovered in the flowthrough of the R-IMAC (for the mix the bands were too faint). PhaE was cleaved in a larger fraction compared to the incubation at 4 °C.

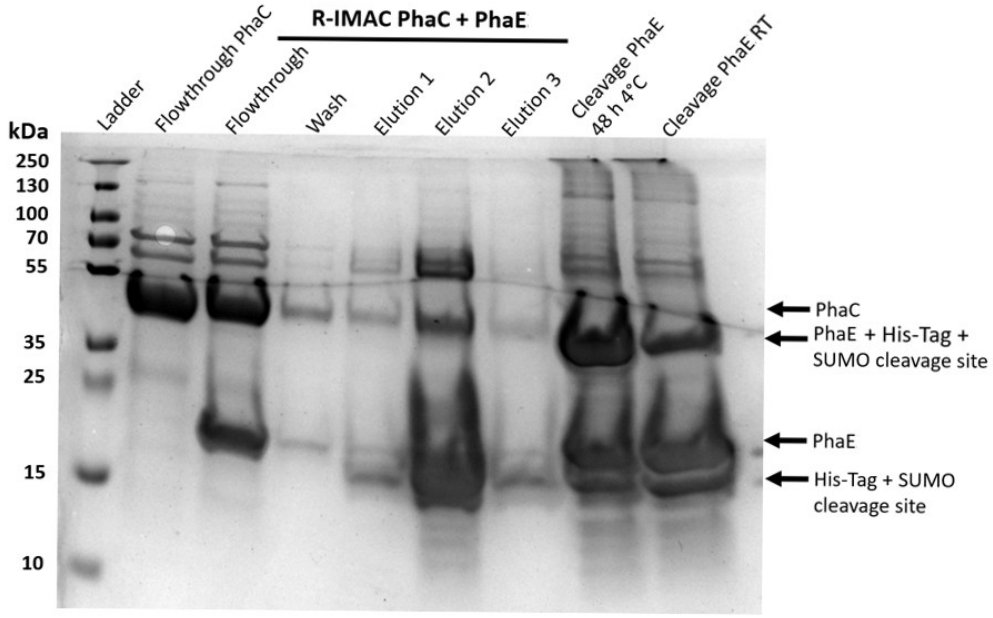

Figure 15: 10% SDS-PAGE gel of R-IMAC flowthrough fractions for PhaC (first sample), the R-IMAC of PhaC and PhaE mixture (next 5 samples), and PhaE cleavage under different conditions: 48 h at 4 °C and overnight at room temperature (RT). Both proteins were identified in the flowthrough from R-IMAC, with some minor contamination visible as thin bands over PhaC. Cleavage fractions showed greater efficiency at RT compared to 4 °C.

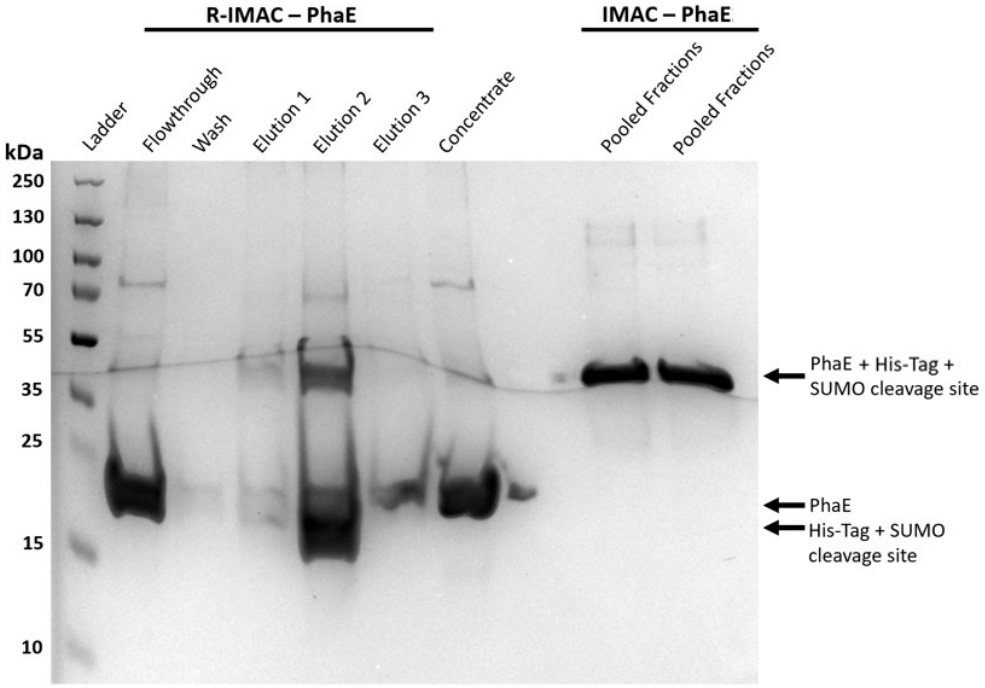

Figure 16: 10% SDS-PAGE gel of R-IMAC fractions for PhaE. Due to the similar size of PhaE (21 kDa) and SUMO-His Tag (12 kDa, but found over 15 kDa), the bands position overlapped. But it could be assumed that PhaE was isolated from the SUMO-His Tag.

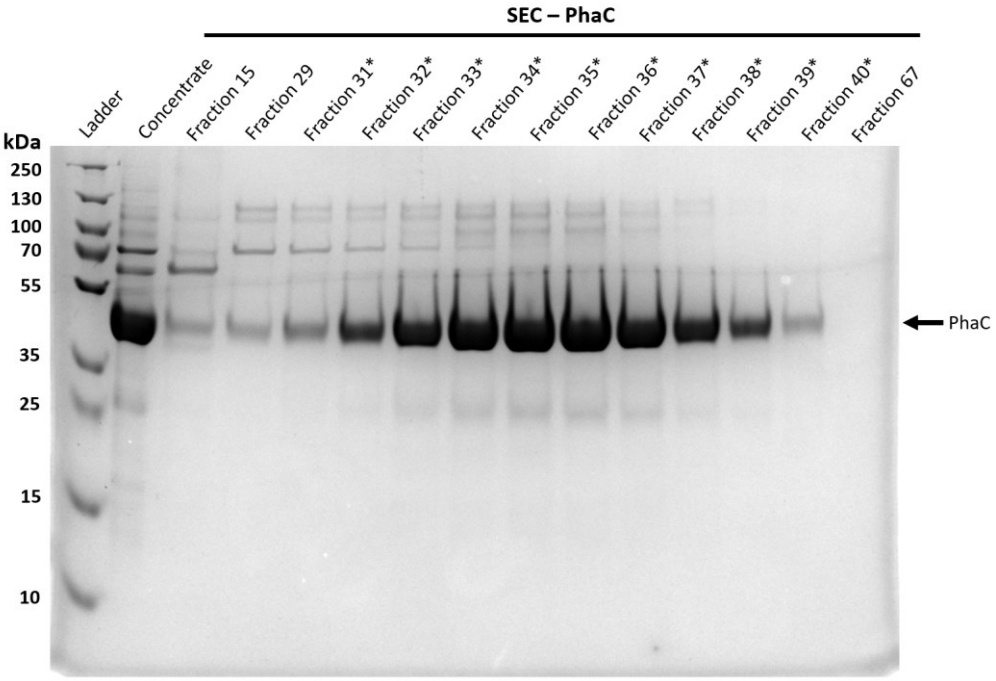

Figure 17: 10% SDS-PAGE gel with the fractions of PhaC from SEC, the enzyme was concentrated mainly between fraction 31 and 39. Some minor contamination was visible as thin bands over PhaC. The fractions with * correspond to the pooled fractions.

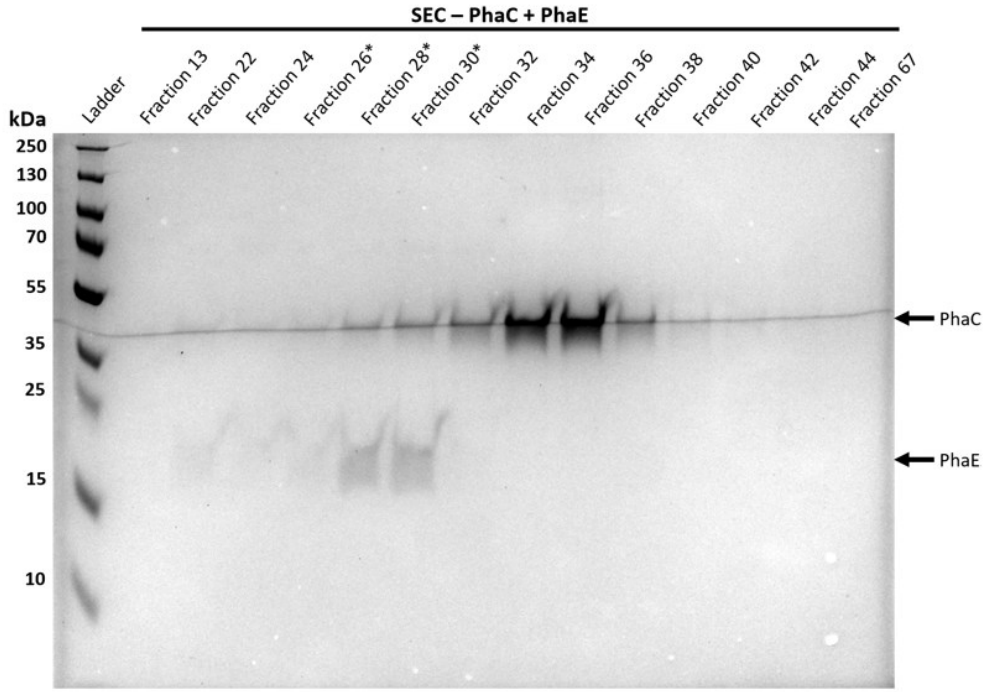

Figure 18: 10% SDS-PAGE gel with the fractions of PhaC and PhaE from SEC. Both proteins are detected between the fractions 22 to 30, and only PhaC between 32 and 38. The fractions with * correspond to the pooled fractions.

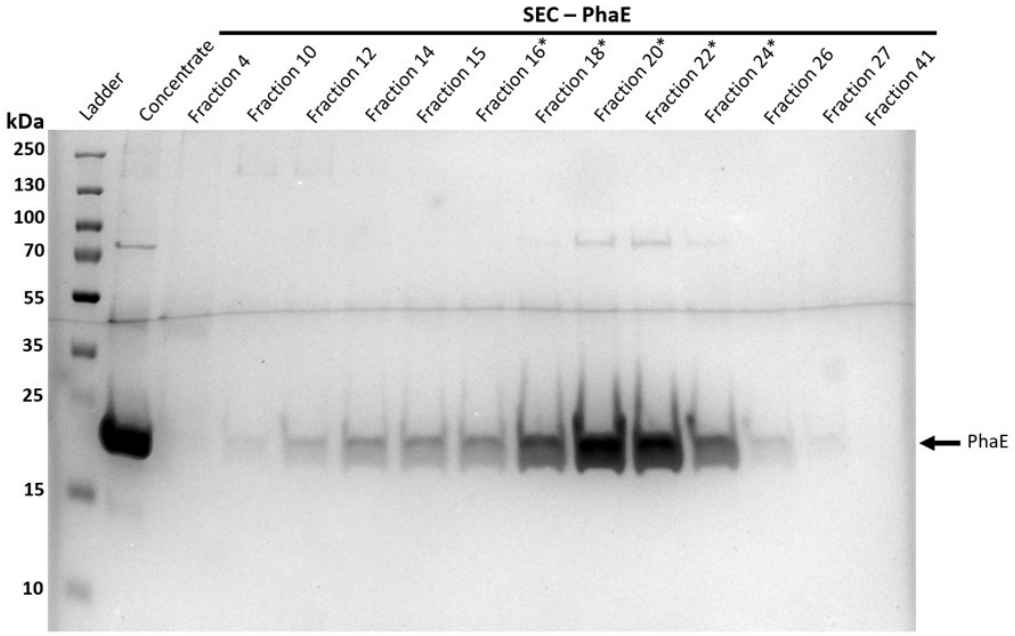

Figure 19: 10% SDS-PAGE gel with the fractions of PhaE from SEC. PhaE could be found from fractions 12 to 26, but only the fractions with * correspond to the pooled.

Mass photometry

Following the results from the SEC purification of the PhaE and PhaC protein mix, which indicated a possible complex formation, mass photometry was conducted to confirm the previous findings. When the proteins were measured individually (Figure 20), PhaE exhibited a possible trimerization (69 kDa – expected value for individual protein of 21.3 kDa) while PhaC was present as monomer. (49 kDa – expected value for individual protein of 43.1 kDa). Analyzes of the assembled complex revealed three distinctive peaks. Two peaks possible represent the PhaC monomer (~45 kDa) and the PhaE trimer (~65 kDa). A new peak at around 111 kDa might depict and a PhaCE complex, with a composition of one subunit of PhaC and three subunits of PhaE (Figure 21).

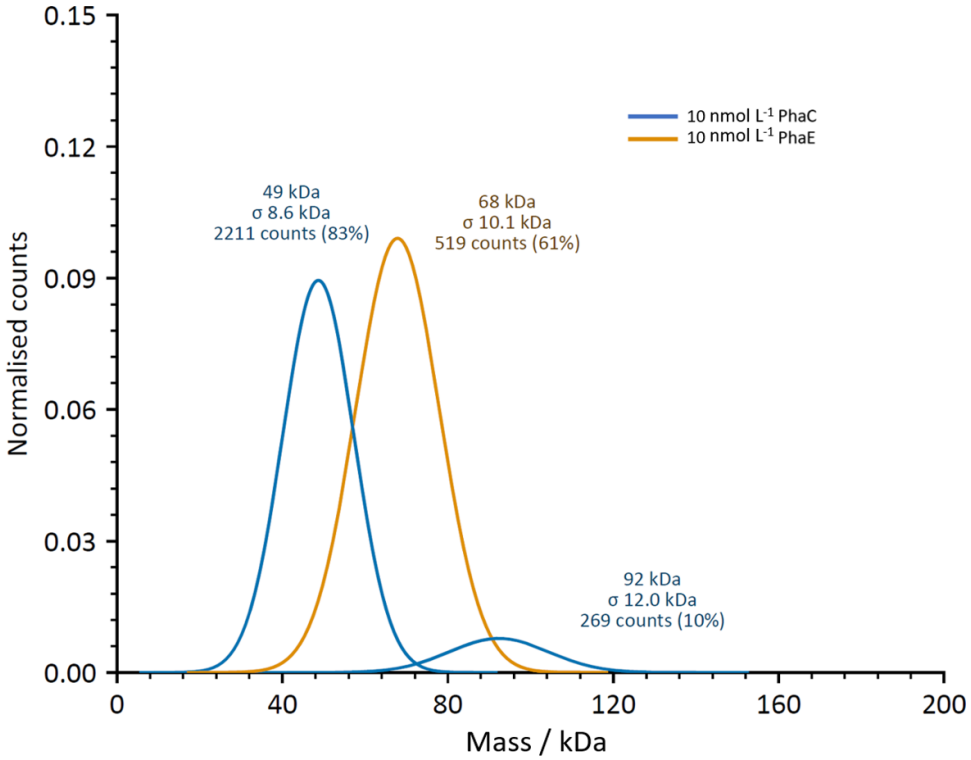

Figure 20: Mass photometry analysis of individual PhaC and PhaE (10 nmol L^{-1}), diluted in 50 mmol L^{-1} Tris/HCl 200 mmol L^{-1} NaCl. The most significant peaks matched molecular weights of 49 kDa, possible monomer of PhaC, and 92 kDa, possible trimer of PhaE.

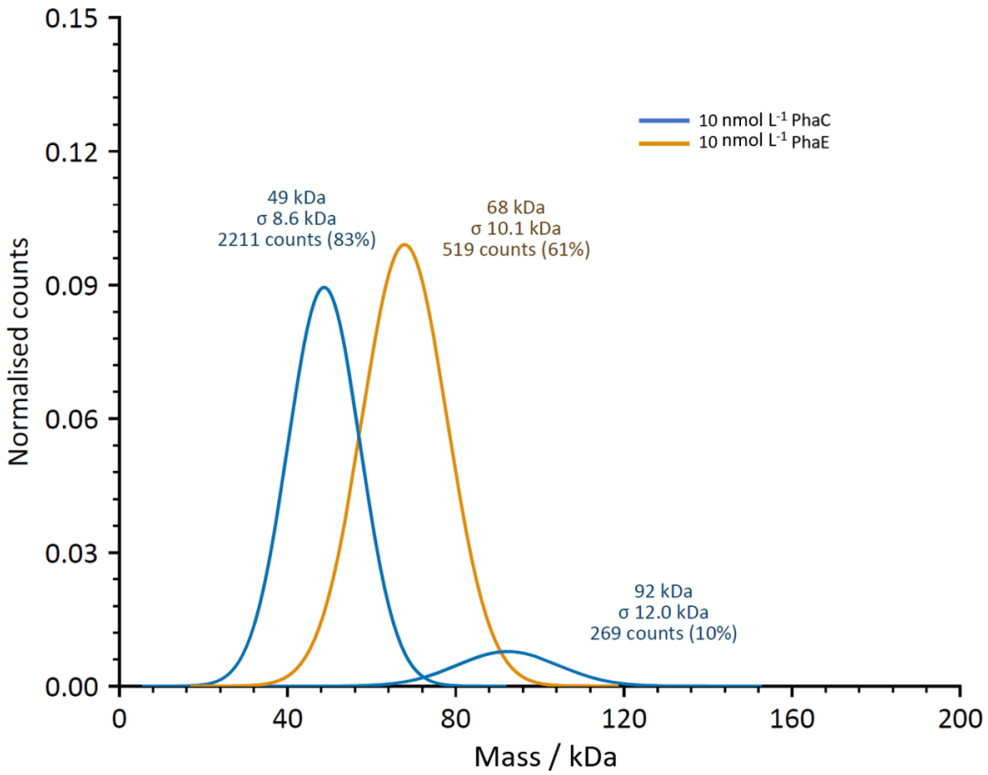

Figure 21: Mass photometry analysis of PhaC and PhaE mixture at different concentrations (10, 20 and 100 nmol L^{-1}). Three peaks were identified, possibly attributed to PhaE dimer (~45 kDa), PhaC (~65 kDa), and a complex of PhaC and PhaE (~111 kDa).

Enzimatic activity and kinetic assay

PhaB exhibited catalytic activity in the presence of NADH and acetoacetyl-CoA (AcAc-CoA). The rate of (R)-3-hydroxybutyryl-CoA (3-HB) formation varied depending on AcAc-CoA concentration, with differences observed in both reaction rates and total consumption times for each substrate concentration (Figure 22). Higher substrate concentrations led to a more rapid initial formation of 3-HB, which subsequently slowed as the reaction progressed. By analyzing the initial reaction rates (Figure 23) in accordance with the Michaelis Menten kinetic model, V_{max} and K_m were determined to be $1.023 \cdot 10^{-3} \pm 4.047 \cdot 10^{-5}$ mmol L^{-1} s^{-1} and $2.809 \cdot 10^{-2} \pm 3.285 \cdot 10^{-3}$ mmol L^{-1}, respectively. Subsequently, k_{cat} and the catalytic efficency (k_{cat}/K_m) were calculated to be 40.920 ± 1.619 s^{-1} and $1.457 \cdot 10^{6} \pm 1.798 \cdot 10^{5}$ (mol L^{-1})$^{-1}$ s^{-1}, respectively.

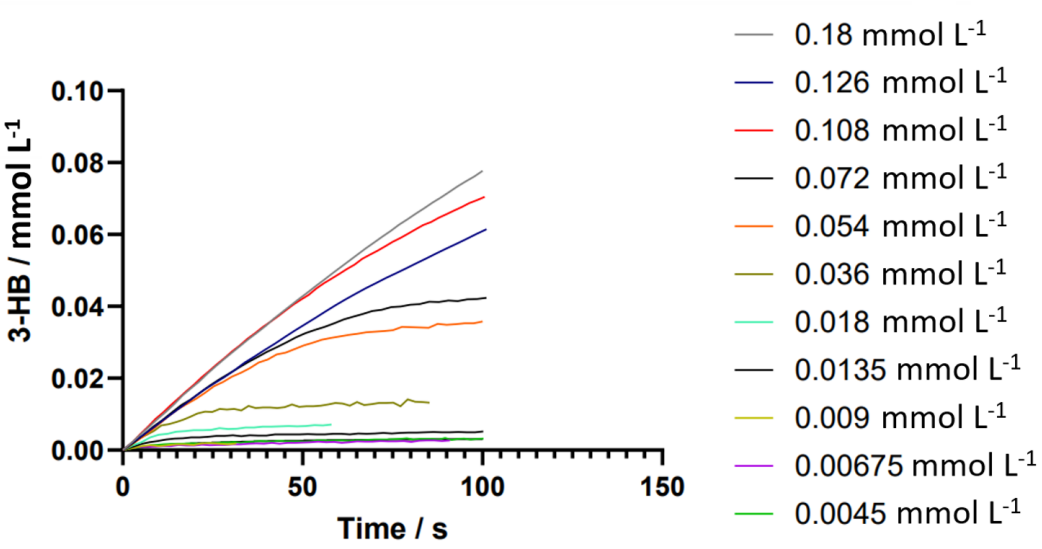

Figure 22: (R)-3-Hydroxybutyryl-CoA (3-HB) generation at different acetoacetyl-CoA (AcAc-CoA) concentrations. Formation rates varied greatly depending on the substrate concentration.

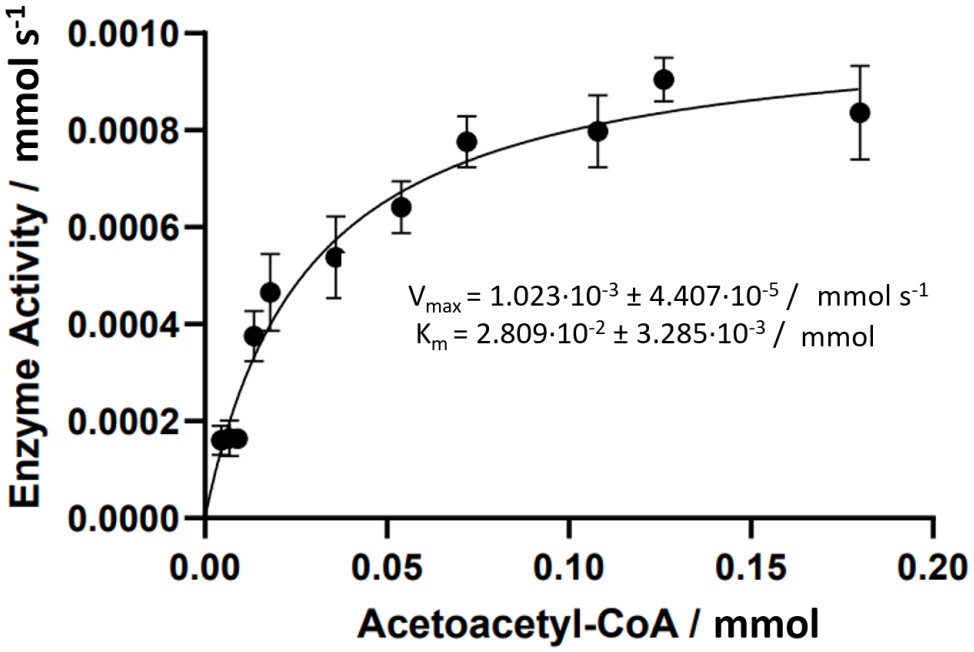

Figure 23: Kinetic assay and Michaelis Menten parameters of PhaB (25 nmol L^{-1}) with acetoacetyl-CoA as a substrate.

Discussion

Although the genes were successfully cloned, proteins PhaAa1 and PhaAb1 were not detected in high or consistent expression levels, possibly due to their role as thiolase, which may disrupt central carbon metabolism in the cells. Specifically, PhaA utilizes acetyl-CoA, a critical metabolite in pathways such as the Krebs cycle and fatty acid biosynthesis. To address these issue, alternative expression strategies should be considered. One approach could involve the expressing of individual subunit in separate expression vectors. Previous studies in Haloarchaea have shown that the enzyme is inactive when either subunit is missing, which would allow controlled expression without immediate enzyme activity [5]. Another possible strategy is to design an inactive fusion protein containing both subunits linked by a protease-sensitive cleavable linker [16]. Following the expression, treatment with a specific protease could release the two subunits, enabling controlled activation of the enzyme. Alternatively, it could be tested if the proteins are soluble when expressed, checking the formation of inclusion bodies [17].

In contrast, the expression of the other enzymes was successful and did not appear to have any toxic effects on the recombinant *E. coli*, likely because they do not interfere with critical metabolic pathways or consume essential metabolites needed for cell viability. To gain a holistic understanding of the complete PHA biosynthesis pathway at a cellular level, complementary metabolomic and transcriptomic analyses could be employed [18]. These techniques would help assess cellular changes and predict the effects of gene expression in other organisms. Such analyses could also reveal metabolic bottlenecks and suggest strategies to improve the supply of metabolic precursors needed for PHA synthesis.

The His and SUMO tag enabled straightforward and efficient purification of the POI, with no apparent interference in protein folding or catalytic activity. As reported, the SUMO tag may have improved enzyme solubility but resulted in an apparent higher molecular weight than the actual protein [12]. Furthermore, the protease ULP1 was successful in removing the purification tags. However, in the case of PhaE, ULP1 did not perform as efficiently, likely due to the trimeric structure of the subunit which makes the SUMO cleavage site less accessible. This issue was resolved by increasing the incubation temperature, which vastly improved the cleavage efficiency.

The co-purification study of the PHA synthase subunits demonstrated that it is feasible to purify both subunits from the same solution, suggesting the potential to purify the proteins directly from a cell co-expressing them. Photometric analysis indicated a possible heterotetrametric structure, consisting of three PhaE subunits and one PhaC subunit. If confirmed, this would be the first report of such a structure. To validate this finding, additional studies are required, including analysis with a native gel and tests of the tetramer's catalytic activity. This novel configuration opens up the possibility of synthesizing a new type of PHA polymer with unique properties not previously reported, potentially offering useful characteristics for industrial applications.

The enzyme PhaB exhibits Michaelis-Menten kinetics, enabling the determination of its catalytic parameters. Although this enzyme does not stand out in terms of substrate affinity or catalytic rate compared to others reported (notably, *C. necator* PhaB has the lowest K_m and highest k_{cat} reported, both with one order of magnitude of difference with the studied enzyme), its kinetic values fall within the typical range for similar enzymes. Specifically, when compared to the ammonia-oxidizing archaeon *N. maritimus*, the enzyme from *N. viennensis* displays a similar substrate affinity but has a lower catalytic activity, with *N. maritimus* demonstrating over twofold greater efficiency in this regard.

Table 4: Reported Michaelis Menten kinetic parameters for PhaB. WT: Wild type; NR: Not reported.

Organism	Enzyme	K_m / mmol L^{-1}	k_{cat} / s^{-1}	k_{cat}/K_m / (mol L^{-1})$^{-1}$ s^{-1}	References
Cupriavidus necator	WT	$5.7 \cdot 10^{-3}$	102	$1.8 \cdot 10^{7}$	[19]
	T173S	$1.36 \cdot 10^{-2}$	361	$2.65 \cdot 10^{7}$	[19]
Synechocystis sp. PCC 6803	WT	12,37	0,93	80	[20]
Ca. Accumulibacter phosphatis	WT	$5.67 \cdot 10^{-2}$	11,6	$2.05 \cdot 10^{5}$	[21]
Nitrosopumilus maritimus	WT	$2.6 \cdot 10^{-2}$	108	$4.05 \cdot 10^{6}$	[7]
Clostridium butyricum	WT	$2.8 \cdot 10^{-2}$	56,7	$2 \cdot 10^{6}$	[22]
	K50A/K54A/L232Y	$1.6 \cdot 10^{-2}$	158,3	$9.83 \cdot 10^{6}$	[22]
Streptomyces coelicolor	WT	$1.8 \cdot 10^{-2}$	NR	NR	[23]
Methylobacterium rhodesianum MB 126	WT	$3 \cdot 10^{-2}$	NR	NR	[24]

To deepen the comparative analysis between sequences and catalytic performances, aligning the sequence with orthologues would be beneficial [25]. This would help to identify closely related enzymes and highly potential advantageous mutations, especially among archaea enzymes, where information remains limited. Furthermore, assessing the enzyme's catalytic activity with alternative electron donors, such as NADPH instead of NADH, could provide valuable insights into how cofactor specificity influences kinetic parameters.

Conclusions

The objectives of this research were partially achieved as the expression, quaternary structure and activity of only certain enzymes could be verified. Particularly, the subunits encoding for the first enzyme in the process (β-ketothiolase PhaAa1/PhaAb1) could not be soluble expressed, possibly due to its substrate affinity to the key metabolite in the central carbon metabolism of the cell.

It was demonstrated that recombinant enzymes with His and SUMO tags can be purified using chromatography techniques, as shown by the purification of the PHA synthetase complex PhaC and PhaC. Additionally, co-purifying the complex from the same protein solution was additionally demonstrated. The potential quaternary structure found for PhaCE was unexpected, as it has not been previously reported in the literature. However, its activity along with the identification and characterizing the specific type of polymer is still to be verified.

The acetoacetyl-CoA reductase (PhaB) was shown to follow Michaelis Menten kinetics, its catalytic efficiency is within the same order of magnitude (10^6 (mol $L^{-1})^{-1}$ s^{-1}) as most of the reported wild-type enzymes. However, its catalytic parameters (k_{cat} and K_m) are less processive than the engineered proteins from *C. necator*. Further experiments are necessary to characterize the potential reversibility of the catalytic process and use of coenzymes.

It is recommended to conduct metabolomic and transcriptomic studies that can identify bottlenecks in precursor metabolites necessary for PHA synthesis (possibly acetyl-CoA and NADH) and cell stress. Subsequently, in an industrial perspective, the gene cassette should be expressed in an organism that consumes a cheap substrate in order to achieve economic feasibility.

Furthermore, this study represents a pioneering effort in characterizing PHA synthesis enzymes from archaea, particularly ammonia-oxidizing archaea (AOA), as previous research has only identified the genes and assessed the reversibility of PhaB.

Bibliography

1. Abby, S. S., Kerou, M. & Schleper, C. Ancestral Reconstructions Decipher Major Adaptations of Ammonia-Oxidizing Archaea upon Radiation into Moderate Terrestrial and Marine Environments. mBio 11, 10.1128/mbio.02371-20 (2020).

2. Sagong, H.-Y., Son, H. F., Choi, S. Y., Lee, S. Y. & Kim, K.-J. Structural Insights into Polyhydroxyalkanoates Biosynthesis. Trends in Biochemical Sciences 43, 790–805 (2018).

3. Samrot, A. V. et al. The Synthesis, Characterization and Applications of Polyhydroxyalkanoates (PHAs) and PHA-Based Nanoparticles. Polymers 13, 3302 (2021).

4. Sharma, V., Sehgal, R. & Gupta, R. Polyhydroxyalkanoate (PHA): Properties and Modifications. Polymer 212, 123161 (2021).

5. Hou, J. et al. Haloarchaeal-Type β-Ketothiolases Involved in Poly(3-Hydroxybutyrate-co-3-Hydroxyvalerate) Synthesis in Haloferax mediterranei. Applied and Environmental Microbiology 79, 5104–5111 (2013).

6. Han, J., Lu, Q., Zhou, L., Liu, H. & Xiang, H. Identification of the polyhydroxyalkanoate (PHA)-specific acetoacetyl coenzyme A reductase among multiple FabG paralogs in Haloarcula hispanica and reconstruction of the PHA biosynthetic pathway in Haloferax volcanii. Appl Environ Microbiol 75, 6168–6175 (2009).

7. Liu, L., Schubert, D. M., Könneke, M. & Berg, I. A. (S)-3-Hydroxybutyryl-CoA Dehydrogenase From the Autotrophic 3-Hydroxypropionate/4-Hydroxybutyrate Cycle in Nitrosopumilus maritimus. Front. Microbiol. 12, (2021).

8. Javidpour, P. et al. Biochemical and Structural Studies of NADH-Dependent FabG Used To Increase the Bacterial Production of Fatty Acids under Anaerobic Conditions. Appl Environ Microbiol 80, 497–505 (2014).

9. Chek, M. F., Hiroe, A., Hakoshima, T., Sudesh, K. & Taguchi, S. PHA synthase (PhaC): interpreting the functions of bioplastic-producing enzyme from a structural perspective. Appl Microbiol Biotechnol 103, 1131–1141 (2019).

10. Zher Neoh, S. et al. Polyhydroxyalkanoate synthase (PhaC): The key enzyme for biopolyester synthesis. Current Research in Biotechnology 4, 87–101 (2022).

11. Kerou, M. et al. Proteomics and comparative genomics of Nitrososphaera viennensis reveal the core genome and adaptations of archaeal ammonia oxidizers. Proceedings of the National Academy of Sciences 113, E7937–E7946 (2016).

12. Marblestone, J. G. et al. Comparison of SUMO fusion technology with traditional gene fusion systems: Enhanced expression and solubility with SUMO. Protein Science 15, 182–189 (2006).

13. Wu, D. & Piszczek, G. Standard protocol for mass photometry experiments. Eur Biophys J 50, 403–409 (2021).

14. Johnson, K. A. & Goody, R. S. The Original Michaelis Constant: Translation of the 1913 Michaelis–Menten Paper. Biochemistry 50, 8264–8269 (2011).

15. Bradford, M. M. A rapid and sensitive method for the quantitation of microgram quantities of protein utilizing the principle of protein-dye binding. Analytical Biochemistry 72, 248–254 (1976).

16. Elleuche, S. Bringing functions together with fusion enzymes—from nature's inventions to biotechnological applications. Appl Microbiol Biotechnol 99, 1545–1556 (2015).

17. Bhatwa, A. et al. Challenges Associated With the Formation of Recombinant Protein Inclusion Bodies in Escherichia coli and Strategies to Address Them for Industrial Applications. Front. Bioeng. Biotechnol. 9, (2021).

18. Zhou, L. et al. Omics-guided bacterial engineering of Escherichia coli ER2566 for recombinant protein expression. Appl Microbiol Biotechnol 107, 853–865 (2023).

19. Matsumoto, K. et al. Directed Evolution and Structural Analysis of NADPH-Dependent Acetoacetyl Coenzyme A (Acetoacetyl-CoA) Reductase from Ralstonia eutropha Reveals Two Mutations Responsible for Enhanced Kinetics. Applied and Environmental Microbiology 79, 6134–6139 (2013).

20. Wang, T. et al. Acetoacetyl-CoA reductase PhaB as an excellent anti-Prelog biocatalyst for the synthesis of chiral β-hydroxyl ester and the molecular basis of its catalytic performance. Molecular Catalysis 514, 111854 (2021).

21. Olavarria, K. et al. An NADH preferring acetoacetyl-CoA reductase is engaged in poly-3-hydroxybutyrate accumulation in Escherichia coli. Journal of Biotechnology 325, 207–216 (2021).

22. Kim, E.-J. et al. Crystal Structure of (S)-3-Hydroxybutyryl-CoA Dehydrogenase from Clostridium butyricum and Its Mutations that Enhance Reaction Kinetics. Journal of Microbiology and Biotechnology 24, 1636–1643 (2014).

23. PACKTER, N. M. & FLATMAN, S. Characterization of acetoacetyl-CoA reductase (3-oxoreductase) from Streptomyces coelicolor: Its possible role in polyhydroxybutyrate biosynthesis. Biochemical Society Transactions 11, 598–599 (1983).

24. Mothes, G. & Babel, W. Methylobacterium rhodesianum MB 126 possesses two acetoacetyl-CoA reductases. Arch. Microbiol. 161, 277–280 (1994).

25. Davidson, A. R. Multiple Sequence Alignment as a Guideline for Protein Engineering Strategies. in Protein Design: Methods and Applications (eds. Guerois, R. & de la Paz, M. L.) 171–181 (Humana Press, Totowa, NJ, 2006). doi:10.1385/1-59745-116-9:171.

Chapter 2

Method for automated cultivation and assessment of physiological and biotechnological parameters of gas-fermenting methanogens

Contribution

My contributions to this chapter included culture maintenance, determination of dry mass coefficient, writing the analysis script, conducting the experiments and device maintenance.

Method for automated high performance closed batch cultivation of gas-utilizing methanogens

Walter Hofmann[1,2,#], Marco Orthofer[3,#], Nicolás Salas Wallach[1,2], Aquilla Ruddyard[1], Markus Ungerank[4], Christian Paulik[3], Simon K.-M. R. Rittmann[1,*]

[1]Archaea Physiology & Biotechnology Group, Department of Functional and Evolutionary Ecology, Universität Wien, Wien, Austria
[2]Acib GmbH, Wien, Austria
[3]Institute for Chemical Technology of Organic Materials, Johannes Kepler Universität Linz, Linz, Austria
[4]Creonia e.U., Perg, Austria

[#]These authors contributed equally to this work

[*]Corresponding author:
Dr. Simon K.-M. R. Rittmann, Privatdoz.
Archaea Physiology & Biotechnology Group
Department of Functional and Evolutionary Ecology
Djerassiplatz 1
Universität Wien
1030 Wien
Austria
Email: simon.rittmann@univie.ac.at

Keywords**:** Microbiology, biotechnology, gas fermentation, microorganisms, anaerobe, methanogenic archaea

Abstract

To advance the utilization of microbial cell factories in gas fermentation processes, their physiological and biotechnological characteristics must be understood. Here, we report on the construction and operation of a novel device, the Gas and Pressure Controller (GPC), which is specifically designed for the automated control of the headspace gas pressure of closed cultivation bottles and facilitates automated gassing, sparging, monitoring and regulation of the headspace volume operated in closed batch cultivation mode in real time.

As proof of concept, the physiological and biotechnological characteristics of four autotrophic, hydrogenotrophic methanogenic archaea were examined to quantify novel physiological limits through the elimination of gas limitation during growth and methane formation. We determined unprecedented high maximum specific methane productivity (qCH_4) values for: *Methanothermobacter marburgensis* of 169.59 ± 12.52 mmol g^{-1} h^{-1}, *Methanotorris igneus* of 420.21 ± 89.46 mmol g^{-1} h^{-1}, *Methanocaldococcus jannaschii* of 364.52 ± 25.50 mmol g^{-1} h^{-1} and *Methanocaldococcus villosus* of 356.38 ± 20.79 mmol g^{-1} h^{-1}. Obtained qCH_4 of *M. marburgensis* is more than 10-fold higher compared to conventional closed batch cultivation set-ups and as high as the highest reported qCH_4 value of *M. marburgensis* from fed-batch gas fermentation in stirred tank bioreactors. Furthermore, the GPC demonstrated reliable functionality with *Methanococcus maripaludis*, operating safely and autonomous during long term cultivation. This novel device enables optimal headspace pressure control, providing flexibility in application for various gas-fermenting biotechnological processes. It facilitates near optimal cultivation conditions in semi-continuous closed batch cultivation mode, the analysis of limiting factors in high-throughput experimental design and allows for automated biomass production of autotrophic, hydrogenotrophic methanogens.

Introduction

In time of limiting resources, microbiology and biotechnology research avenues focus on establishing sustainable production processes. A complete transition towards sustainability may not be solely achieved through one technology but requires a synergy of multiple technologies from different industrial sectors and advances from various scientific fields. Two promising and rapidly emerging biotechnological fields are gas fermentation [1,2] and archaea biotechnology [3,4]. Archaea are a group of prokaryotic microorganisms that exhibit unique biochemical, metabolic and physiological properties that allow application in a wide variety of industrial applications [3,5,6]. Despite their physiological and biotechnological potential, archaea remain largely underexplored in both scientific research and technological applications. However, many different compounds can be nowadays produced by archaea [3,7] and major advancement in archaea biotechnology have been recently achieved [8–11], with a few archaeal production processes currently being scaled-up beyond lab-scale [3]. Significant improvements using archaea have also been made in the context of gas fermentation processes, converting gaseous C1 compounds into gaseous or liquid compounds. In this regard, biohydrogen production through the water gas shift reaction [12–14] as well as the conversion of carbon dioxide (CO_2) and molecular hydrogen (H_2) into methane (CH_4) [15–17] have been thoroughly studied. These bioprocesses may act as carbon utilization avenues, reducing global carbon emissions by converting inorganic carbon into organic material through autotrophic organisms.

Methanogenic archaea (methanogens) [18,19] are anaerobic organisms and possesses ecological flexibility that allows them to inhabit various anoxic environments including the gastrointestinal tract [20] and could possibly thrive in extraterrestrial environments [21]. They utilize a wide range of different substrate types including methyl compounds, acetate and C1 compounds [22]. Autotrophic, hydrogenotrophic methanogens are archaeal cell factories for H_2/CO_2 to CH_4 conversion [17,23,23,24] and may be employed for proteinogenic amino acid production [8–11,25,26]. However, a major obstacle that remains is to characterize methanogens in high-throughput screening settings – before bioprocess development shall be initiated. Examining the physiological boundaries of methanogens under comparable and highly reproducible cultivation conditions is therefore essential for identifying and prioritizing strains for their subsequent optimization. Several studies already emphasize the importance of bioprocess factors for regulating the physiological output of methanogens, including gassing rates, pH, stirring rates, temperature, media composition and dilution rates in various cultivation settings [15–17,27,28].

Anaerobic cultivation of gas-utilizing microorganisms must meet specific requirements, including the prevention of molecular oxygen (O_2) exposure, as O_2 is toxic to varying degrees for the strict anaerobic organisms [29,30]. The most used cultivation technique in anaerobic microbiology and biotechnology laboratories is closed batch, commonly performed in serum bottles [16,29–31] and, in the case of autotrophic, hydrogenotrophic methanogens, under slight overpressure conditions [31]. Later, scale-up of bioprocesses occurs in bioreactors, during which continuous supply of gaseous substrates in fed-batch [32] or continuous culture mode (both liquid and gas feed) is employed [15]. The bottleneck in closed batch, but also in bioreactors, is (usually) not the catalysis rate of the biomass, but the gas transfer from the gas into the liquid phase. It is therefore necessary to optimize the gas transfer rate (GTR) using biochemical bioengineering methods [27,33]. This can be achieved by increasing the partial pressure of the respective gas, which is why gas fermentations are specifically carried out under elevated pressure [16,21,28,33], or though increasing the gas-liquid mass transfer coefficient (k_La) [33]. Cultivation in closed batch cultivation mode is usually performed before process development is initiated or for obtaining seeding cultures for inoculation [27]. This is due to the cost-effectiveness, low expertise requirements of operators and suitability for high-throughput experiments compared to operating bioreactors. Successful

outcomes of closed batch cultivations include the assessment of physiological parameters by investigating the methane evolution rates of autotrophic, hydrogenotrophic methanogens [16], studies of analysis of growth behavior under elevated heavy metals and volatile fatty acids concentration [34] as well as media optimization studies [16,32]. Furthermore, closed batch cultivations are an integral part of biomass production pipelines [35]. However, during closed batch mode, sub-optimal supply of the gaseous substrate prohibits balanced growth shifting the growth kinetics to a disproportionate pattern, labelling it unsuitable for modelling and scale up of biomethanation processes. Therefore, optimizing cultivation conditions in closed batch setups is crucial to be able to draw significant conclusions in screening experiments, even in a small-scale high-throughput design.

In this article, we present the functionality and operation of an innovative device, designed for automated gassing, purging, sparging and pressurizing of sealed microbial cultivation bottles independent of the process volume for closed batch cultivations – the Gas and Pressure Controller (GPC). This novel apparatus allows for continuous real-time pressure monitoring throughout the cultivation process. In this proof-of-concept study, convenient quantification of gas conversion and CH_4 production kinetics of five autotrophic, hydrogenotrophic methanogens is demonstrated. The utilization of the GPC facilitates the application of a specific stoichiometry during gas conversion according to the metabolic requirements of the organisms, which leads to a noticeable pressure drop during gas fermentation. The GPC overcomes gas limitations by constant and automated adaptation of the headspace gas pressure, therefore allowing optimal growth in unimpeded conditions. This combination of the advantages of closed batch gas fermentation under gas-unlimited conditions was previously not possible and represents a major leap forward in closed batch cultivation techniques.

Materials and methods

Strains and media

For the proof-of-concept demonstration, five autotrophic, hydrogenotrophic methanogens *Methanothermobacter marburgensis* DSM 2133, *Methanotorris igneus* DSM 5666, *Methanocaldococcus jannaschii* DSM 2661, *Methanocaldococcus villosus* DSM 22612 and *Methanococcus maripaludis* S0001 were cultivated in closed batch utilizing the GPC. *M. maripaludis* S0001 is a mutated strain and originates from the wild-type strain S2. It was generated by deleting the gene encoding for the hypoxanthine phosphoribosyltransferase (MMP0145) and introducing the rep gene from the Methanococcus shuttle vector pURB500 [36,37]. The cultivation medium '282c_18' was used for *M. villosus*, while '282c_30' was applied for both *M. jannaschii* and *M. igneus*. Exact media compositions were derived from a previous study [16], with a single modification of omitting $NaHCO_3$. The defined medium for *M. marburgensis* was prepared identical to the previously published recipe [34]. The cultivation media for *M. maripaludis* was applied as previously described [35]. However, sodium acetate was excluded from the recipe, as the metabolism of *M. maripaludis* was shifted to CO_2 as sole carbon source. All methanogens were cultivated according to their optimal pH and temperature. The pH was adjusted aerobically before complementing the media with Na_2S and L-Cysteine. To demonstrate pH changes under anaerobic, CO_2 saturated conditions with elevated pressure and following the addition of alkaline solution Na_2S, the defined media (MM) was pressurized to 15 bar absolute and analyzed at 65 °C and room temperature (RT). These experiments were conducted using the simultaneous bioreactor system (SBRS-II) (Orthofer *et al*., submitted for publication). The cultures were supplied with a premixed gas (20 Vol.-% CO_2 in H_2) (Air Liquide GmbH, Schwechat, Austria) as gaseous

substrate and was introduced manually through an offline gassing manifold (pre-culture) or automated with the GPC.

Closed batch cultivation – pre-cultures

The pre-cultures of the four thermophilic/hyperthermophilic methanogens were cultivated in pressure-resistant 500 mL Schott bottles (DURAN® pressure plus+ GL 45; DWK Life Sciences GmbH, Wertheim, Germany) using established closed batch system technique, adapted for larger culture volumes of 200 mL [31]. The anaerobic bottles were sealed with butyl rubber stoppers and fastened with perforated caps (Ochs Laborbedarf, Bovenden, Germany). The pre-culture of *M. maripaludis* was initially cultivated in serum bottles before performing GPC experiments as previously established [31]. All bottles were anaerobized by a total of ten repetitions of gassing and subsequent vacuuming to 0.5 bar with H_2/CO_2 (4:1) prior to inoculation. Incubation of pre-cultures were performed by pressurizing to 1.5 bar for Schott bottles and 3 bar overpressure for serum bottles. Sterile conditions were ensured by connecting a 0.20 µm cellulose acetate filter (9055511; LLG Labware, Meckenheim, Germany) while gassing and pressure measurements with a digital manometer (303005.0003; Keller, Winterthur, Switzerland). Growth was observed by measuring the optical density (OD) with a Specord 200 Plus spectrophotometer (823-0200P2; Analytik Jena, Jena, Germany) at 578 nm. The thermophilic/hyperthermophilic hydrogenotrophic methanogens were incubated using a GFL 1083 shaking water bath (Gesellschaft für Labortechnik mbH, Burgwedel, Germany) filled with heating bath fluid ROTITHERM® (Carl Roth GmbH + Co. KG, Karlsruhe, Germany). The internal temperature was maintained according to the specific temperature requirements. Set optimal temperatures were 65 °C for *M. marburgensis*, 88 °C for *M. igneus*, 80 °C for *M. villous* and 85 °C for *M. jannaschii* with a constant unidirectional agitation of 100 rpm during the pre-culture phase. *M. maripaludis* was cultivated in a Premium Double Layer Shaking Incubator 170L ZWYR-2102C (LABWIT Scientific, Burwood East, VIC, 3151) at 37 °C and 180 rpm orbital shaking. An overview of the cultivation conditions is shown in Table 1.

Determination of dry biomass weight

To analyze the specific CH_4 production rate (qCH_4) of the methanogen, a conversion factor (x) for optical density to dry biomass was determined for investigated methanogen except for *M. maripaludis*. The cultures were prepared as described above. Filters (Whatman® regenerated cellulose RC58 filter discs 0.2 µm, Cytiva, Massachusetts, US) were dried overnight at 105 °C and weighed the following day. The OD_{578} of the cell suspension was measured, the diluted cultures filtered (10 mL) in triplicates and subsequently washed three times with the corresponding medium. The filters were subsequently dried overnight at 105 °C and the total weight of the filters measured. Detected dry biomass can be subsequently converted to the initial OD_{578}.

GPC

Application and set-up of the GPC

One GPC unit consists of four individual channels and allows for the supply and exhaust of gas in four pressurized cultivation vessels (Figure S1, Figure S2, Figure S3). Four external gas connections are available and can be used to supply different gases to the culture. The gas flow is

regulated by 8 Solenoid valves (SV) (SV1-8, Figure S1 and Figure S2) (1913CA302; Ningbo Brando Hardware Co., Ltd., Zhejiang, China) placed in two parallel rows. Molecular nitrogen (N_2) supply (Figure S2, valve position #8) (not used) and a 4:1 H_2/CO_2 gas bottle (Figure S2, valve position #7) were connected while one open position (Figure S2, valve position #5) functioning as an off-gas discharge to ventilate the headspace volume. The inlet pressure was adjusted using the pressure regulators situated in the lab. Additional downstream throttle valves were integrated for better fine tuning (Figure S1, NV1-4; Figure S2). Opening two valves in parallel directs the gas flow from the high-pressure laboratory gas lines (~5 bar) to the lower-pressure cultivation bottles. If pressure needs to be released from the cultivation bottles, the gas is vented through an exhaust valve (valve position #5). A total of four distinct and autonomously executable sequence programs in CSV format can be generated and uploaded to the controller. Real-time pressure changes are monitored using manometers (Figure S1, PIC 1-4; Figure S2, M1-4) (RL-131-II-1A; Anhui Ruiling Meter Manufacturing Co. Ltd, Anhui, China) respectively. All elements are interconnected with pressure resistant tubing (Master-Tube PUR 98A – Masterflex, Gelsenkirchen, Germany). The GPC was fitted in a fume hood to facilitate a rapid extraction of released gases. Two additional devices are placed outside and contain power supply, system control and facilitate data monitoring and recording. In order to maintain anaerobic conditions inside the serum bottles, a T-Fitting connector is used to join the valve and manometer tubing, with the remaining position connected to a pressure-resistant bottle using a Luer-Lock adapter (male) with a sterile needle. PTFE gas tape is applied to all connections (Manometer, T Fitting, needle) to ensure tight sealing of the system. The cultivation bottles were placed in the corresponding incubator. The same incubators were employed as previously described. For the mesophilic strains, the gas lines were conducted through an opening on the side of the incubator into its interior and connected to the cultivation bottles. During mesophilic cultivation, a sterile filter was installed directly after the valves (Figure S2, SV5-8) to increase the sterility of the system.

Standard operating procedure of the GPC

A precise gassing layout must be defined before the start of cultivation and uploaded to the controller as a CSV file via a micro-SD card. Two sets of experiments were conducted to illustrate the functionality of the system. To assess physiological parameters of *M. marburgensis, M. igenus, M. villous* and *M. jannaschii* the GPC was paused after each methanation cycle and the optical density (OD_{578}) measured. The unidirectional agitation rate was set to 250 rpm to facilitate maximum gas entry into the liquid phase. The cultivation of *M. maripaludis* was performed over several days without biomass detection to facilitate unsupervised cultivation at orbital shaking of 180 rpm. Therefore, the methanation phase was looped with the flushing of the cultivation bottles (20x) to guarantee automated gas supply during the cultivation. Prior to the methanation process and during sampling steps, the headspace volume of the culture vessel is exchanged by pressurizing with H_2/CO_2 gas mixture followed by subsequent release (Flushing phase). At the start of each methanation phase, a pressure of 4 bar absolute is applied for cultivation in serum bottles and 2.5 bar for Schott bottles. The gas consumption, determined as the absolute pressure drop, was set to 1 bar $cycle^{-1}$ in the case of *M. marburgensis* and *M. maripaludis* and 0.5 bar $cycle^{-1}$ for the hyperthermophilic organism in order to increase the total amount of gassing cycles. An overview and detailed description of used programs can be found in the supplementary materials (Figure S4).

The following protocol delineates growth of autotrophic, hydrogenotrophic methanogens for biomass production and quantitatively assessment of their methanation. Unless specified otherwise, all preparatory procedures were performed in an anaerobic glove box (Vinyl Anaerobic

Chambers; Coy Laboratory Products Inc, Michigan, USA). A single controller was utilized to monitor and supply gas to three individual cultures simultaneously (n=3), while an additional negative control was cultivated (not shown).

Inoculation

a Harvest the pre-cultures in active growth phase by centrifugation at 5000 g for 15 min (RT)
b Discard the supernatant and re-suspend the pellet in fresh medium ($OD_{578} \sim 0.05$)

Transfer 30 mL of re-suspended culture into a 60 mL serum bottle and seal as previously described

Note: *M. maripaludis* is known to be a fragile organism due to its thin S-layer [35,38], therefore centrifugation was avoided during the inoculation process and was performed with a sterile needle and syringe. *M. maripaludis* was cultivated in 1 L pressure resistant Schott bottles with a total of 204.175 mL culture volume (2 Vol.-% inoculum).

1 Start cultivation
   a Place culture vessel into pre-heated incubator and wait until process temperature is reached
   b Switch on the GPC
   c Attach a sterile needle to the tubing (luer lock)
   d Start the program and wait until air is flushed out of the tubing, then penetrate the septum with the needle
   e Initiate methanation phase by start shaking of the incubator after target pressure is reached
2 Sampling (optional)
   a After the automatic stop of the gassing station, the injection needle can be pulled out carefully from the septum
   b Remove the serum bottle from the incubator and take a sample (0.7 mL) with a sterile syringe and needle for measuring optical density
   c Reinsert the bottle and repeat steps 2 d-e. to restart the methanation phase
3 End experiment
   After completing the experiment, the agitation can be stopped and the needle removed from the cultivation bottle

Data analysis

An algorithm was developed for fast and easy processing of the raw data in a singular step and was subsequently executed on Matlab 2021b (MathWorks; Natick, Massachusetts, USA). It allows for trimming and smoothing of the raw data as well as the calculation of the most important physiological parameters. A sampling rate of 10 sec was directly configured within the GPC software to minimize the initial amount of data points.

The following filters were applied to facilitate accurate data trimming and were executed sequentially.

i Elimination of data points below a specified pressure threshold (*min-Pressure*). The experiment stops when a certain pressure threshold is reached. Therefore, data points below this limit do not represent the actual pressure evolution.
ii Organization of data into cycles. A cycle is defined from the maximum pressure to a defined threshold or minimum recorded pressure. Data that does not meet this definition is eliminated.

iii Elimination of short-duration cycles (*len_cycles*): Due to the differentiated re-pressurization of the cultures, the pressure gauges are affected by the opening and closing of valves, resulting in small cycles that are removed.

iv Elimination of cycles with no activity (*pressure_drop*). Cycles devoid of a minimum pressure drop of 50 mbar imply no catalytic activity and are removed.

v Elimination of data points that are not consecutive within a cycle. It is anticipated that the data within each cycle progresses sequentially and, at most, deviates by a factor of 2 times the measurement time.

A preset of variables can be manually adjusted to allow for individual evaluation of a wide range of different pressure kinetics. This involves the *move_max* function, which erases a specific number of data points following the peak pressure point after the initial trimming steps. The *calculation* value determines the number of data points used for calculation, while the *average* function adjusts the smoothing factor. CH_4 production was quantified based on the stoichiometry of the biomethanation reaction from H_2/CO_2 as previously described.[31]. This calculation is based on the pressure drop concomitant to the methanation, converting five mol of gaseous substrate to 1 mol of CH_4 (I, II)

$$\text{(I) } p_{CH4} = \frac{p_{before} - p_{after}}{4} [Pa]$$

$$\text{(II) } MER = \frac{\Delta n_{CH4}}{\Delta t * V} [mmol L^{-1} h^{-1}]$$

As it is assumed that only around 5% of the carbon flux is directed into the biomass, the biomass production was omitted for the mass balance and full conversion of CO_2 into CH_4 assumed [39]. The volumetric methane evolution rate (MER / mmol L^{-1} h^{-1}), the conversion rate / mbar h^{-1} and the produced mol of CH_4 (n_{CH4} / mol) are calculated over the whole cultivation time automatically with the algorithm. Additionally, the specific CH_4 production rate (qCH_4 / mmol g^{-1} L^{-1}), biomass concentration (dry cell weight) (x / g L^{-1}), biomass production rate (r_x / g L^{-1} h^{-1}) and the growth yield (Y_{CH4} / g $mmol^{-1}$) can additionally be calculated. Calculations of qCH_4 are based on the final MER values of each cycle, coinciding with the time point at which growth was monitored. The results are plotted against the cultivation time (T_cult / h) which represents the duration of the experiment without accounting for the time intervals between the methanation cycles. Two different versions of the algorithm are provided. The standard version assumes biomass data is available, while in the second version (v2), biomass-specific values are calculated only if a biomass file is present. The culture volume ($V_{culture}$ / mL), the total gas volume in the headspace ($V_{headspace}$ / mL), and possibly the OD_{578} to dry biomass coefficient (x) were additionally supplied. A reduction in culture volume and an increase in headspace volume of 0.7 mL resulting from sampling were considered after each cycle. An overview of all parameters can be found in Table 1. Definition of the cultivation time and calculation of the specific growth rate (exponential formulation) (μ / h^{-1}) were performed separately.

The homogeneity of variance was tested in between cycles with a Levene's test. Statistical relevance was verified further with an ANOVA and subsequent Post hoc analysis (only performed for the thermophilic/hyperthermophilic organisms). Only common cycles before reaching the inflection point were examined.

Table 1: Overview of all cultivation parameters and variables specific to each organism. Volumes displayed refer to cultivation with the GPC. $V_{headspace}$ / mL is the total volume of gas from both the bottle headspace and the tubing. Variables for fine-tuned calculation of physiological parameters are given in timepoints (10 s).

Strain	T / °C	pH	$V_{culture}$ / mL	$V_{headspace}$ / mL	Δ pressure / bar cycle^{-1}	x	calculation	average	move_max
M. marburgensis	65	7	30	38.228	1	0.393	12	9	10
M. igneus	88	5.7	30	44.889	0.5	0.429	10	9	1
M. villosus	80	6.5	30	38.228	0.5	0.334	10	9	5
M. jannaschii	85	6	30	44.889	0.5	0.635	6	5	10
M. maripaludis	37	6.9	204.175	1006.025	1	-	50	30	30

Results

Measured OD_{578} to dry biomass coefficients for all methanogens are listed in Table 1. Cultures of *M. igneus* exhibited biomass aggregates and results did not show good linear regression in comparison to the other methanogens (Figure S5). Investigating the pH at elevated headspace pressure revealed significant differences between different temperatures. At 65 °C the pH stabilizes to around 6, while at RT the pH drops to approximately 4.6 (Figure S6). During cultivation of the thermophilic and hyperthermophilic methanogens a decrease in headspace pressure was visible right after of the cultivation, accelerating over time, indicating instant metabolic activity and growth of the microorganisms (Figure S7-10). This resulted in a steady decrease in cultivation time and shortening of the cycles, paralleled by an increase in the turnover rate until an inflection point is reached (Figure 1), which is reflected in the peak of MER before gradually decreasing (Figure 2). In the experiment with *M. marburgensis*, the decrease in metabolic activity additionally pinpoints the inflection point of the qCH_4, but not of Y_{CH4}, which was detected two cycles earlier (Figure 3). The hyperthermophilic methanogens demonstrate different gas fermentation characteristics due to putative liquid limitations, whereby qCH_4 reaches its maximum only during the initial one to two time points, while the inflection point, and simultaneous drop in MER, align more closely with the Y_{CH4} peak, revealing a relative push into the direction of energy conversion after catalytic inhibition occurred. Biomass production exceeded – except for *M. jannaschii* – albeit at a slower pace after the inflection point had been reached. *M. marburgensis*, *M. igneus* and *M. jannaschii* reached exponential growth with maximum growth rates of 0.55 ± 0.06 h^{-1}, 1.86 ± 0.10 h^{-1}, and 2.64 ± 0.10 h^{-1} respectively, while *M. villosus* showed only linear behavior (1.03 ± 0.13 h^{-1}). This was also evidenced by the trends observed at the MER, where *M. villosus* displayed a different pattern, characterized by a slower initial increase but prolonged MER peak. *M. jannaschii* exhibited the highest MER of 58.24 ± 1.20 mmol L^{-1} h^{-1}, followed by *M. igneus*, *M. marburgensis* and *M. villosus* with 54.07 ± 6.63 mmol L^{-1} h^{-1}, 37.61 ± 3.37 mmol L^{-1} h^{-1} and 26.37 ± 0.61 mmol L^{-1} h^{-1} with *M. villosus*, respectively. The hyperthermophilic methanogens reach similar maxima in their biomass production, while *M. marburgensis* displayed the highest observed OD_{578} of 0.8223 ± 0.0601. However, in terms of qCH_4, the hyperthermophiles exceed *M. marburgensis* with rates of 420.21 ± 33.39 mmol g^{-1} h^{-1} for *M. igneus*, 364.52 ± 25.50 mmol g^{-1} h^{-1} for *M. jannschii*, and 356.38 ± 20.79 mmol g^{-1} h^{-1} for *M. villosus*. After reaching the highest value at the start of the experiments, a decrease is observed shortly thereafter. This contrasts with *M. marburgensis*, where a more stable qCH_4 is achieved (max at 169.59 ± 12.52 mmol g^{-1} h^{-1}) over a longer period until the inflection point is reached. For an overview of the maximum values, please refer to Table 2. Considering the CH_4 produced in moles also reveals either an exponential or linear progression (Figure S11). Methanation by *M. maripaludis* was detected after a lag phase of approximately 10 h (Figure 4, Figure S12, Figure S13) and showed exponential increase until an inflection point is reached. A decline in MER is apparent afterwards until the end of the methanation cycle leads to re-gassing of the cultivation bottles (Figure 4, Figure S13). MER_{max} was typically observed during the second cycle, followed by a mostly linear decrease until the headspace volume was replenished. The maximum MER drops with subsequent gassing cycles, while the duration of these cycles progressively increases.

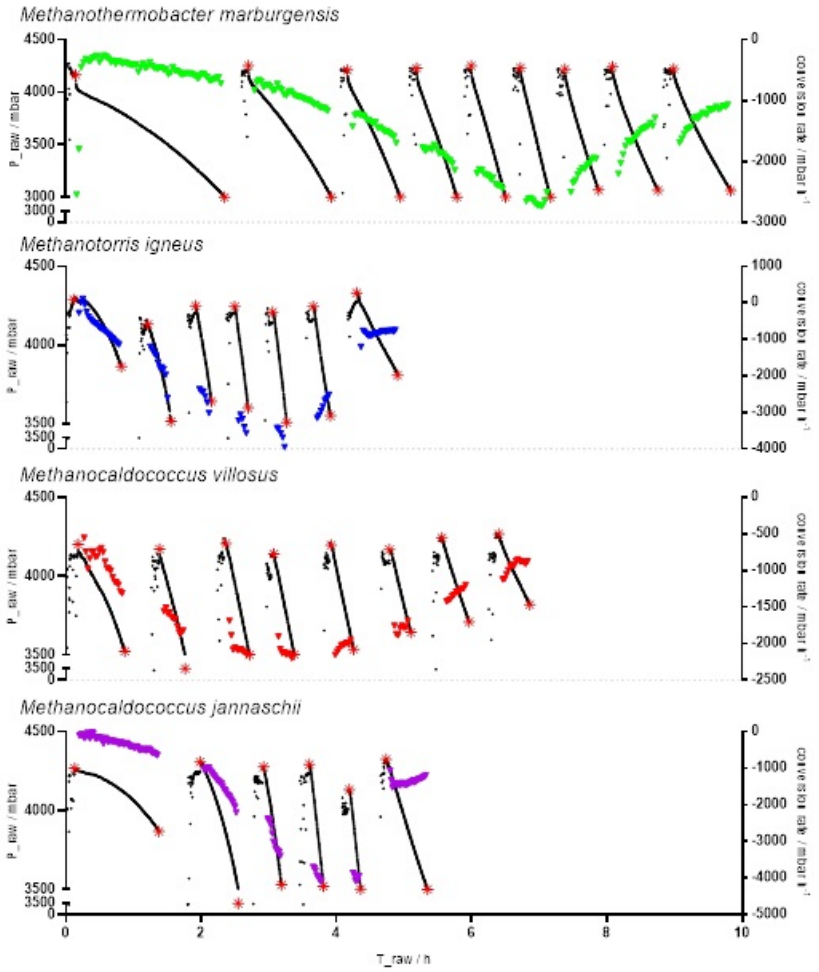

Figure 1 Overview of the pressure kinetics of the thermophilic/hyperthermophilic autotrophic and hydrogenotrophic methanogens. Black dots indicate raw data (prior to trimming and smoothing) of the first replicate. Start and end of the cultivation time is highlighted by red stars. The conversion rates / mbar h^{-1} are shown in color.

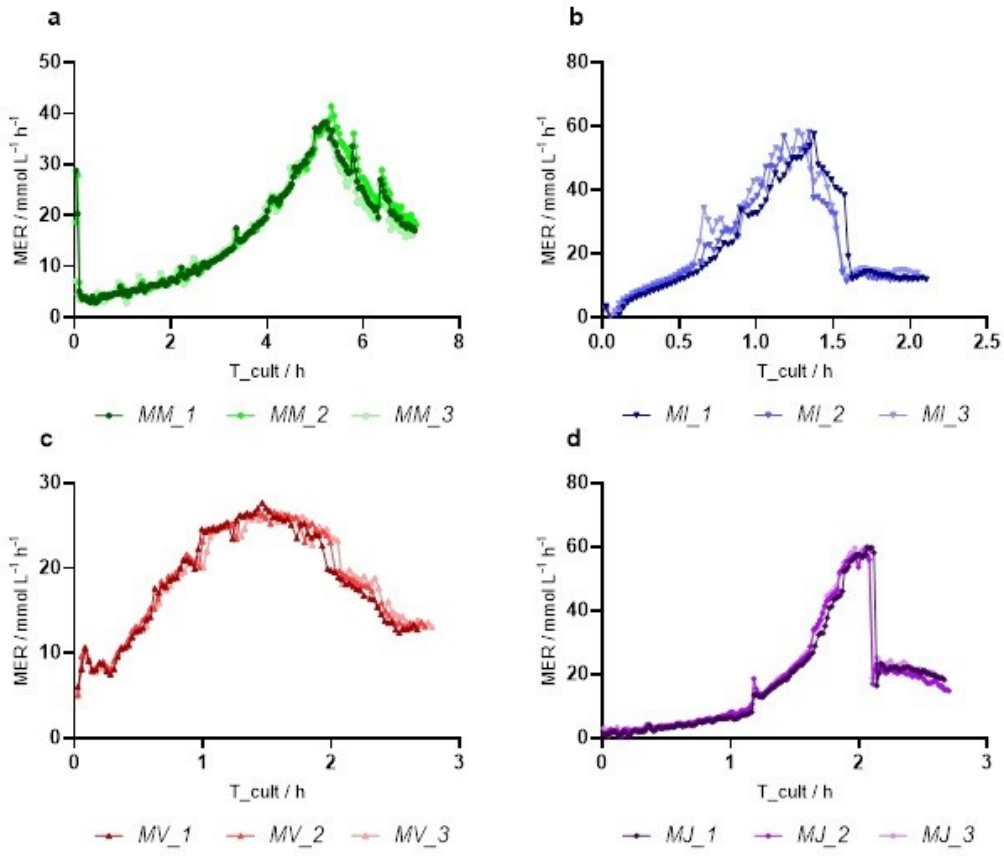

Figure 2 MER / mmol L^{-1} h^{-1} determined over the cultivation time for (a) *M. marburgensis* (*MM*), (b) *M. igneus* (*MI*), (c) *M. villosus* (*MV) a*nd (d) *M. jannaschii* (*MJ*). All experiments are n=3. Individual experiments are shown.

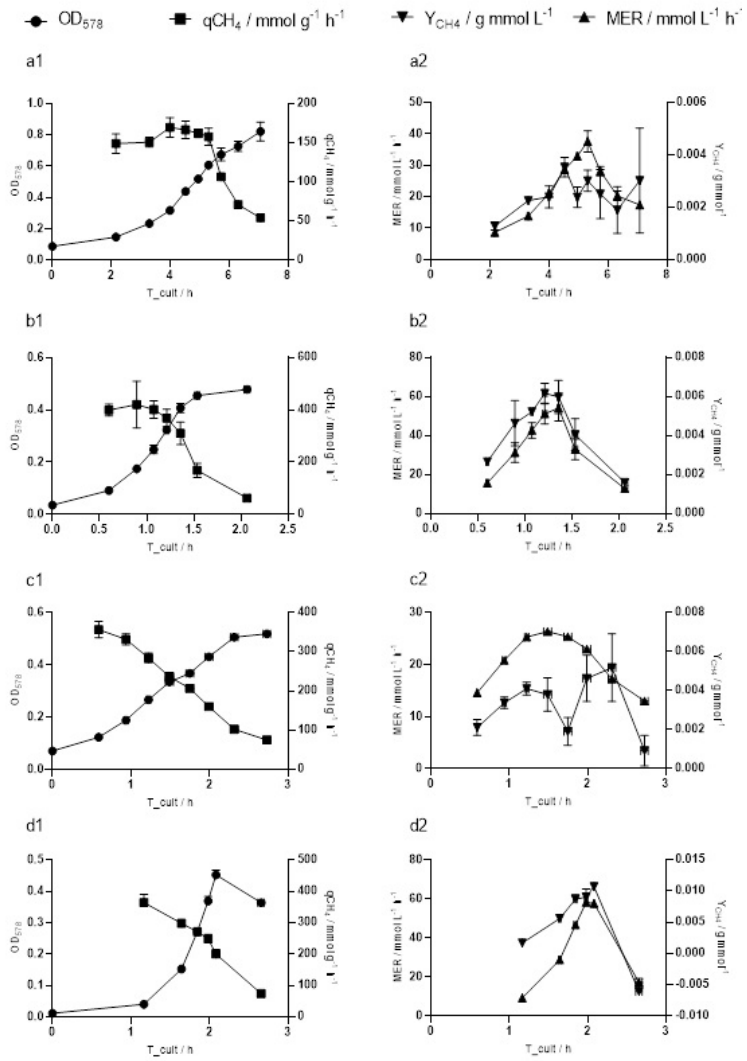

Figure 3: Overview of OD_{578}, MER / mmol L^{-1} h^{-1}, qCH_4 / mmol g^{-1} h^{-1} and Y_{CH4} g $mmol^{-1}$ strain specific values plotted over cultivation time. Shown results from (a1-2) *M. marburgensis*, (b1-2) *M. igneus*, (c1-2) *M. villosus* and (d1-2) *M. jannaschii* represent measured values at the end of each cycle. Horizontal error bars are explained due to slight differences in the cycle length.

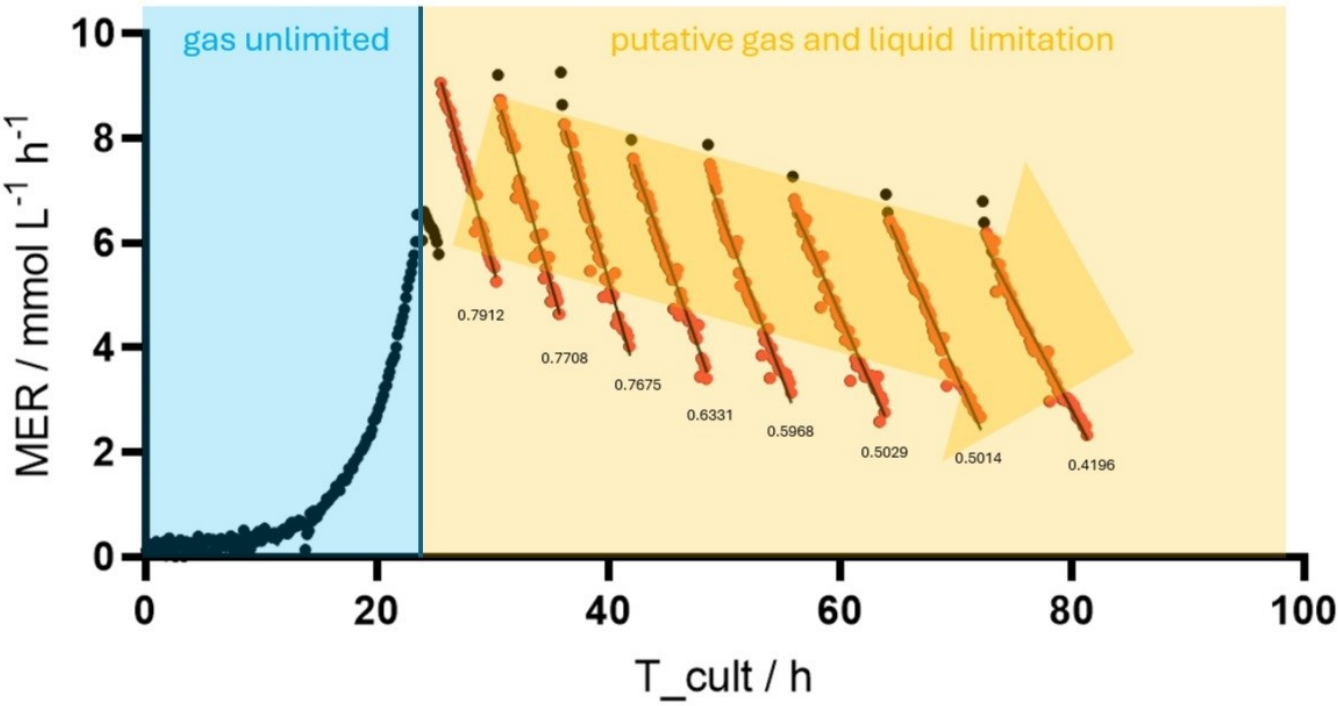

Figure 4: MER / mmol L-1 h-1 determined over an extended cultivation time (86 h) for *M. maripaludis*. Phases of putative gas and liquid limitation are indicated. Slopes were calculated from linear regression, Only the first experiment is shown. Experiment was performed in triplicates (n=3). Additional experiments can be found in the supplementary materials (Figure S13).

Table 2: Measured physiological and biotechnological characteristics of the thermophilic/hyperthermophilic methanogens. Maximum detected values are displayed. Given values for YCH4 / g mmol-1 represent data at the inflection point. All experiments are n=3.

	OD_{578}	x / g L^{-1}	μ / h^{-1}	MER / mmol L^{-1} h^{-1}	qCH_4 / mmol g^{-1} h^{-1}	Y_{CH4} / g $mmol^{-1}$
M. marburgensis	0.8223 ± 0.0601	0.32 ± 0.02	0.55 ± 0.06	32.99 ± 0.13	169.59 ± 12.52	0.0030 ± 0.0004
M. igneus	0.4781 ± 0.0024	0.20 ± 0.00	1.86 ± 0.10	54.07 ± 6.63	420.21 ± 89.46	0.0060 ± 0.0008
M. villosus	0.5190 ± 0.0031	0.17 ± 0.00	1.04 ± 0.13	26.37 ± 0.61	356.38 ± 20.79	0.0038 ± 0.0009
M. jannaschii[1]	0.4526 ± 0.0153	0.29 ± 0.01	2.64 ± 0.10	58.24 ± 1.20	364.52 ± 25.50	0.0090 ± 0.0013

[1] Two OD measurements missing

Discussion

Set-up constraints of the GPC

The quantification of CH_4 production kinetics is based on its partial pressure and can be calculated from the pressure kinetics apparent during methanation [31]. Ensuring the gas tightness of the system is therefore of utmost importance and regular testing for the closure of the system is highly advised. Inaccuracy may arise through additional pressure loss, facilitated by damage to the rubber stopper. Excessive shaking can subject the needle to extreme stress, potentially causing breakage or wear of the rubber stopper. To mitigate possible risks, only new rubber stoppers were used. Due to the high cultivation temperature and the high re-gassing rate in some experiments, water vapor may form and accumulate within the pipes during the experiment. To prevent any liquids from entering the valves or the manometer, it is crucial to design the length of the tubes in a manner that allows condensation of water vapor to occur within the tubes. An attached sterile filter upstream of the cultivation bottle led to clocking due to vapor formation and deterred gas stream and pressure monitoring. However, sterile filters were installed during cultivation under mesophilic conditions, due to longer tubing and lower temperatures. To further facilitate sterile conditions, the tubing can be removed and autoclaved prior to conducting the experiments. In order to achieve an automated operation that ensures safe release and re-pressurizing of cultivation bottles, unwanted contact between the needle and liquid has to be avoided. This can occur frequently during heavy shaking and significantly increases the risk of culture being drawn into the system, leading to subsequent contamination and potential damage. A significant improvement would be the combination with a non-invasive OD sensor, which would eliminate processing time when measuring biomass concentrations.

Data evaluation and uncertainty analysis

The application of several data filtering steps was successful in eliminating background data, present during the pressurizing phase at the beginning of each cycle. Due to the dissolution of gases into the liquid phase, a strong aberrant pressure loss occurs at the beginning of the cultivation cycles, which must be mitigated, due to an exaggerated CH_4 production visible as sharp spikes in the MER plots. More rigorous data trimming results in greater data loss and must therefore be adjusted individually based on the organism and the experimental goals. However, preserving the complete cultivation duration is of minor importance when comparing physiological parameters. The methanation kinetics and biomass production kinetics must be evaluated separately, as the actual cultivation time differs from the cycles determined by the algorithm due to data trimming and data processing. Therefore, the CH_4 production kinetics and the timepoint of biomass monitoring do not align accurately. The time intervals for calculating the growth rate were determined manually, based on the assumption that no significant metabolic activity occurs during pause of the GPC and the subsequent shutdown of the shaker. This is evident from the short pressure interval right before shaking and the GPC begins monitoring the headspace pressure. This pressure remains stable when cultivating *M. marburgensis*, while most cycles of the hyperthermophiles show an increase, presumably because the process temperature has not yet been reached. However, shaking rapidly induces biomethanation and biomass production suggesting that the discussed time interval can be neglected.

Comparison of growth and CH_4 production kinetics

Four different autotrophic, hydrogenotrophic methanogens were chosen and are among the highest performing CH_4 producers so far identified [16]. *M. marburgensis and M. jannaschii* additionally exhibits a broad range of fed-batch or continuous culture cultivations data [15,40] or possess genetic tools [41,42], while biotechnology and physiological studies concerning *M. igneus* and *M. villosus* are scarce.

Many gas fermentation bioprocesses are inhibited by either liquid or gas limiting conditions, a situation particularly present during closed batch cultivations. To improve GTR into the liquid phase an enlargement of the gas-liquid boundary is required, frequently achieved by rigorous stirring or shaking, or by increasing the driving force through applying barophilic conditions [15,16,28,33]. In order to push the metabolic activity of observed organism to the limits, even in closed batch cultivation mode, the unidirectional shaking was set to maximum while the GPC provides excess of gaseous substrate. During the experiments, no gas limitation was observed, as indicated in the acceleration of the conversion rate until an inflection point, defined as the timepoint where maximum conversion (k_{min} / bar h^{-1}) and MER_{max} occurs, is reached [28]. It was not possible to measure the k_La using established methods, as the gassing in and gassing out method with O_2 is only applicable in fed batch fermentation with the appropriate probe, preferable with a short response time. Although probes for measuring H_2, CO_2, or CH_4 are available, they are not commonly used in closed batch systems.

The k_{min} determined for all experiments were around two to four times (2.8 to 4.1 bar h^{-1}) higher than the previously inspected values at 10 bar (max 1.52 ± 0.27 bar h^{-1}) and challenging most maximum conversion rates at 50 bars (0.85 ± 0.64 to 5.11 ± 0.55 bar h^{-1}) [16]. It should be noted that our system allows for GTRs that are comparable to, or higher than those achieved in high-pressure experiments. However, making a precise statement about physiological properties was not possible, as the biomass was omitted during the analysis.

The inflection point, signaling the peak in MER, marks the precise moment when a putative liquid limitation occurs and, except for *M. igneus*, where one inflection point is off by one cycle, remains consistent within the experimental group. *M. marburgensis* shows optimal performance for about 7.06 h, in contrast to hyperthermophilic methanogens that reach the inflection point earlier, after 3 h for *M. igneus*, 3.3 h for *M. villosus*, and 3.7 h for *M. jannaschii*. Additionally, *M. igneus* and *M. jannaschii* show a sudden decrease in MER after reaching liquid limitation. Catalytic inhibition in *M. marburgensis* arises later, coinciding with a stable qCH_4 up to that point. The hyperthermophilic methanogens decrease in qCH_4 highlight early limitation right from the start of the cultivation and review different degrees of optimization potential of cultivation media and show specific differences between thermophilic and hyperthermophilic organisms. While the media of *M. marburgensis* was intensely optimized regarding trace elements (Schönheit et al., 1980; Abdel Azim et al., 2018), the hyperthermophilic 282c media was mostly unchanged or had been substituted with yeast extract or peptone for heterotrophic growth [44], therefore compulsory inhibition of methanogenesis arise early. However, a thorough analysis of the limiting factors requires investigating the specific media requirements and conducting experimental testing of methanation under conditions of limitation or saturation. Previous studies highlight the correlation between trace elements on biomethanation efficiency [17,32]. A limitation in trace element is therefore probable, deriving from lower absolute amounts and potentially higher demands and specificity, but might only explain the limitation localized by the inflection point. Additionally,

the biological availability of chloride versus sulfate-based media needs to be verified. The necessity of Selenium (Se) for growth of methanogens was also reported, due to Se being part of enzymes responsible for energy metabolism [45]. It can be assumed that selenite concentration is underrepresented, as higher concentrations were shown to be beneficial [40]. The trends of qCH_4 could also be a consequence of carbon regulation. The experiments indicate that during the initial phase of cultivation, the carbon flux shifts toward biomass production and shows a reversed trend after reaching the inflection point (Figure 3). Therefore, the qCH_4 decreases as the carbon flux in the biomass increases. This goes along with the theory that during sufficient nutrient supply, biomass growth is increased while the metabolism is less efficient. Conversely, under substrate limitation, growth decreases, but metabolic activity increases [46]. This effect is more pronounced during hyperthermophilic growth, as during cultivation of *M. marburgensis,* where Y_{CH4} at the inflection point correlates with qCH_{4max}, both exhibiting a positive trend that contradicts the proposed carbon flow regulation. Another possible explanation could be the instability of hyperthermophilic growth, where the rapid turnover leads to quick cell division and lysis, resulting in fewer enzymatically active cells overall. Furthermore, the pH was not measured during the experiment, as measuring pH in a closed environment is a highly inversive process. This is a known problem during closed batch gas fermentations and is extra challenging in anaerobic environments. An investigation of pH values under elevated pressures illustrates the decrease in CO_2 solubility under elevated temperatures. It can therefore be assumed that the influence of the pressure as well as the CO_2 solubility and consumption on the pH is limited under thermophilic and hyperthermophilic conditions.

The highest observed specific growth rate of *M. marburgensis* ($\mu_{max} = 0.55 \pm 0.06\ h^{-1}$) was lower than the previously proposed (Schönheit et al., 1980) and confirmed [32] optimum of $0.69\ h^{-1}$. However, earlier experiments were carried out under optimized conditions in bioreactors [32]. The qCH_{4max} of 169.59 ± 12.52 mmol $g^{-1}\ h^{-1}$ is, under consideration of the standard deviation, almost equal to the maximum reported qCH_4 [32], which is another indicator that the system during that time is not limited by the gas transfer or by liquid media depletion but by the physiology of the organism itself. Ascertained qCH_{4max} from *M. igneus*, *M. jannaschii*, *M. villous* were the highest ever recorded of any methanogen only challenged by Peillex *et al*. [47]. Here, reported qCH_4 values exceed other published data by several factors, along with significant variations, potentially not reflecting actual physiological limits of *M. marburgensis* [17]. The newly determined specific growth rates of the hyperthermophilic methanogens were, to our research, additionally the highest that had ever been reported [16,40,44,48]. Investigating qCH_4, MER, μ and Y_{CH4} shows lack of homogeneity in some cycles. Therefore, the statistical analysis was not conducted with the complete data set. Statistical relevance was found in the first cycle of qCH_4 between *M. marburgensis* and the hyperthermophiles but not between the hyperthermophilic organisms themselves. This highlights the methanation capacities between organisms of different temperature regimes. The biomethanation capacities of tested hyperthermophiles are probably too closely related to detect meaningful differences.

Long term cultivation with *M. maripaludis*

M. maripaludis is one of the best studied autotrophic, hydrogenotrophic methanogens and exhibit an advanced molecular toolkit, including CRISPR-mediated genome editing, that labels the organism as a valuable cell factory well-suited for physiological studies and the production of a wide range of different products [36,49–53]. As a result, increased efforts have been made towards improving biotechnological capability, such as in the production of biomass [35].

M. maripaludis was successfully cultivated over 80 h while constant monitoring and adjusting of the headspace pressure. Figure 4 and Figure S13 delineate the gas consumption during cultivation with suboptimal culture to headspace volume ratio. While the exponential increase in MER after the lag phase suggests exponential growth behavior, an inflection point is reached soon after, signaling the transfer from gas unlimited to limited conditions. Afterward, a decreasing trend in the MER, starting anew with each gassing cycle, can be observed. It is assumed that during gas limited conditions and biomass saturation the MER matches the GTR. Since the GTR is the product of the k_La and the driving force (Δc) from the gas to the liquid phase, and a stable k_La is assumed during the cultivation process, the MER can be considered a direct function of the pressure. However, the total CH_4 production decreases with each cycle, accompanied by an increase in cultivation time, evident by the reduced slope and the transition to more curved methanation kinetics over time. This hypothesis requires further testing, as cultivation results obtained from *M. maripaludis* using CO_2 as carbon source reveal liquid limitations as early as the second cycle. This is evidenced by a decline in MER at consistent pressure levels across successive methanation cycles (Figure S14), a trend also apparent in the wavelike pattern of the total amount of produced CH_4 in mol (Figure S15).

In conclusion: The GPC facilitates automated gassing of a wide range of different cultivation bottles in closed batch settings and allows for monitoring and regulation of the headspace gas pressure in real time over virtually unlimited duration. Here, the GPC has been specifically used to elucidate physiological and biotechnological characteristics of autotrophic, hydrogenotrophic methanogens. Further testing is needed to adapt the system for other gas conversion processes, such as those that support microbial activity followed by a fixed stoichiometry. First, the GPC allows quantification of physiological limits of autotrophic, hydrogenotrophic methanogens by eliminating gas limitation during growth of organisms and facilitates near optimal cultivation conditions in closed batch setups. As a result, previously unknown and very high qCH_4 values for three hyperthermophilic methanogens have been determined. Second, the device can accurately determine the occurrence of liquid limitations by visualizing the conversion point of metabolic inhibition. This allows for conclusions about limiting components and can be further exploited by high-throughput experiments. Third, the GPC may act as a tool for generating biomass on a large scale and by reaching specific growth rates that would not be possible in established manual closed batch cultivation settings. Finally, the GPC demonstrates application flexibility towards various applications in the fields of gas fermentation with hydrogenotrophic methanogens and archaea biotechnology.

Declarations

Ethics approval and consent to participate
Not applicable.

Consent for publication
Not applicable.

Availability of data and materials
The datasets generated and/or analysed during the current study are available in the PHAIDRA repository of Universität Wien, https://doi.org/10.25365/phaidra.518; https://doi.org/10.25365/phaidra.519; https://doi.org/10.25365/phaidra.597; https://doi.org/10.25365/phaidra.598

Competing interests
MU has competing interests as the owner of Creonia e.U.. All other authors declare not to have any competing interests.

Funding
The Österreichische Forschungsförderungsgesellschaft (FFG) funded this research through the FlaeXMethan project (grant 888509). Research was funded by The COMET center ACIB: Next Generation Bioproduction is funded by BMK, BMAW, SFG, Standortagentur Tirol, Government of Lower Austria und Vienna Business Agency in the framework of COMET – Competence Centers for Excellent Technologies. The COMET-Funding Program is managed by the Austrian Research Promotion Agency FFG.

Authors' contributions
WH, NSW and AR conducted experiments. MO and MU designed the GPC. MU wrote the GPC code. NSW and WH wrote the Matlab code. WH and NSW visualized data. MU, CP and SK-MRR conceived, designed, and supervised research. WH and SK-MRR wrote the manuscript. MU, CP and SK-MRR acquired funding.

Acknowledgements
Open access funding provided by the University of Vienna.

References

1. Liew, F. E. et al. Carbon-negative production of acetone and isopropanol by gas fermentation at industrial pilot scale. Nat Biotechnol 40, 335–344 (2022).
2. Woern, C. & Grossmann, L. Microbial gas fermentation technology for sustainable food protein production. Biotechnol Adv 69, 108240 (2023).
3. Pfeifer, K. et al. Archaea Biotechnology. Biotechnol Adv 47, 107668 (2021).
4. Straub, C. T. et al. Biotechnology of extremely thermophilic archaea. FEMS Microbiology Reviews 42, 543–578 (2018).
5. Carr, S. & Buan, N. R. Insights into the biotechnology potential of *Methanosarcina*. Front Microbiol 13, (2022).
6. Aparici-Carratalá, D., Esclapez, J., Bautista, V., Bonete, M.-J. & Camacho, M. Archaea: current and potential biotechnological applications. Res Microbiol 174, 104080 (2023).
7. Rittmann, S. K.-M. R., Pfeifer, K., Palabikyan, H., Ergal, İ. & Schuster, B. Archaea in der Biotechnologie. Biospektrum 27, 96–98 (2021).
8. Rittmann, S. K.-M. R. et al. Method for fermentatively producing norvaline. (2023).
9. Rittmann, S. K.-M. R. et al. Method for producing amino acids in a bioreactor. (2023).
10. Rittmann, S. K.-M. R. et al. Method for producing amino acids in a bioreactor with methanogenic microorganisms. (2023).
11. Rittmann, S. K.-M. R. et al. Method for producing amino acids with methanogenic microorganisms in a bioreactor. (2023).
12. Rittmann, S. K.-M. R. et al. One-carbon substrate-based biohydrogen production: microbes, mechanism, and productivity. Biotechnol Adv 33, 165–177 (2015).
13. Kim, M.-S. et al. Enhancement of the hydrogen productivity in microbial water gas shift reaction by *Thermococcus onnurineus* NA1 using a pressurized bioreactor. Int J Hydrogen Energ 42, 27593–27599 (2017).
14. Kim, M.-S. et al. CO-Dependent H2 Production by Genetically Engineered *Thermococcus onnurineus* NA1. Appl Environ Microbiol 79, 2048–2053 (2013).
15. Seifert, A. H., Rittmann, S. & Herwig, C. Analysis of process related factors to increase volumetric productivity and quality of biomethane with *Methanothermobacter marburgensis*. Appl Energy 132, 155–162 (2014).
16. Mauerhofer, L.-M. et al. Hyperthermophilic methanogenic archaea act as high-pressure CH4 cell factories. Commun Biol 4, 289 (2021).
17. Rittmann, S. K.-M. R., Seifert, A. H. & Bernacchi, S. Kinetics, multivariate statistical modelling, and physiology of CO2-based biological methane production. Appl Energy 216, 751–760 (2018).
18. Lyu, Z., Shao, N., Akinyemi, T. & Whitman, W. B. Methanogenesis. Curr Biol 28, R727–R732 (2018).

19. Lyu, Z., Rotaru, A.-E., Pimentel, M., Zhang, C.-J. & Rittmann, S. K.-M. R. Editorial: The methane moment - Cross-boundary significance of methanogens: Preface. Front Microbiol 13, (2022).

20. Borrel, G. et al. *Methanomethylophilus alvi* gen. nov., sp. nov., a Novel Hydrogenotrophic Methyl-Reducing Methanogenic Archaea of the Order Methanomassiliicoccales Isolated from the Human Gut and Proposal of the Novel Family Methanomethylophilaceae fam. nov. Microorg 11, 2794 (2023).

21. Taubner, R.-S. et al. Biological methane production under putative Enceladus-like conditions. Nat Commun 9, 748 (2018).

22. Kurth, J. M., Op Den Camp, H. J. M. & Welte, C. U. Several ways one goal—methanogenesis from unconventional substrates. Appl Microbiol Biotechnol 104, 6839–6854 (2020).

23. Rittmann, S. K.-M. R., Seifert, A. H. & Krajete, A. Biomethanisierung — ein Prozess zur Ermöglichung der Energiewende? Biospektrum 20, 816–817 (2014).

24. Rittmann, S. K.-M. R. A Critical Assessment of Microbiological Biogas to Biomethane Upgrading Systems. Adv Biochem Eng Biotechnol 151, 117–135 (2015).

25. Taubner, R.-S. et al. Lipidomics and Comparative Metabolite Excretion Analysis of Methanogenic Archaea Reveal Organism-Specific Adaptations to Varying Temperatures and Substrate Concentrations. mSyst 8, e0115922 (2023).

26. Reischl, B. et al. Quantitative analysis of amino acid excretion by *Methanothermobacter marburgensis* under N2-fixing conditions. Sci Rep 15, 3755 (2025).

27. Rittmann, S., Seifert, A. & Herwig, C. Essential prerequisites for successful bioprocess development of biological CH4 production from CO2 and H2. Crit Rev Biotechnol 35, 141–151 (2015).

28. Pappenreiter, P. A., Zwirtmayr, S., Mauerhofer, L., Rittmann, S. K. R. & Paulik, C. Development of a simultaneous bioreactor system for characterization of gas production kinetics of methanogenic archaea at high pressure. Eng Life Sci 19, 537–544 (2019).

29. Mauerhofer, L.-M. et al. Methods for quantification of growth and productivity in anaerobic microbiology and biotechnology. Folia Microbiol 64, 321–360 (2019).

30. Hanišáková, N., Vítězová, M. & Rittmann, S. K.-M. R. The Historical Development of Cultivation Techniques for Methanogens and Other Strict Anaerobes and Their Application in Modern Microbiology. Microorg 10, 412 (2022).

31. Taubner, R.-S. & Rittmann, S. K.-M. R. Method for Indirect Quantification of CH4 Production via H2O Production Using Hydrogenotrophic Methanogens. Front Microbiol 7, 532 (2016).

32. Abdel Azim, A. et al. The physiology of trace elements in biological methane production. Bioresour Technol 241, 775–786 (2017).

33. Takors, R. et al. Using gas mixtures of CO, CO2 and H2 as microbial substrates: the do's and don'ts of successful technology transfer from laboratory to production scale. Microb Biotechnol 11, 606–625 (2018).

34. Abdel Azim, A., Rittmann, S. K.-M. R., Fino, D. & Bochmann, G. The physiological effect of heavy metals and volatile fatty acids on *Methanococcus maripaludis* S2. Biotechnol Biofuels 11, 301 (2018).

35. Palabikyan, H. et al. Scale-up of biomass production by *Methanococcus maripaludis*. Front Microbiol 13, (2022).

36. Walters, A. D., Smith, S. E. & Chong, J. P. J. Shuttle Vector System for *Methanococcus maripaludis* with Improved Transformation Efficiency. Appl Environ Microbiol 77, 2549–2551 (2011).

37. Long, F., Cheung, C.-Y., Whitman, W. B., Cook, G. M. & Ronimus, R. S. Using genome comparisons of wild-type and resistant mutants of *Methanococcus maripaludis* to help understand mechanisms of resistance to methane inhibitors. Access Microbiol 3, 000244 (2021).

38. Jones, W. J., Paynter, M. J. B. & Gupta, R. Characterization of *Methanococcus maripaludis* sp. nov., a new methanogen isolated from salt marsh sediment. Arch Microbiol 135, 91–97 (1983).

39. Schill, N., Van Gulik, W. M., Voisard, D. & Von Stockar, U. Continuous cultures limited by a gaseous substrate: Development of a simple, unstructured mathematical model and experimental verification with *Methanobacterium thermoautotrophicum*. Biotechnol Bioeng 51, 645–658 (2000).

40. Mukhopadhyay, B., Johnson, E. F. & Wolfe, R. S. Reactor-Scale Cultivation of the Hyperthermophilic Methanarchaeon *Methanococcus jannaschii* to High Cell Densities. Appl Environ Microbiol 65, 5059–5065 (1999).

41. Susanti, D., Frazier, M. C. & Mukhopadhyay, B. A Genetic System for *Methanocaldococcus jannaschii*: An Evolutionary Deeply Rooted Hyperthermophilic Methanarchaeon. Front Microbiol 10, (2019).

42. Fink, C. et al. A Shuttle-Vector System Allows Heterologous Gene Expression in the Thermophilic Methanogen *Methanothermobacter thermautotrophicus* DH. mBio 12, (2021).

43. Schönheit, P., Moll, J. & Thauer, R. K. Growth parameters (Ks, μmax, Ys) of *Methanobacterium thermoautotrophicum*. Arch Microbiol 127, 59–65 (1980).

44. Topçuoğlu, B. D., Meydan, C., Nguyen, T. B., Lang, S. Q. & Holden, J. F. Growth Kinetics, Carbon Isotope Fractionation, and Gene Expression in the Hyperthermophile *Methanocaldococcus jannaschii* during Hydrogen-Limited Growth and Interspecies Hydrogen Transfer. Appl Environ Microbiol 85, e00180-19 (2019).

45. Grahame, D. A. & Stadtman, T. C. Redox Enzymes of Methanogens: Physicochemical Properties of Selected, Purified Oxidoreductases. in Methanogenesis: Ecology, Physiology, Biochemistry & Genetics (ed. Ferry, J. G.) 335–359 (Springer US, Boston, MA, 1993). doi:10.1007/978-1-4615-2391-8_8.

46. Molenaar, D., van Berlo, R., de Ridder, D. & Teusink, B. Shifts in growth strategies reflect tradeoffs in cellular economics. Mol Syst Biol 5, 323 (2009).

47. Peillex, J.-P., Fardeau, M.-L. & Belaich, J.-P. Growth of *Methanobacterium thermoautotrophicum* on H2-CO2: High CH4 productivities in continuous culture. Biomass 21, 315–321 (1990).

48. Miller, J. F., Shah, N. N., Nelson, C. M., Ludlow, J. M. & Clark, D. S. Pressure and Temperature Effects on Growth and Methane Production of the Extreme Thermophile *Methanococcus jannaschii*. Appl Environ Microbiol 54, 3039–3042 (1988).

49. Goyal, N., Zhou, Z. & Karimi, I. A. Metabolic processes of *Methanococcus maripaludis* and potential applications. Microb Cell Fact 15, 107 (2016).

50. Bao, J., De Dios Mateos, E. & Scheller, S. Efficient CRISPR/Cas12a-Based Genome-Editing Toolbox for Metabolic Engineering in *Methanococcus maripaludis*. ACS Synth Biol 11, 2496–2503 (2022).

51. Li, J. et al. CRISPR-Cas9 Toolkit for Genome Editing in an Autotrophic CO 2 -Fixing Methanogenic Archaeon. Microbiol Spectr 10, e01165-22 (2022).

52. Xu, Q. et al. A robust genetic toolbox for fine-tuning gene expression in the CO2-Fixing methanogenic archaeon *Methanococcus maripaludis*. Metab Eng 79, 130–145 (2023).

53. Du, Q. et al. An improved CRISPR and CRISPR interference (CRISPRi) toolkit for engineering the model methanogenic archaeon *Methanococcus maripaludis*. Microb Cell Fact 23, 239 (2024).

General discussion

Pfeifer *et al*. highlight that biotechnological applications in archaea exhibit varying levels of development, with the most advanced and well-understood applications focusing on gas fermentation (methane and hydrogen) and the industrial utilization of their enzymes [1]. This work presents novel advances in two key areas of archaeal biotechnology. First, the enzymatic pathway for polyhydroxyalkanoate (PHA) production is partially characterized for the first time in archaea different than the traditionally well studied haloarchaea. Second, a device is developed and operated that allows for the cultivation of autotrophic hydrogenotrophic methanogens in batch cultivation mode without gaseous substrate limitations, combined with automated analysis to determine physiological and biotechnological relevant parameters of the organism.

The study conducted in the first chapter represents the first reported characterization of the PHA biosynthesis pathway in an ammonia-oxidizing archaea, specifically in *N. viennensis*. The identification and expression of the *phaAa1*, *phaAb1*, *phaB*, *phaC*, and *phaE* genes reveal similarities with PHA biosynthesis pathways in other microorganisms and suggests synthesis of SCL PHAs. For instance, the β-ketothiolase of *N. viennensis* consists of two different subunit (PhaAa1 and PhaAb1), a feature shared with other investigated archaea, such as haloarchaea [24]. However, the challenging expression of soluble cytosolic β-ketothiolase in *E. coli* might indicate toxic effects to the host organism, possibly due to acetyl-CoA depletion, a central metabolite in multiple metabolic pathways. On the other hand, the acetoacetyl-CoA reductase (PhaB) was successfully purified and performed kinetic assays confirmed its activity of the enzyme, with the kinetic parameters falling within the average range of other reported PhaB enzymes in both bacteria and archaea (k_{cat}/K_m between 2 and $9 \cdot 10^6$ $(mol\ L^{-1})^{-1}\ s^{-1}$) [25–31]. Despite this promising result, the wild-type PhaB kinetics are almost 20 times less efficient than the engineered-optimized PhaB from *C. necator*. A particularly interesting discovery is the possible heterotetrameric conformation of PHA synthase (PhaCE), as most previously described PHA synthases have been homodimeric or heterodimeric [32,33]. This uncommon structure might confer a different specificity for PHA polymerization or be promiscuous and accept other monomers [34], suggesting that the synthesized polymer could differ from traditional PHB and PHV, opening new possibilities for producing bioplastics with unique properties. However, further experiments are required to confirm this hypothesis. The determination of the other enzymes' kinetic parameters is needed to fully characterize the pathway and propose improvements based on protein and metabolic engineering. These results will not only expand our understanding of PHA biosynthesis in archaea but also pave the way for more bioprospection in archaea searching for new biodegradable bioplastics.

In the second chapter, a novel device called the Gas and Pressure Controller (GPC) was developed and validated for monitoring and controlling headspace gas pressure in batch for the cultivation of hydrogenotrophic methanogens. The ability to regulate the pressure eliminates gaseous substrate limitations, enhancing the screening for relevant physiologically and biotechnological parameters. Furthermore, these advances represent a significant step in optimizing the cultivation of hydrogenotrophic methanogen and their application in biotechnological processes.

A key component of the GPC is a MATLAB-implemented algorithm that processes the raw data by eliminating background data and reducing noise by data smoothing as well as organizing the data into methanation cycles. While this approach results in some data loss, it allows for the reproducible and fast determination of key parameters. The calculation is facilitated by the pressure drop monitored in real time, specifically the methane evolution rate (MER) and the

specific methane productivity (qCH_4). These parameters are essential for standardizing and comparing cultures with in literature-reported data.

The values obtained in this proof-of-concept study for the four evaluated methanogens are unprecedented in literature [35–37], with methane production rates of 169.59 ± 12.52 mmol g^{-1} h^{-1}, 420.21 ± 89.46 mmol g^{-1} h^{-1}, 364.52 ± 25.50 mmol g^{-1} h^{-1} and of 356.38 ± 20.79 mmol g^{-1} h^{-1} for *M. marburgensis, M. igneus, M. jannaschii* and *M. villosus*, respectively. In some cases, the CH_4 production rates in batch cultures exceeded previously reported values by more than tenfold. This novel finding suggests that eliminating gaseous limitations through real time pressure control and monitoring, significantly enhances methanogen metabolism, allowing them to reach their full physiological potential. Moreover, removing gaseous limitations shifts optimization efforts toward liquid substrates, enabling the fine-tuning of media to meet the specific needs of each microorganism.

This new cultivation setting provides a standardized and efficient method for evaluating various organisms and metabolic pathways involving gas consumption in biotechnological applications, such as biological CH_4 and H_2 production. The calculation of the physiological parameters bridges archaeal biotechnology and industrial applications by offering precise values for reactor scaling and substrate conversion. These findings open the possibility of applying methanogens to reduce reliance on fossil-based natural gas and contribute to industrial decarbonization.

While the GPC introduced significant innovations, there is potential for further optimization. Integrating real-time depressurization analysis and OD measurements would enhance culture control, streamline automation, and improve usability. Additionally, precise quantification of CO_2 conversion into CH_4 or biomass would serve as a key metric for evaluating metabolic efficiency.

References

1. Pfeifer, K. *et al.* Archaea Biotechnology. *Biotechnology Advances* **47**, 107668 (2021).
2. Fox, P. F., Guinee, T. P., Cogan, T. M. & McSweeney, P. L. H. Cheese: Historical Aspects. in *Fundamentals of Cheese Science* (eds. Fox, P. F., Guinee, T. P., Cogan, T. M. & McSweeney, P. L. H.) 1–10 (Springer US, Boston, MA, 2017). doi:10.1007/978-1-4899-7681-9_1.
3. Brogren, C.-H. Louis Pasteur—The life of a controversial scientist with a prepared mind, driven by curiosity, motivation, and competition. *APMIS* **132**, 7–30 (2024).
4. Kafarski, P. Rainbow code of biotechnology. *Chemik* **66**, 811–816 (2012).
5. Juhas, M., Reuß, D. R., Zhu, B. & Commichau, F. M. Bacillus subtilis and Escherichia coli essential genes and minimal cell factories after one decade of genome engineering. *Microbiology* **160**, 2341–2351 (2014).
6. Dikicioglu, D., Wood, V., Rutherford, K. M., McDowall, M. D. & Oliver, S. G. Improving functional annotation for industrial microbes: a case study with *Pichia pastoris*. *Trends in Biotechnology* **32**, 396–399 (2014).
7. Duncker, K. E., Holmes, Z. A. & You, L. Engineered microbial consortia: strategies and applications. *Microbial Cell Factories* **20**, 211 (2021).
8. Cabrera, Ma. Á. & Blamey, J. M. Biotechnological applications of archaeal enzymes from extreme environments. *Biological Research* **51**, 37 (2018).
9. Baker, B. J. *et al.* Diversity, ecology and evolution of Archaea. *Nat Microbiol* **5**, 887–900 (2020).
10. Aparici-Carratalá, D., Esclapez, J., Bautista, V., Bonete, M.-J. & Camacho, M. Archaea: current and potential biotechnological applications. *Research in Microbiology* **174**, 104080 (2023).
11. Ammonia-Oxidizing Archaea (AOA) Play with Ammonia-Oxidizing Bacteria (AOB) in Nitrogen Removal from Wastewater - Yin - 2018 - Archaea - Wiley Online Library. https://onlinelibrary.wiley.com/doi/full/10.1155/2018/8429145.
12. Huang, L. *et al.* Ammonia-oxidizing archaea are integral to nitrogen cycling in a highly fertile agricultural soil. *ISME COMMUN.* **1**, 1–12 (2021).
13. Taubner, R.-S. *et al.* Lipidomics and Comparative Metabolite Excretion Analysis of Methanogenic Archaea Reveal Organism-Specific Adaptations to Varying Temperatures and Substrate Concentrations. *mSyst* **8**, e0115922 (2023).
14. Reischl, B. *et al.* Quantitative analysis of amino acid excretion by Methanothermobacter marburgensis under N2-fixing conditions. *Sci Rep* **15**, 3755 (2025).
15. Vera, M., Schippers, A., Hedrich, S. & Sand, W. Progress in bioleaching: fundamentals and mechanisms of microbial metal sulfide oxidation – part A. *Appl Microbiol Biotechnol* **106**, 6933–6952 (2022).
16. Innovations in Copper: Mining & Extraction: Producing copper nature's way: Bioleaching. https://www.copper.org/publications/newsletters/innovations/2004/05/producing_copper_natures_way_bioleaching.html.

17. GHG emissions of hydrogen and its derivatives – Global Hydrogen Review 2024 – Analysis. *IEA* https://www.iea.org/reports/global-hydrogen-review-2024/ghg-emissions-of-hydrogen-and-its-derivatives.

18. Akhlaghi, N. & Najafpour-Darzi, G. A comprehensive review on biological hydrogen production. *International Journal of Hydrogen Energy* **45**, 22492–22512 (2020).

19. Lyu, Z., Shao, N., Akinyemi, T. & Whitman, W. B. Methanogenesis. *Current Biology* **28**, R727–R732 (2018).

20. Sagong, H.-Y., Son, H. F., Choi, S. Y., Lee, S. Y. & Kim, K.-J. Structural Insights into Polyhydroxyalkanoates Biosynthesis. *Trends in Biochemical Sciences* **43**, 790–805 (2018).

21. Sharma, V., Sehgal, R. & Gupta, R. Polyhydroxyalkanoate (PHA): Properties and Modifications. *Polymer* **212**, 123161 (2021).

22. Obruca, S. *et al.* Novel unexpected functions of PHA granules. *Appl Microbiol Biotechnol* **104**, 4795–4810 (2020).

23. Samrot, A. V. *et al.* The Synthesis, Characterization and Applications of Polyhydroxyalkanoates (PHAs) and PHA-Based Nanoparticles. *Polymers* **13**, 3302 (2021).

24. Hou, J. *et al.* Haloarchaeal-Type β-Ketothiolases Involved in Poly(3-Hydroxybutyrate-co-3-Hydroxyvalerate) Synthesis in Haloferax mediterranei. *Applied and Environmental Microbiology* **79**, 5104–5111 (2013).

25. Liu, L., Schubert, D. M., Könneke, M. & Berg, I. A. (S)-3-Hydroxybutyryl-CoA Dehydrogenase From the Autotrophic 3-Hydroxypropionate/4-Hydroxybutyrate Cycle in Nitrosopumilus maritimus. *Front. Microbiol.* **12**, (2021).

26. Matsumoto, K. *et al.* Directed Evolution and Structural Analysis of NADPH-Dependent Acetoacetyl Coenzyme A (Acetoacetyl-CoA) Reductase from Ralstonia eutropha Reveals Two Mutations Responsible for Enhanced Kinetics. *Applied and Environmental Microbiology* **79**, 6134–6139 (2013).

27. Wang, T. *et al.* Acetoacetyl-CoA reductase PhaB as an excellent anti-Prelog biocatalyst for the synthesis of chiral β-hydroxyl ester and the molecular basis of its catalytic performance. *Molecular Catalysis* **514**, 111854 (2021).

28. Olavarria, K. *et al.* An NADH preferring acetoacetyl-CoA reductase is engaged in poly-3-hydroxybutyrate accumulation in *Escherichia coli*. *Journal of Biotechnology* **325**, 207–216 (2021).

29. Kim, E.-J. *et al.* Crystal Structure of (S)-3-Hydroxybutyryl-CoA Dehydrogenase from Clostridium butyricum and Its Mutations that Enhance Reaction Kinetics. *Journal of Microbiology and Biotechnology* **24**, 1636–1643 (2014).

30. PACKTER, N. M. & FLATMAN, S. Characterization of acetoacetyl-CoA reductase (3-oxoreductase) from Streptomyces coelicolor: Its possible role in polyhydroxybutyrate biosynthesis. *Biochemical Society Transactions* **11**, 598–599 (1983).

31. Mothes, G. & Babel, W. Methylobacterium rhodesianum MB 126 possesses two acetoacetyl-CoA reductases. *Arch. Microbiol.* **161**, 277–280 (1994).

32. Chek, M. F., Hiroe, A., Hakoshima, T., Sudesh, K. & Taguchi, S. PHA synthase (PhaC): interpreting the functions of bioplastic-producing enzyme from a structural perspective. *Appl Microbiol Biotechnol* **103**, 1131–1141 (2019).

33. Zher Neoh, S. *et al.* Polyhydroxyalkanoate synthase (PhaC): The key enzyme for biopolyester synthesis. *Current Research in Biotechnology* **4**, 87–101 (2022).

34. Chae, T. U. *et al.* Biosynthesis of poly(ester amide)s in engineered Escherichia coli. *Nat Chem Biol* 1–11 (2025) doi:10.1038/s41589-025-01842-2.

35. Peillex, J.-P., Fardeau, M.-L. & Belaich, J.-P. Growth of *Methanobacterium thermoautotrophicum* on H2□CO2: High CH4 productivities in continuous culture. *Biomass* **21**, 315–321 (1990).

36. Abdel Azim, A. *et al.* The physiology of trace elements in biological methane production. *Bioresour Technol* **241**, 775–786 (2017).

37. Rittmann, S. K.-M. R., Seifert, A. H. & Bernacchi, S. Kinetics, multivariate statistical modelling, and physiology of CO2-based biological methane production. *Applied Energy* **216**, 751–760 (2018).

Appendix

Chapter 1: Supplementary Material

Supplementary Table 1 Initial velocities of PhaB with different acetoacetyl-CoA (AcAc-CoA) concentrations

Tested Initial velocity	AcAc-CoA / mmol L^{-1}	Initial velocity (IV)	IV-Blank	Average	Standard deviation
IV1	0.0045	$1.886 \cdot 10^{-4}$	$1.758 \cdot 10^{-4}$	$1.396 \cdot 10^{-4}$	$2.873 \cdot 10^{-5}$
		$1.617 \cdot 10^{-4}$	$1.489 \cdot 10^{-4}$		
		$1.339 \cdot 10^{-4}$	$1.211 \cdot 10^{-4}$		
		$1.252 \cdot 10^{-4}$	$1.124 \cdot 10^{-4}$		
IV2	0.00675	0.0001229	$1.101 \cdot 10^{-4}$	$1.436 \cdot 10^{-4}$	$3.475 \cdot 10^{-5}$
		$1.840 \cdot 10^{-4}$	$1.712 \cdot 10^{-4}$		
		$1.886 \cdot 10^{-4}$	$1.758 \cdot 10^{-4}$		
		$1.299 \cdot 10^{-4}$	$1.171 \cdot 10^{-4}$		
IV3	0.009	$1.499 \cdot 10^{-4}$	$1.371 \cdot 10^{-4}$	$1.431 \cdot 10^{-4}$	$1.537 \cdot 10^{-5}$
		$1.587 \cdot 10^{-4}$	$1.459 \cdot 10^{-4}$		
		$1.393 \cdot 10^{-4}$	$1.265 \cdot 10^{-4}$		
		$1.757 \cdot 10^{-4}$	$1.629 \cdot 10^{-4}$		
IV4	0.0135	$3.267 \cdot 10^{-4}$	$3.139 \cdot 10^{-4}$	$3.444 \cdot 10^{-4}$	$4.947 \cdot 10^{-5}$
		$4.310 \cdot 10^{-4}$	$4.182 \cdot 10^{-4}$		
		$3.396 \cdot 10^{-4}$	$3.268 \cdot 10^{-4}$		
		$3.316 \cdot 10^{-4}$	$3.188 \cdot 10^{-4}$		
IV5	0.018	$3.455 \cdot 10^{-4}$	$3.327 \cdot 10^{-4}$	$4.294 \cdot 10^{-4}$	$7.513 \cdot 10^{-5}$
		$4.641 \cdot 10^{-4}$	$4.514 \cdot 10^{-4}$		
		$5.260 \cdot 10^{-4}$	$5.132 \cdot 10^{-4}$		
		$4.332 \cdot 10^{-4}$	$4.204 \cdot 10^{-4}$		
IV6	0.036	$4.892 \cdot 10^{-4}$	$4.764 \cdot 10^{-4}$	$4.9829 \cdot 10^{-4}$	$8.5835 \cdot 10^{-5}$
		$4.438 \cdot 10^{-4}$	$4.310 \cdot 10^{-4}$		
		$6.002 \cdot 10^{-4}$	$5.875 \cdot 10^{-4}$		
IV7	0.054	$6.215 \cdot 10^{-4}$	$6.087 \cdot 10^{-4}$	$5.968 \cdot 10^{-4}$	$1.075 \cdot 10^{-4}$
		$6.299 \cdot 10^{-4}$	$6.171 \cdot 10^{-4}$		
		$5.357 \cdot 10^{-4}$	$5.229 \cdot 10^{-4}$		
		$6.514 \cdot 10^{-4}$	$6.386 \cdot 10^{-4}$		
IV8	0.072	$7.957 \cdot 10^{-4}$	$7.829 \cdot 10^{-4}$	$7.2542 \cdot 10^{-4}$	$5.2322 \cdot 10^{-5}$
		$7.009 \cdot 10^{-4}$	$6.881 \cdot 10^{-4}$		
		$7.181 \cdot 10^{-4}$	$7.053 \cdot 10^{-4}$		
IV9	0.108	$7.081 \cdot 10^{-4}$	$6.953 \cdot 10^{-4}$	$7.459 \cdot 10^{-4}$	$7.555 \cdot 10^{-5}$
		$8.127 \cdot 10^{-4}$	$7.999 \cdot 10^{-4}$		
		$8.258 \cdot 10^{-4}$	$8.130 \cdot 10^{-4}$		
		$6.881 \cdot 10^{-4}$	$6.754 \cdot 10^{-4}$		
IV10	0.126	$8.610 \cdot 10^{-4}$	$8.482 \cdot 10^{-4}$	$8.4683 \cdot 10^{-4}$	$9.2731 \cdot 10^{-5}$
		$8.156 \cdot 10^{-4}$	$8.028 \cdot 10^{-4}$		

		$9.022 \cdot 10^{-4}$	$8.894 \cdot 10^{-4}$		
IV11	0.18	$8.569 \cdot 10^{-4}$	$8.441 \cdot 10^{-4}$	$7.8178 \cdot 10^{-4}$	$4.3301 \cdot 10^{-5}$
		$6.883 \cdot 10^{-4}$	$6.755 \cdot 10^{-4}$		
		$8.386 \cdot 10^{-4}$	$8.258 \cdot 10^{-4}$		

Chapter 2: Supplementary Material

Supplementary material to: Method for automated high performance closed batch cultivation of gas-fermenting methanogens

Walter Hofmann[1,2,#], Marco Orthofer[3,#], Nicolás Salas Wallach[1,2], Aquilla Ruddyard[1], Markus Ungerank[4], Christian Paulik[3], Simon K.-M. R. Rittmann[1,*]

[1]Archaea Physiology & Biotechnology Group, Department of Functional and Evolutionary Ecology, Universität Wien, Wien, Austria
[2]Acib GmbH, Wien, Austria
[3]Institute for Chemical Technology of Organic Materials, Johannes Kepler Universität Linz, Linz, Austria
[4]Creonia e.U., Perg, Austria

[#]These authors contributed equally to this work

[*]Corresponding author:
Dr. Simon K.-M. R. Rittmann, Privatdoz.
Archaea Physiology & Biotechnology Group
Department of Functional and Evolutionary Ecology
Djerassiplatz 1
Universität Wien
1030 Wien
Austria
Email: simon.rittmann@univie.ac.at

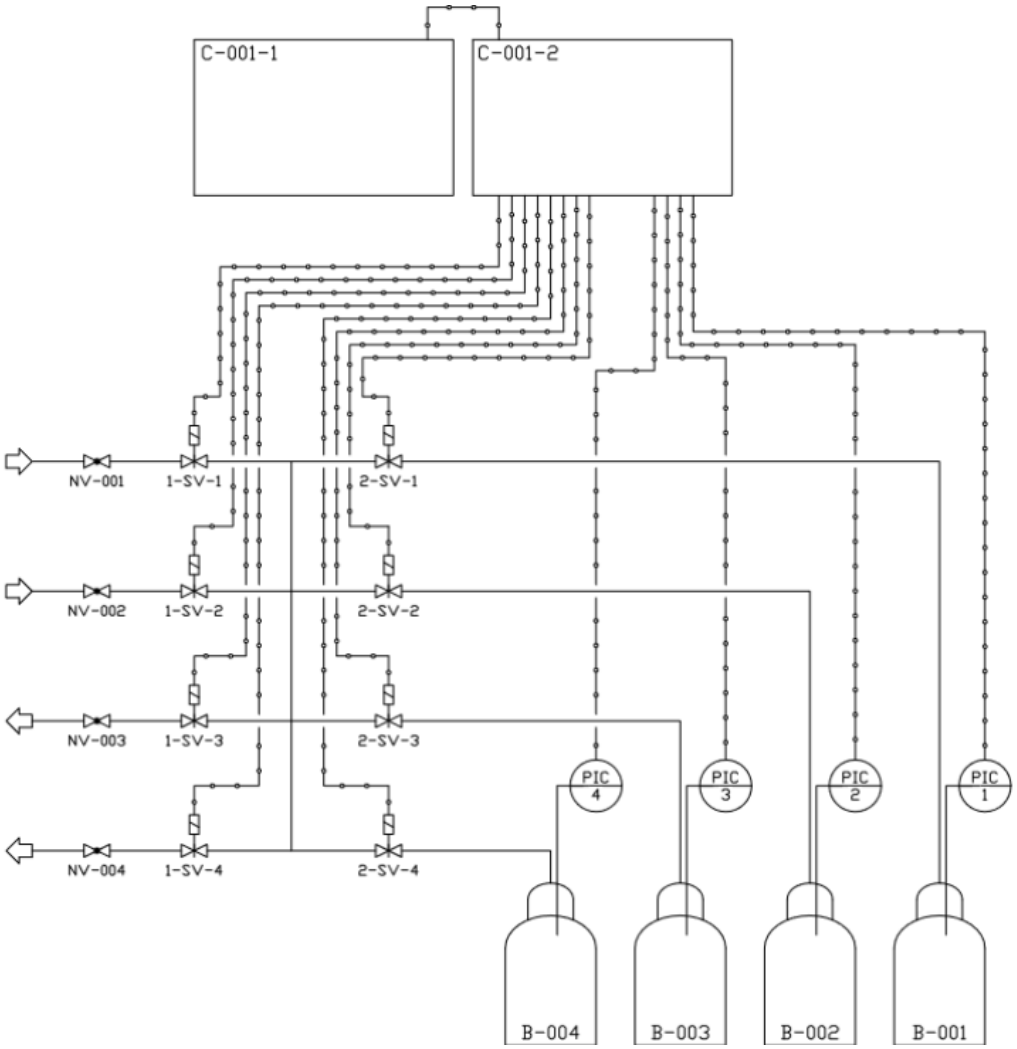

Figure S1: Instrumentation diagram of the GPC. One unit consists of eight valves (SV1-8) equipped with four pressure sensors (PIC1-4) and four throttling valves (NV1-4) connected to a controlling device allowing for pressure monitoring of four cultivation bottles simultaneously. Individual components are connected via pressure resistant tubing.

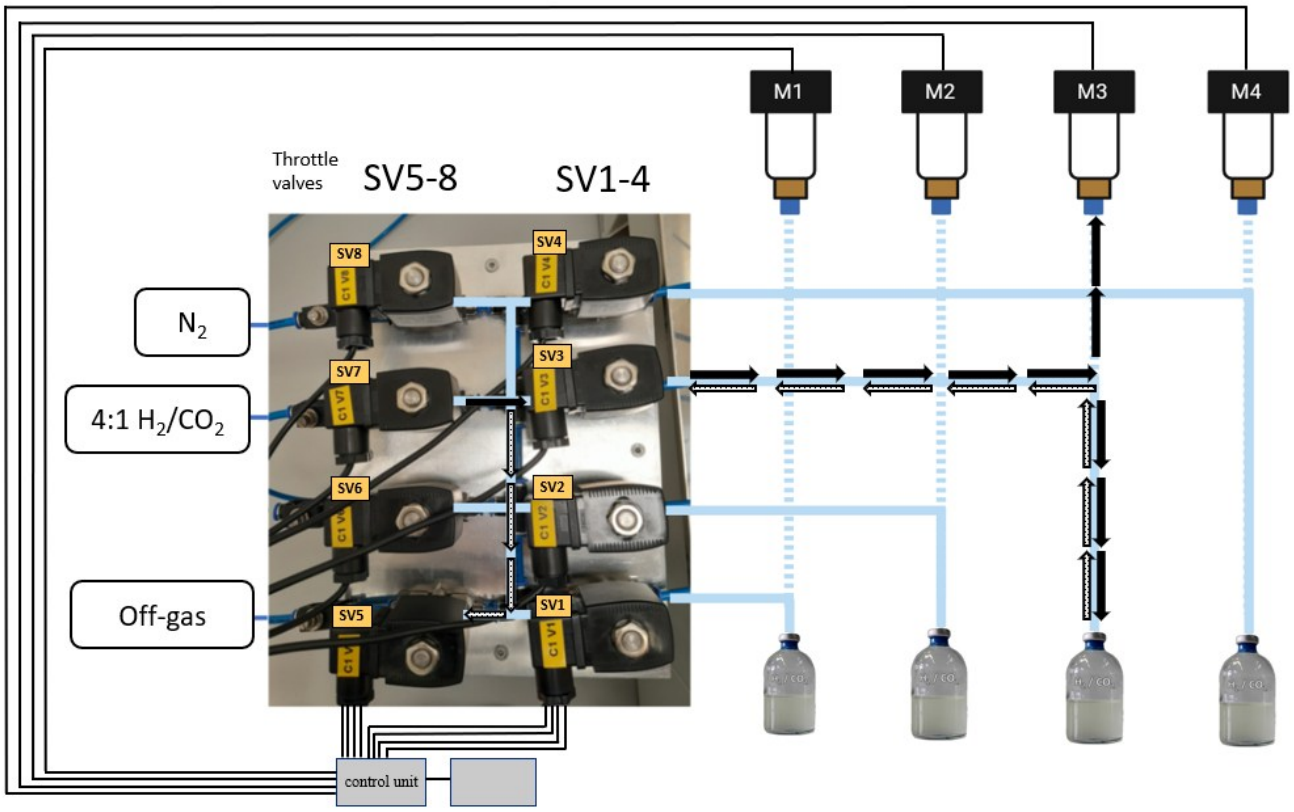

Figure S2: Technical setup of the GPC and illustration of its functionality. Eight valves (SV1–SV8) are arranged in two parallel rows and connected to a control device along with four pressure sensors (M1–M4) and four throttling valves. All components are interconnected using pressure-resistant tubing. Valves 7 and 9 are opened simultaneously, allowing the gas (H_2/CO_2) to stream into the serum bottles, resulting in a pressure buildup (black arrows). During sparging, Valves 5 and 8 are opened, reducing the pressure in the serum bottles (white arrows). The flushed gas is safely discarded through the fume hood (Sterile filters not shown).

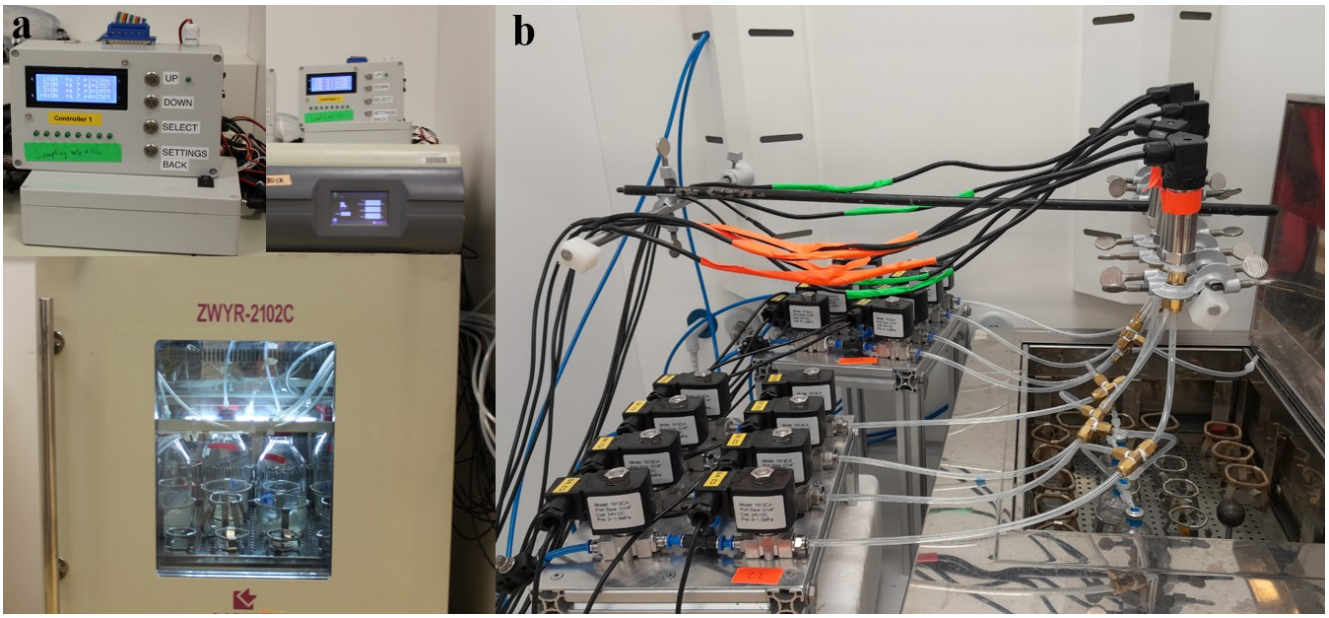

Figure S3: Images of the experimental setup of the GPC. a. The gas lines are introduced into the air incubator from the side and attached to the bottles. The controlling system for data monitoring and power supply is additionally shown. b. GPC set-up in the fume hood.

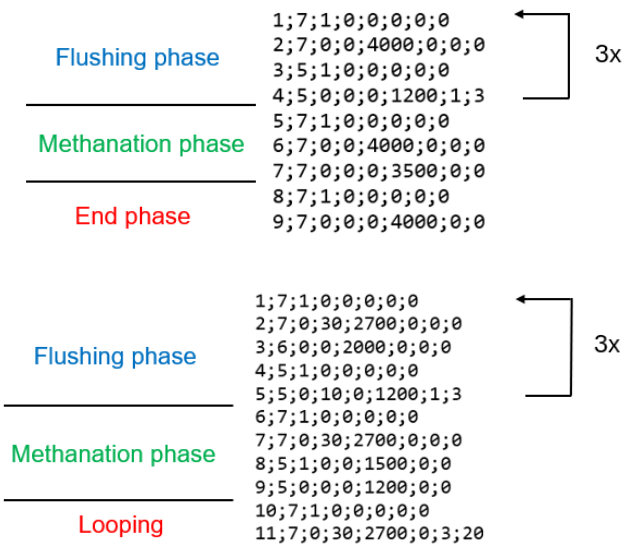

Figure S4: Representation of the programs used in CSV format. Left: Program used for cultivation of thermophilic/hyperthermophilic methanogens. After the end phase, one methanation cycle concludes and OD_{578} is measured. Right: Program applied for autonomous overnight cultivation with *Methanococcus maripaludis*. After the methanation phase the culture is repressurized and looped back to the flushing phase (20x). Prior to operation, the required program must be defined and comprise of a series of executable steps. Column 1 (Step): Program step with consecutive number (1-30); Column 2 (valve): Number of the valve to be opened or closed (5,6,7 or 8) (Note: Valves 1 to 4 are automatically controlled); Column 3 (statusValve): 0 for closed valve, 1 opens the corresponding valve; Column 4 (ValveOnTime): Indicates the maximum opening time of the valve in seconds; Column 5 (PressureHigher): The step ends when the detected pressure in mbar is higher than the set pressure value; Column 6 (PressureLower): The step ends when the measured pressure in mbar is lower than the set pressure value; Column 7 (Jump): The program continues with the step specified after the criteria in columns 4, 5 or 6 is met; Column 8 (Number of jumps): Indicates the number of times the program should repeat the step specified in column 7. All valves can also be controlled manually.

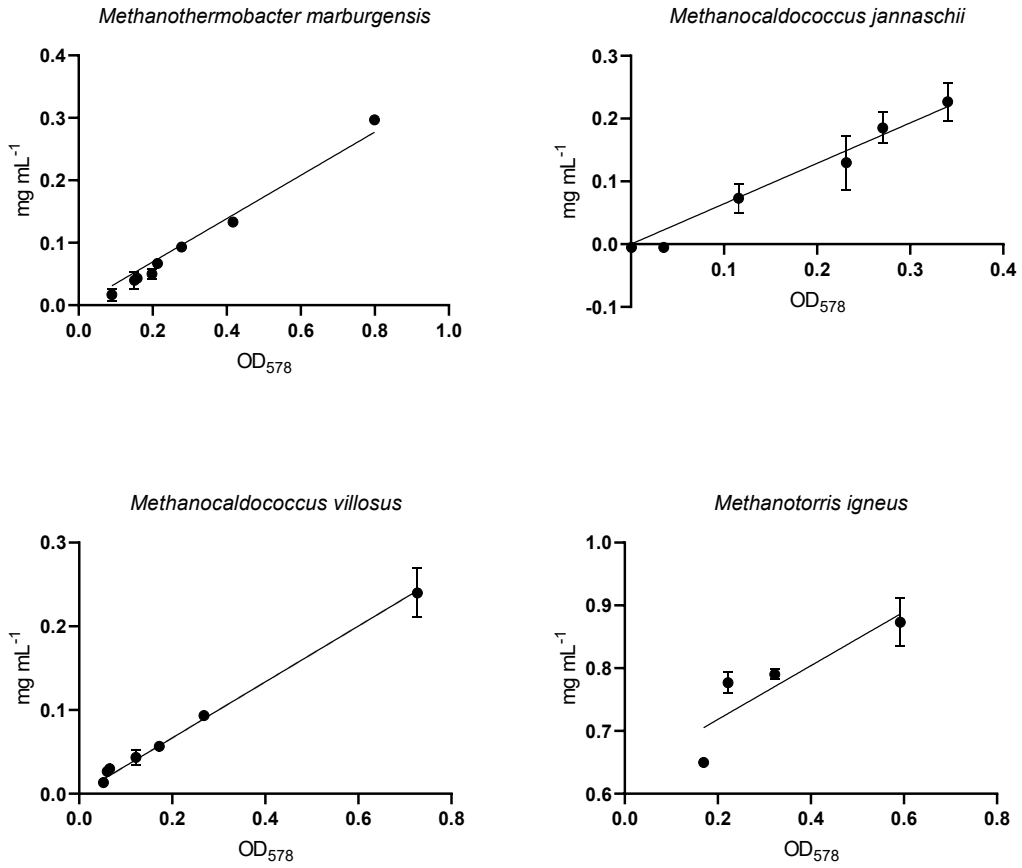

Figure S5: Dry biomass in mg mL^{-1} blotted over OD_{578}. Linear regression forced through zero (except *M. igneus*). Slope determines the OD_{578} to dry biomass coefficient x.

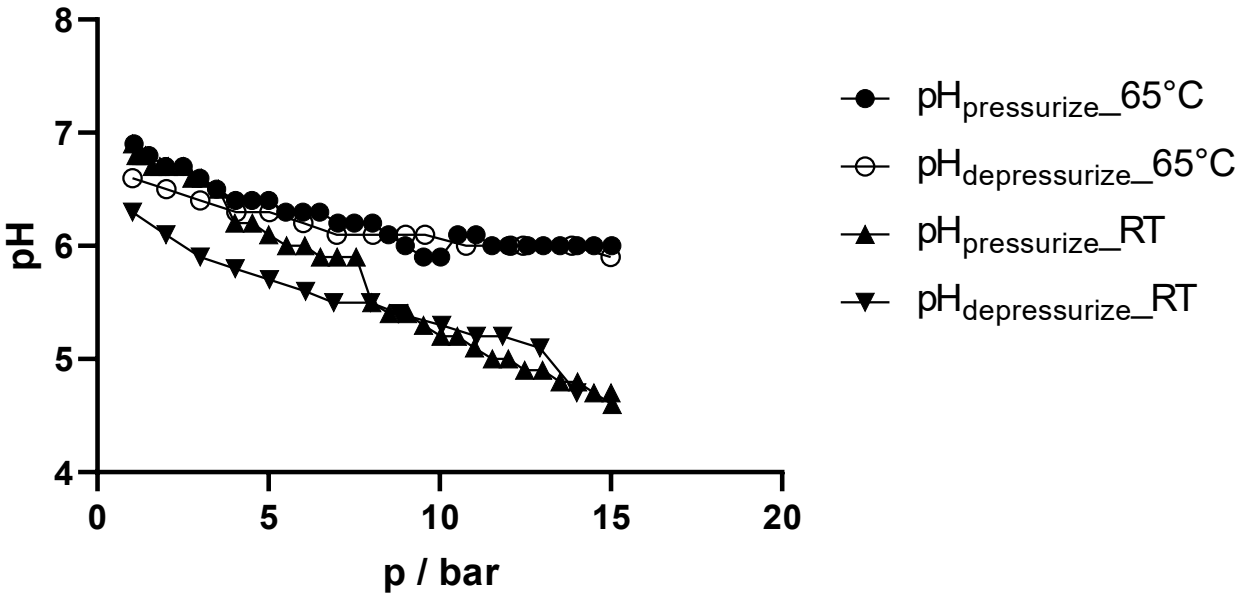

Figure S6: The pH dependence on bar overpressure was analyzed using a 4:1 H_2/CO_2 gas mixture at room temperature (RT) and 65°C. pH measurements were taken during the pressurization and depressurization of the medium.

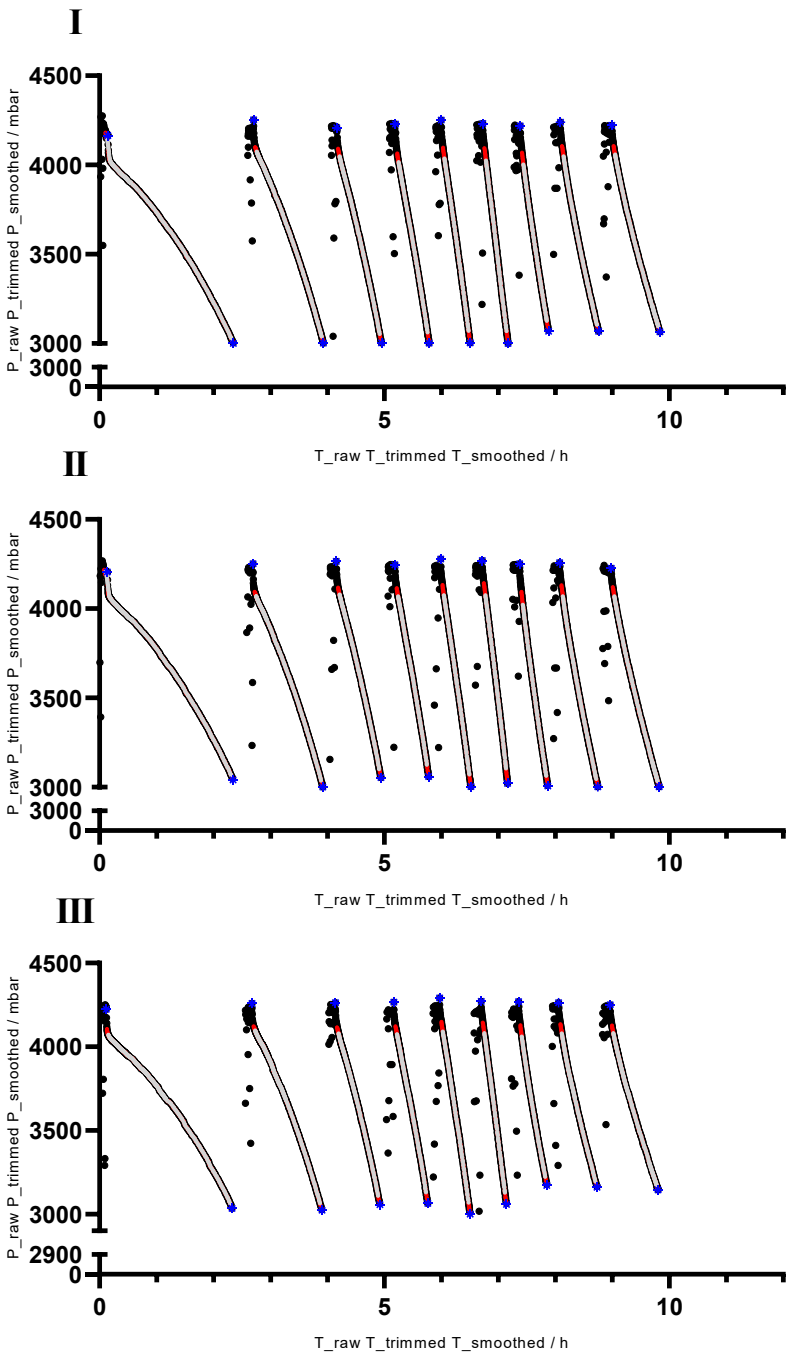

Figure S7: Pressure kinetics (in bar overpressure) of the methanation experiments of *M. marburgensis* in triplicate design. Raw data (black) represents values extracted from the GPC. Trimmed data (red) are obtained after applying data filtering. The smoothed data set (grey) represents pressure kinetics after applying the smoothing factor and is used for subsequent calculation of the physiological parameters. Cultivation time used for calculation of μ / h^{-1} is highlighted in blue and represent start and beginning of a cultivation cycle (total 9).

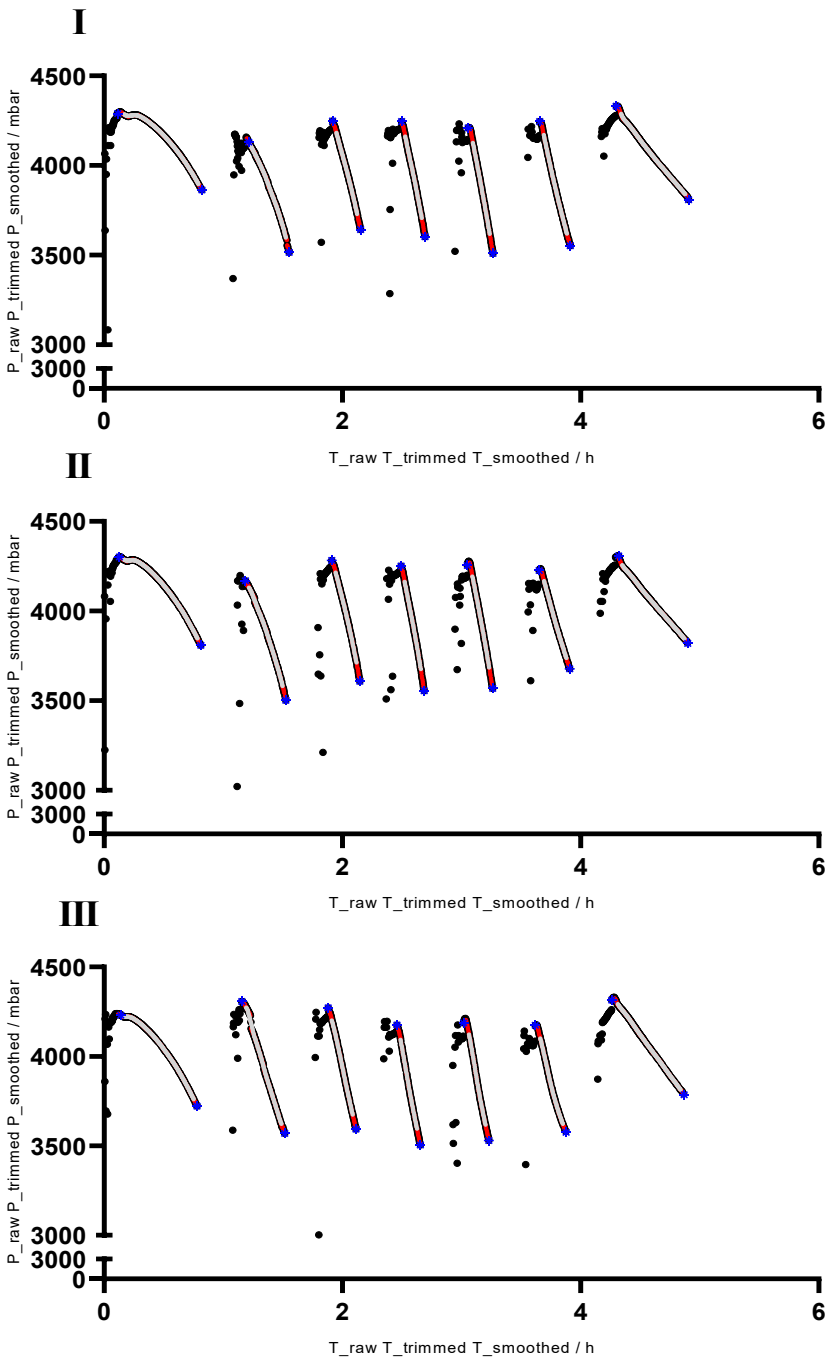

Figure S8: Pressure kinetics (in bar overpressure) of the methanation experiments of *M. igneus* in triplicate design. Raw data (black) represents values extracted from the GPC. Trimmed data (red) are obtained after applying data filtering. The smoothed data set (grey) represents pressure kinetics after applying the smoothing factor and is used for subsequent calculation of the physiological parameters. Cultivation time used for calculation of μ / h^{-1} is highlighted in blue and represent start and beginning of a cultivation cycle (total 7).

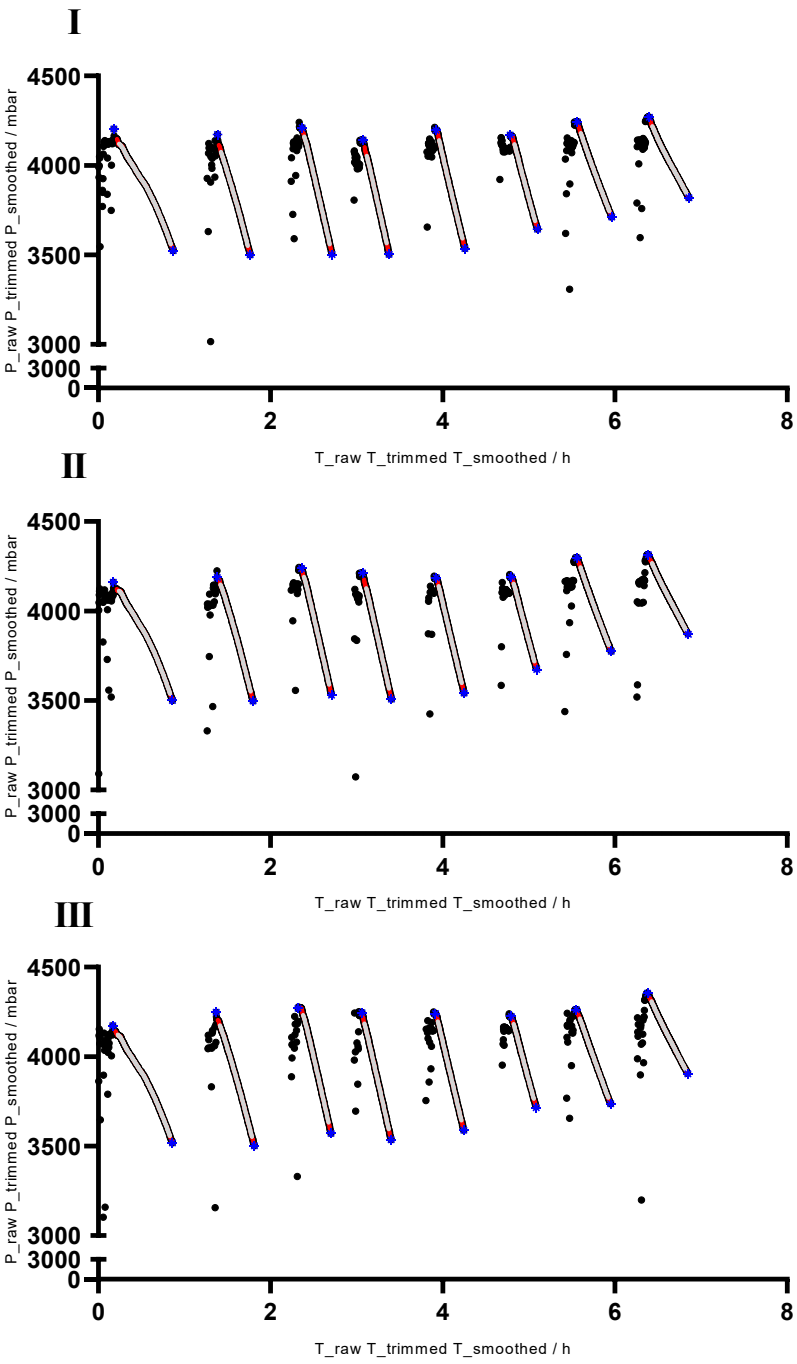

Figure S9: Pressure kinetics (in bar overpressure) of the methanation experiments of *M. villosus* in triplicate design. Raw data (black) represents values extracted from the GPC. Trimmed data (red) are obtained after applying data filtering. The smoothed data set (grey) represents pressure kinetics after applying the smoothing factor and is used for subsequent calculation of the physiological parameters. Cultivation time used for calculation of μ / h^{-1} is highlighted in blue and represent start and beginning of a cultivation cycle (total 8).

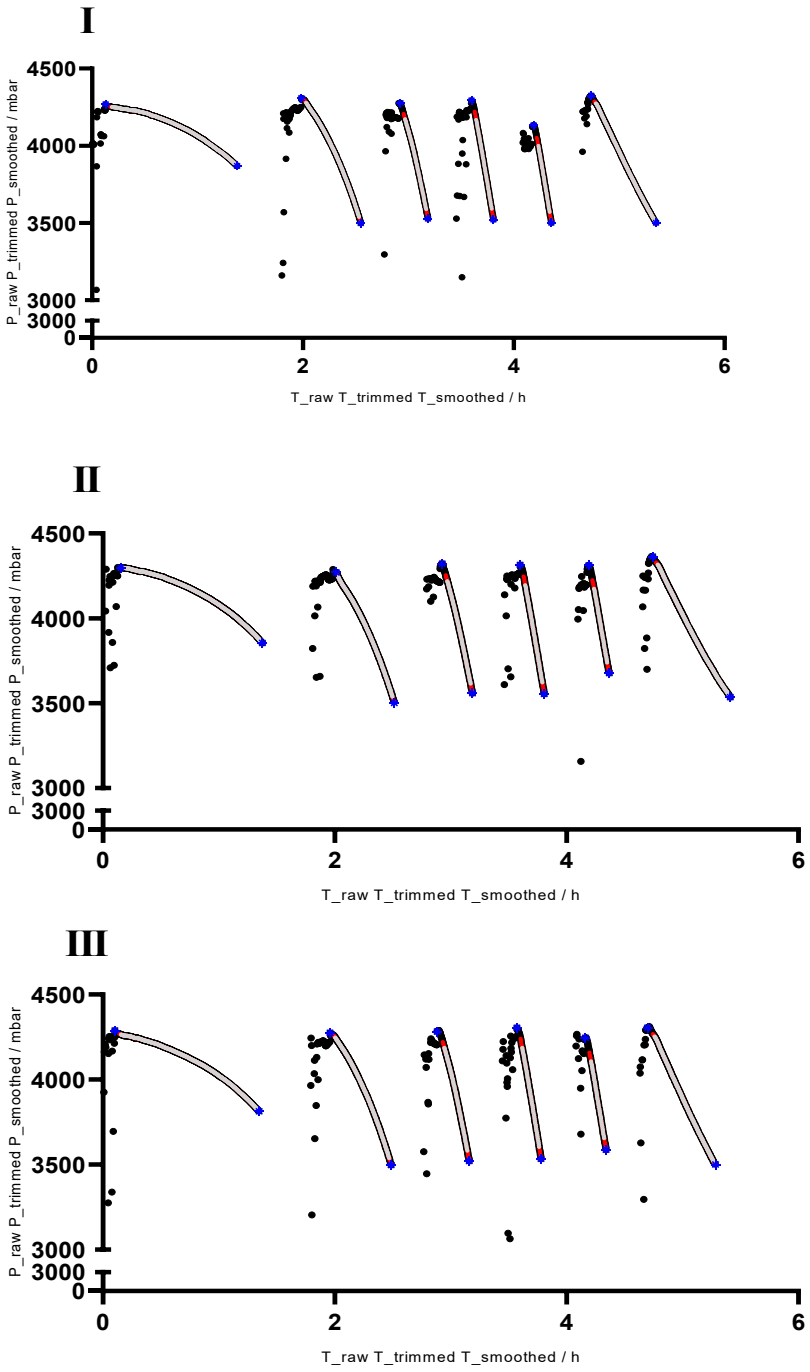

Figure S10: Pressure kinetics (in bar overpressure) of the methanation experiments of *M. jannaschii* in triplicate design. Raw data (black) represents values extracted from the GPC. Trimmed data (red) are obtained after applying data filtering. The smoothed data set (grey) represents pressure kinetics after applying the smoothing factor and is used for subsequent calculation of the physiological parameters. Cultivation time used for calculation of μ / h^{-1} is highlighted in blue and represent start and beginning of a cultivation cycle (total 6).

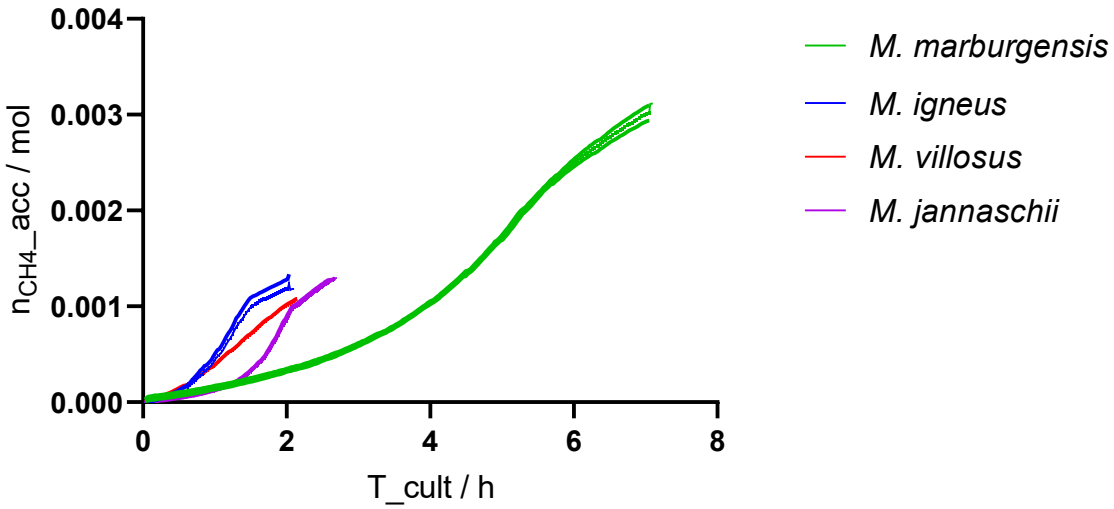

Figure S11: Accumulated moles of CH_4 produced determined in real time over the cultivation time. All experiments were performed in triplicates. Standard deviations are indicated via parallel lines.

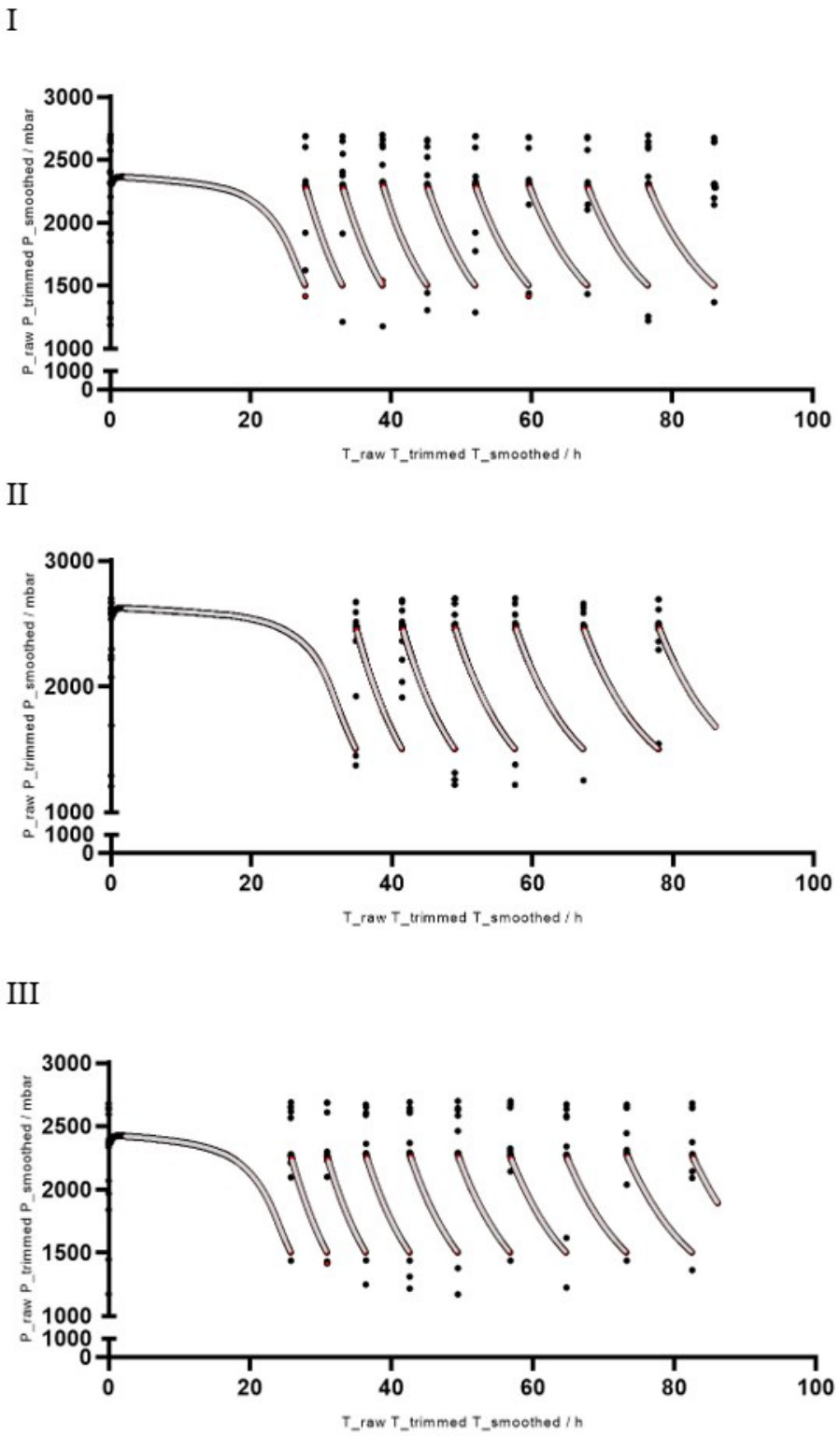

Figure S12: Pressure kinetics (in bar overpressure) of the methanation experiments of *M. maripaludis* in triplicate design. Raw data (black) represents values extracted from the GPC. Trimmed data (red) are obtained after applying data filtering. The smoothed data set (grey) represents pressure kinetics after applying the smoothing factor and is used for subsequent calculation of the physiological parameters.

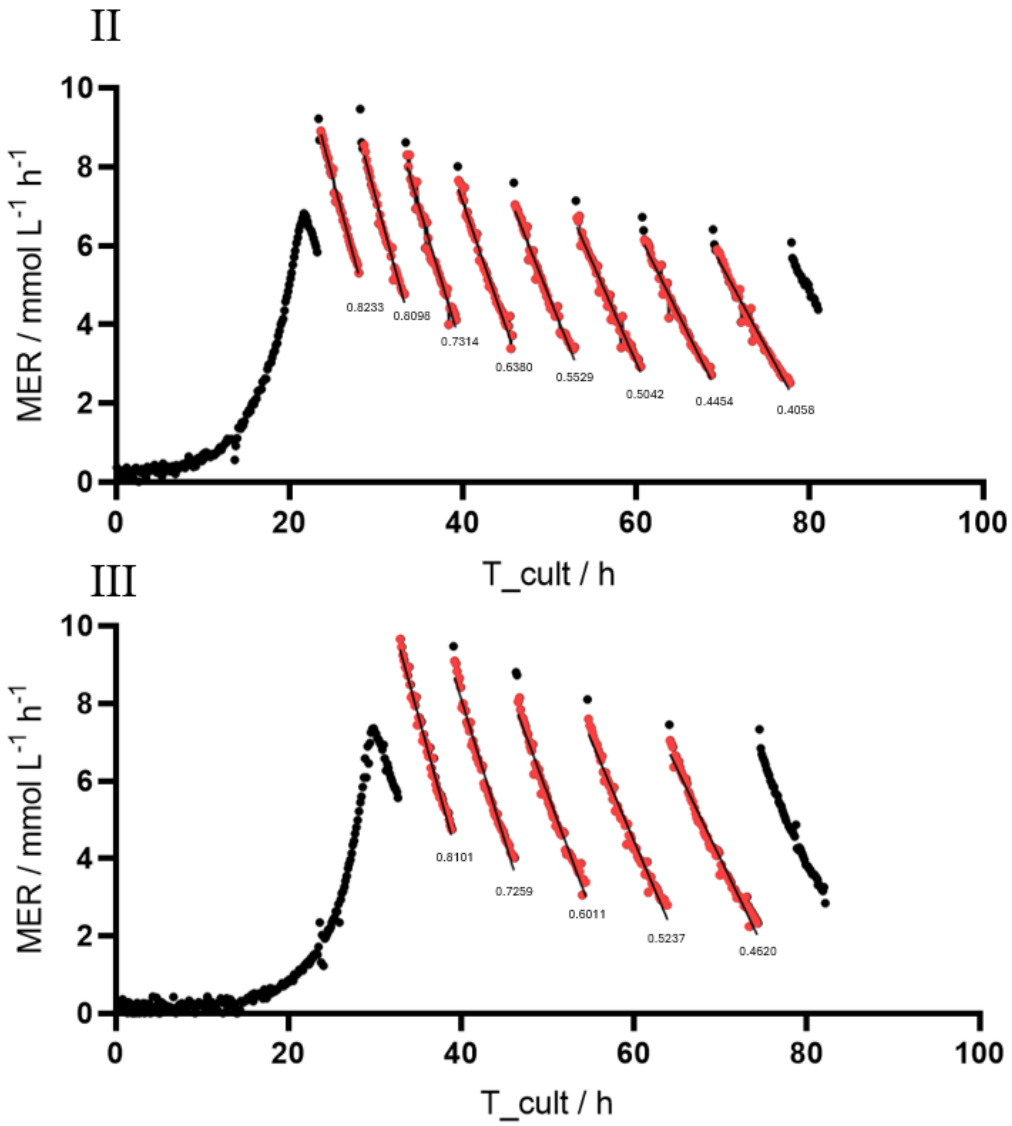

Figure S13: Methanation kinetics of *M. maripaludis* cultivation. Experiments were conducted in triplicate, with a single experiment shown in Figure 4. The slope of the linear regression was calculated for each cycle.

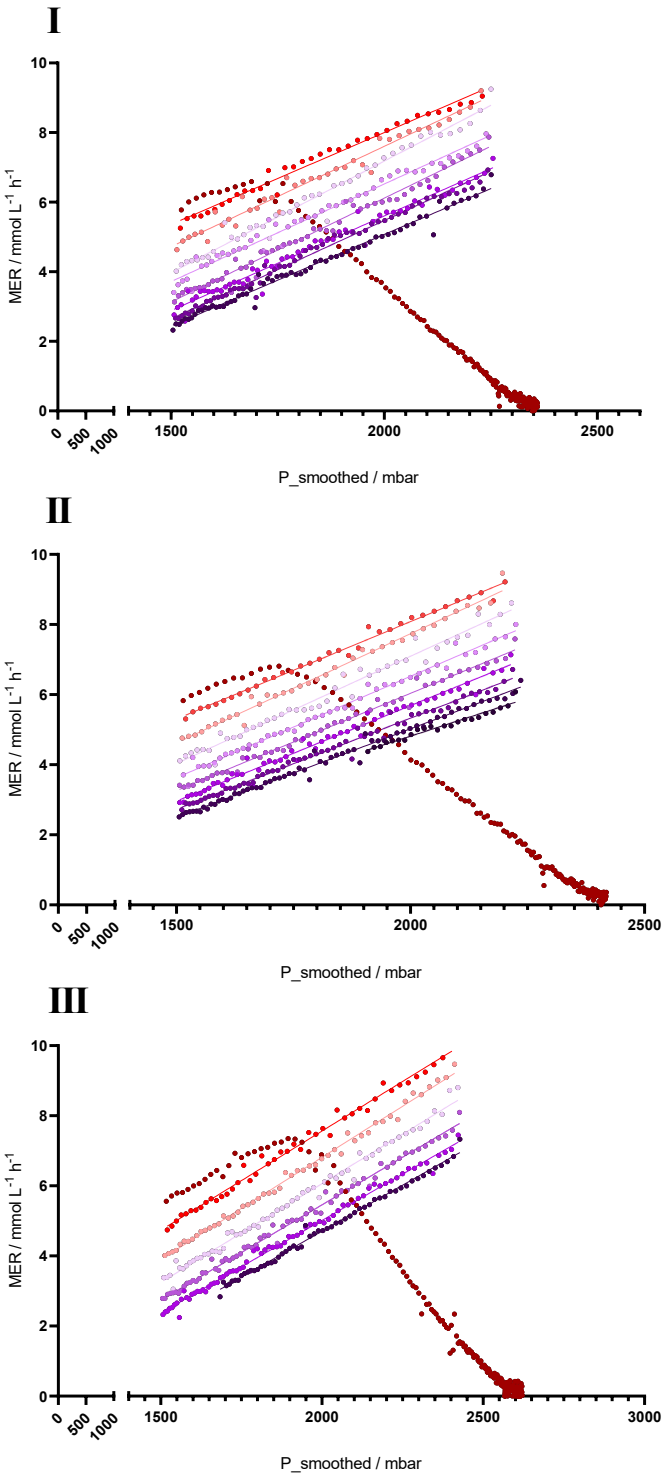

Figure S14: The MER for *M. maripaludis* is plotted against the corresponding pressure. Individual gassing cycles are represented using a color gradient, ranging from dark red to purple.

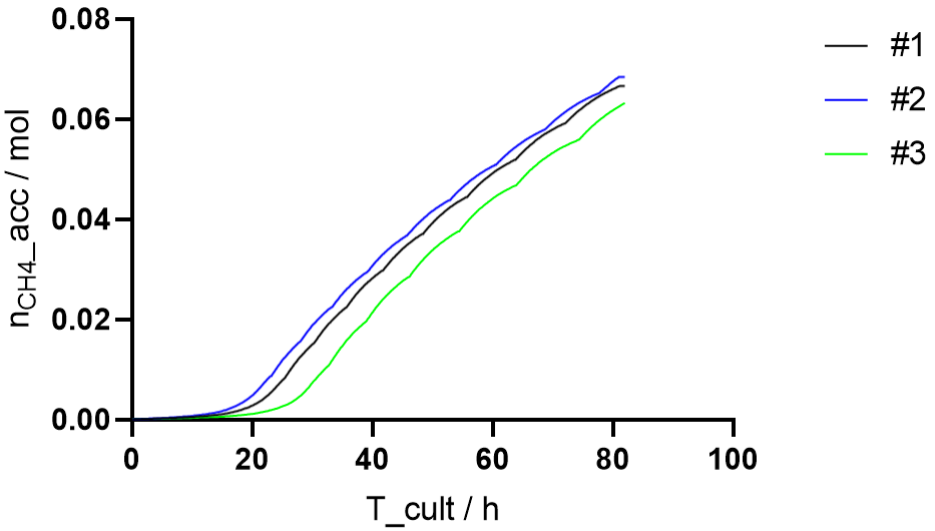

Figure S15: Accumulated moles of CH_4 produced determined in real time over the cultivation time for *M. maripaludis*. All experiments were performed in triplicates. Individual experiments are shown.